Phase Relations and Thermodynamic Properties of Spinelloid Phases in the System Mg_2SiO_4–Fe_2SiO_4–Fe_3O_4 at high Temperatures and Pressures
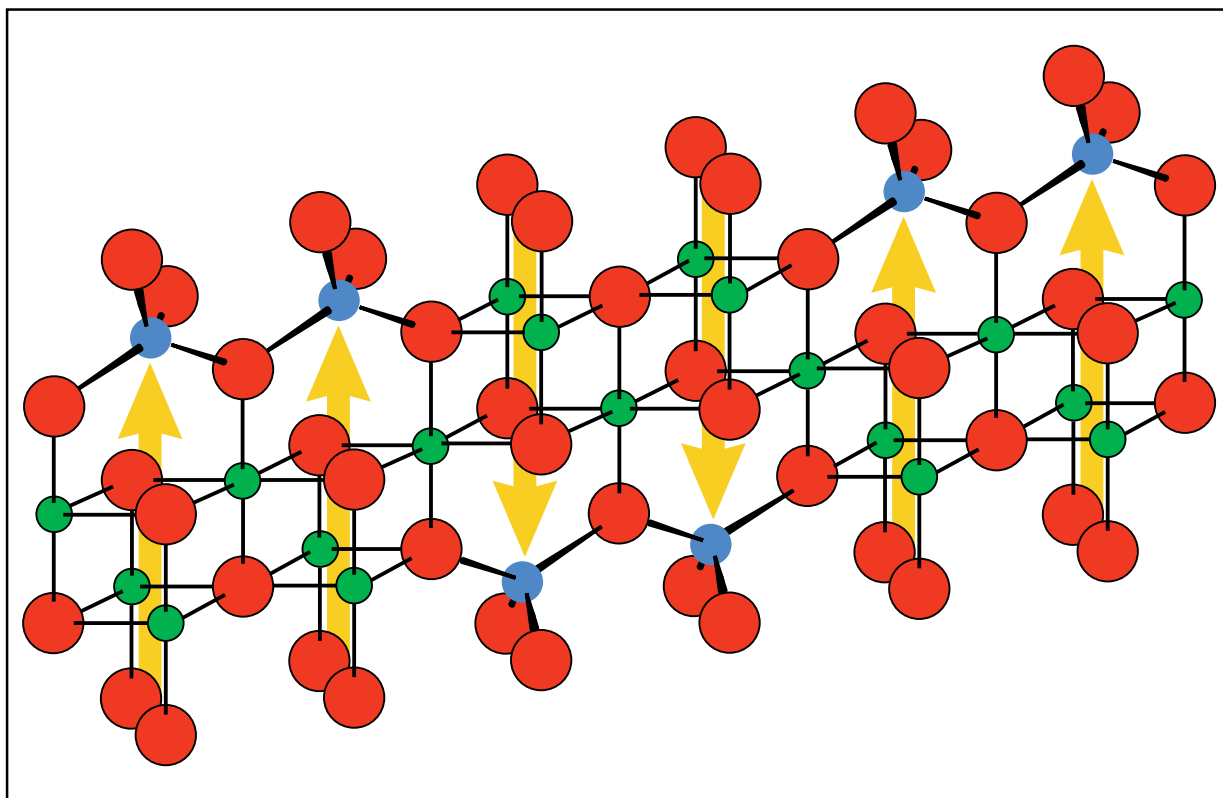
Dissertation

submitted to the
Combined Faculties for Natural Sciences and Mathematics
of the Ruperto-Carola University, Heidelberg, Germany
for the degree of
Doctor of Natural Sciences

presented by

Diplom-Mineraloge Mario Koch
born in Ludwigshafen/Pfalz

May 2003

Table of contents

1. Introduction

1.1. Mantle mineralogy and seismic discontinuities

During the past few decades major progress has been made from controlled laboratory experimentation on understanding the chemical and physical properties of mantle minerals and rocks covering almost the entire pressure and temperature range of the Earth's mantle. From these observations we have a reasonably clear picture of what the Earth's mantle should be composed of and look like. The uppermost part of the mantle is dominantly composed of two principal rock types, namely peridotites (olivine-pyroxene) and to a lesser extent eclogites (garnet-pyroxene), which are widely distributed as local segregations (Fig. 1.1). With the steady development of newer and better experimental techniques to generate higher and higher pressures and temperatures it was only a question of time before some light was shed on the constituents of the lower parts of the mantle. Ringwood and Major (1966) discovered several new phase transformations including those of magnesian olivine to spinel and a spinel-like (beta) phase, later to be named wadsleyite.

DEPTH   **DENSITY**
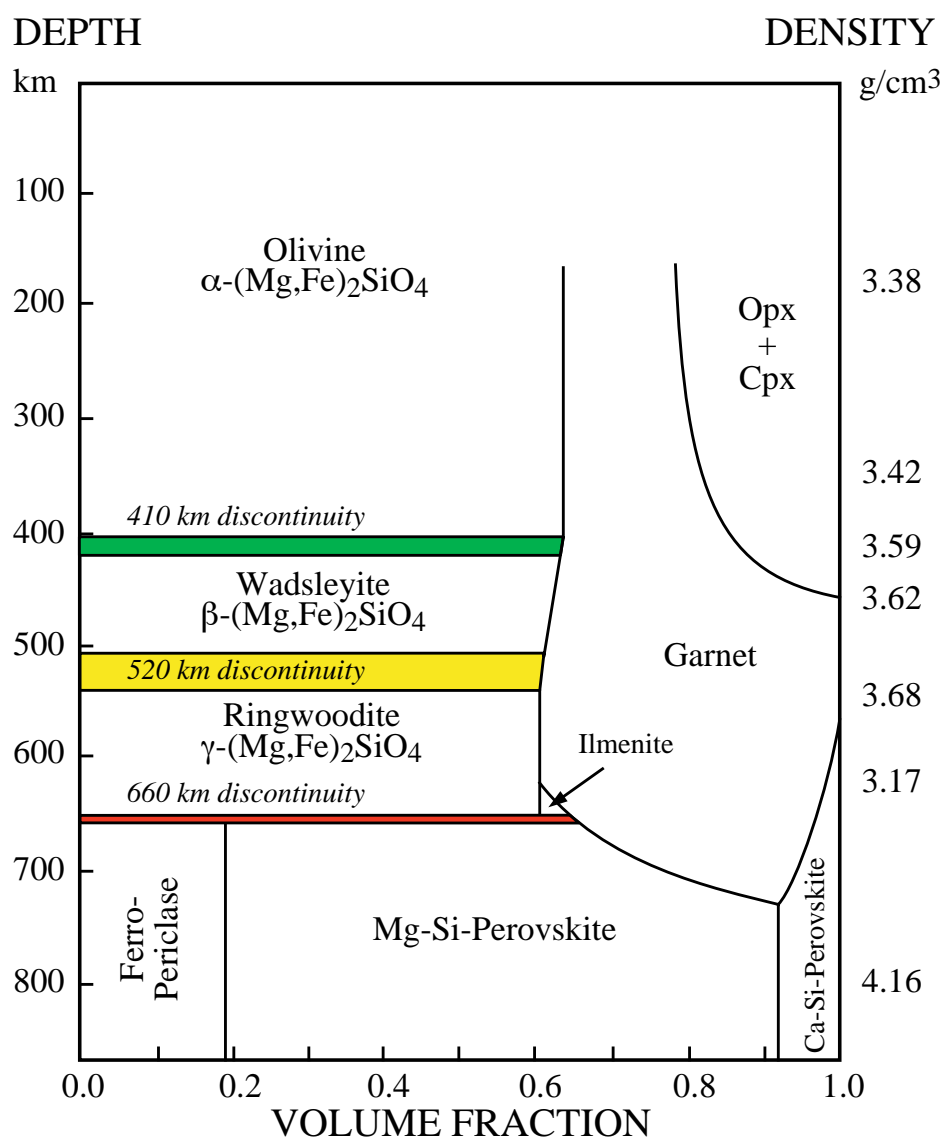
Fig. 1.1: Mineral assemblages in a mantle of pyrolite, or model peridotite composition modified after Ringwood (1991). Densities are given as zero-pressure densities.

They also found a transformation of several silicate pyroxenes into a new type of garnet containing up to 25% octahedrally coordinated silicon (majorite) as well as a magnesian and pure $CaSiO_3$ perovskite at even higher pressures (Fig. 1.1; Ringwood 1967; Ringwood & Major 1971).

On the basis of seismic velocity distributions and the above mentioned phase relations the mantle can be subdivided into three different main regions. The upper mantle encompasses the region between the Mohorovicic discontinuity, marking the base of the crust, and the first major seismic discontinuity at about 410 km depth. The next major seismic discontinuity occurs near a depth of 660 km (compare Fig. 1.1), and the region between these two discontinuities is referred to as the transition zone which also includes a smaller discontinuity at about 520 km (Fig. 1.2). The lower mantle comprises the largest region ranging from the 660 km discontinuity down to the core, which is encountered at a depth of about 2900 km.
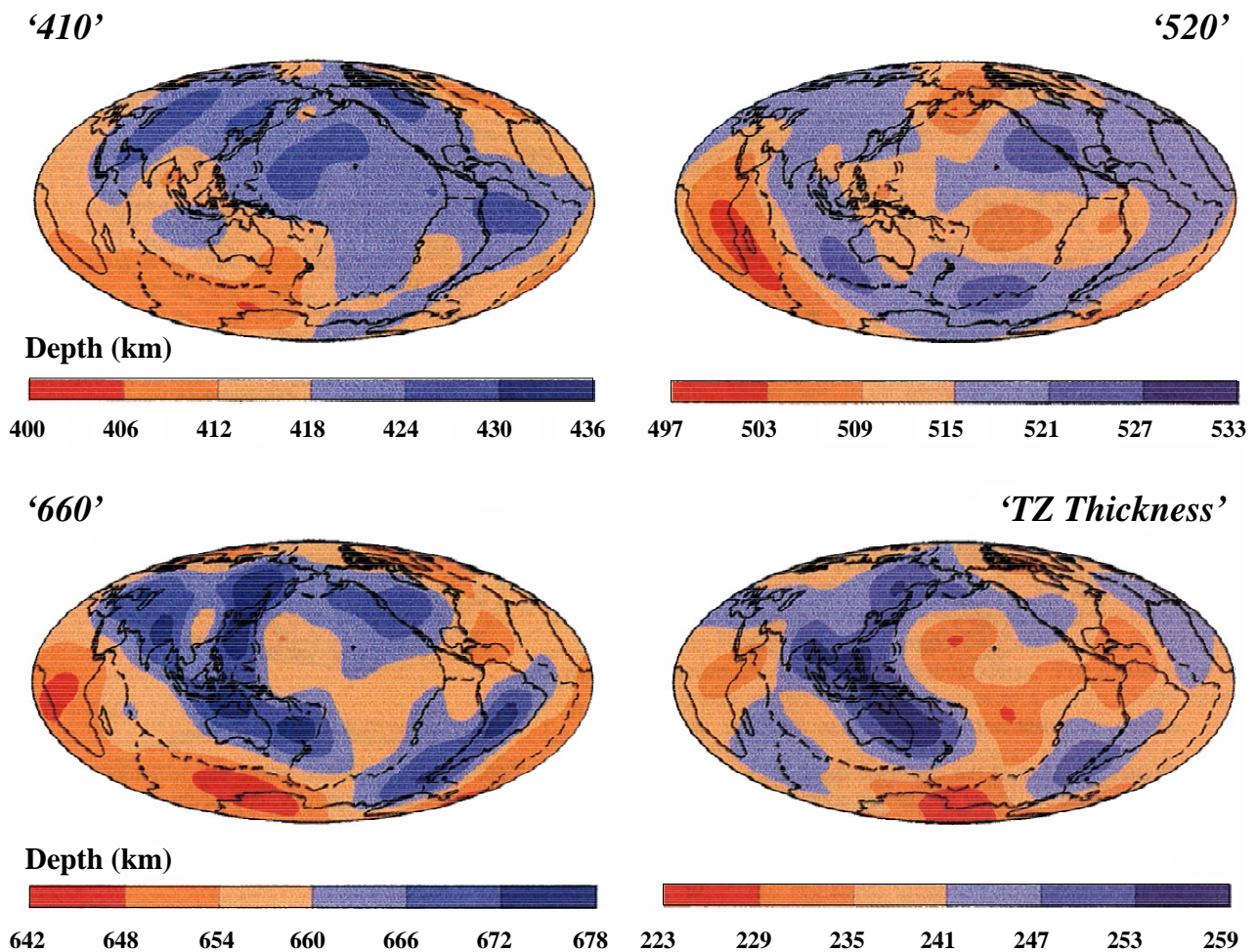
Fig. 1.2: Upper mantle discontinuity topography modified after Flanagan and Shearer (1998). The scale under the first three diagrams indicates the variation in depth at which the discontinuities are observed worldwide. In the lower right diagram TZ stands for transition zone, and here the scale portrays the overall thickness of this zone in the mantle.

The phase relations in the system Mg_2SiO_4–Fe_2SiO_4 illustrated in Figure 1.3 play a key role in determining the mantle structure around depths of 410 km and have been successively refined during the last 35 years as well as successfully correlated to detailed seismic observations. Today it is widely accepted that the seismic discontinuity at 410 km is mainly related to the pressure induced

reconstructive phase transformation of Mg-rich olivine to wadsleyite. The depth interval over which the transition occurs ranges from 4 to 20 km at estimated temperatures of 1400-1700 °C. Wadsleyite has a denser structure than olivine, yielding in a density increase of about 8% due to the phase transition (Ringwood 1991; Flanagan & Shearer 1998).
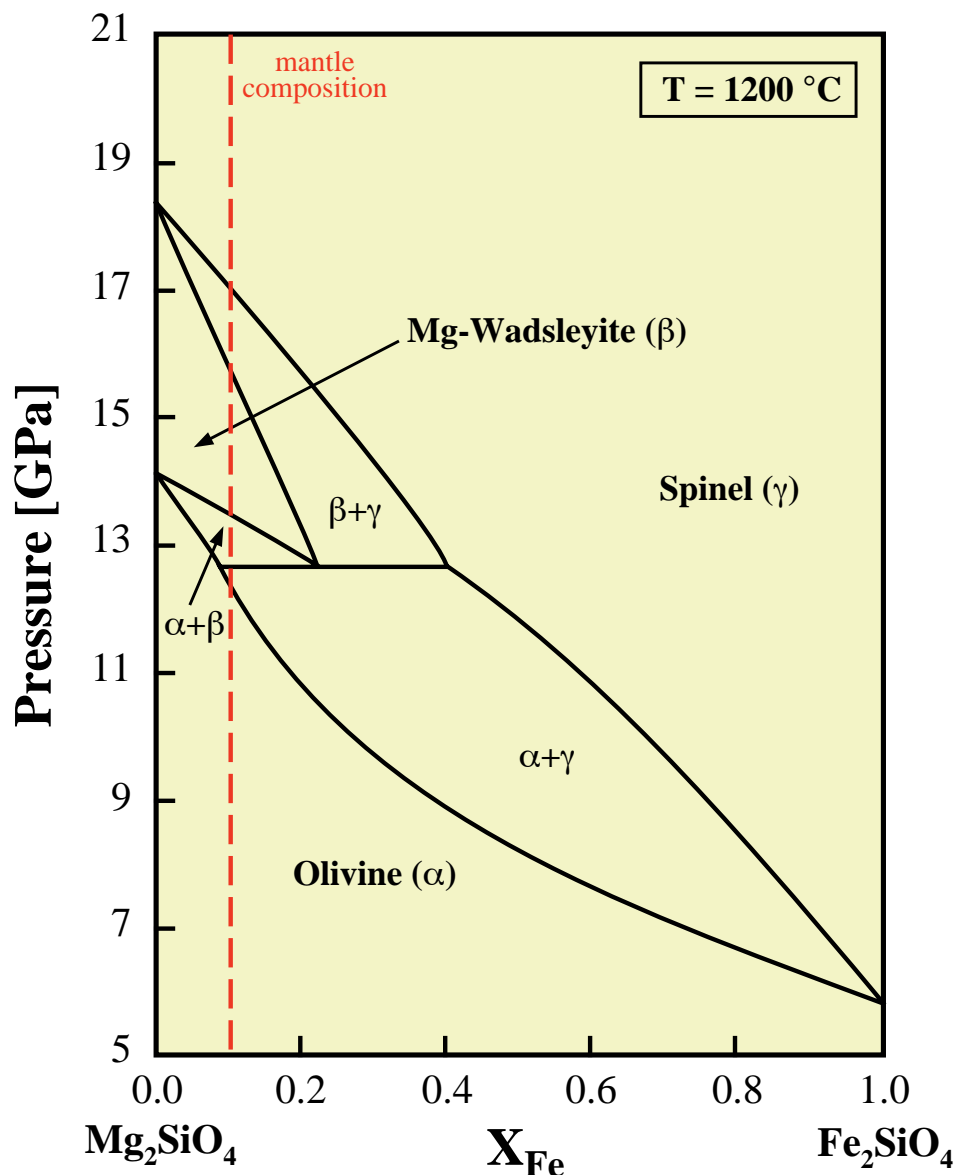
Fig. 1.3: Phase relations in the binary system Mg_2SiO_4–Fe_2SiO_4 as a function of pressure at 1200 °C modified after Fei et al. (1991). At lower temperatures the phase boundaries shift towards lower pressures. Mg-wadsleyite is the only intermediate phase stable in this system. The dashed red line represents a mantle bulk composition.

At a somewhat greater depth of ~520 km and temperatures of 1500 °C, wadsleyite transforms into the spinel structure (γ-phase or ringwoodite) which has recently been related to a smaller and much broader discontinuity accompanied by a density increase of about 2% (Figs. 1.1, 1.2, 1.3; Shearer 1990, 1996). In a similar fashion, the 660 km discontinuity is attributable to the disproportionation reaction of $(Mg,Fe)_2SiO_4$ spinel to $(Mg,Fe)SiO_3$ perovskite and $(Mg,Fe)O$ ferro-periclase at temperatures of ~1600 °C (Fig. 1.1). With an ~4 km width, this discontinuity is remarkably sharp and the reaction involves a large density increase of about 11% (Ringwood 1991).

1.2. Spinelloids

During the high-pressure transformation of olivine to spinel various intermediate phases can exist, such as wadsleyite in the $(Mg,Fe)_2SiO_4$ system. In the $NiAl_2O_4$–Ni_2SiO_4 system (Fig. 1.4) a total of five different intermediate phases have been identified that are closely related to the spinel lattice and structure (Ma 1974; Akaogi et al. 1982).
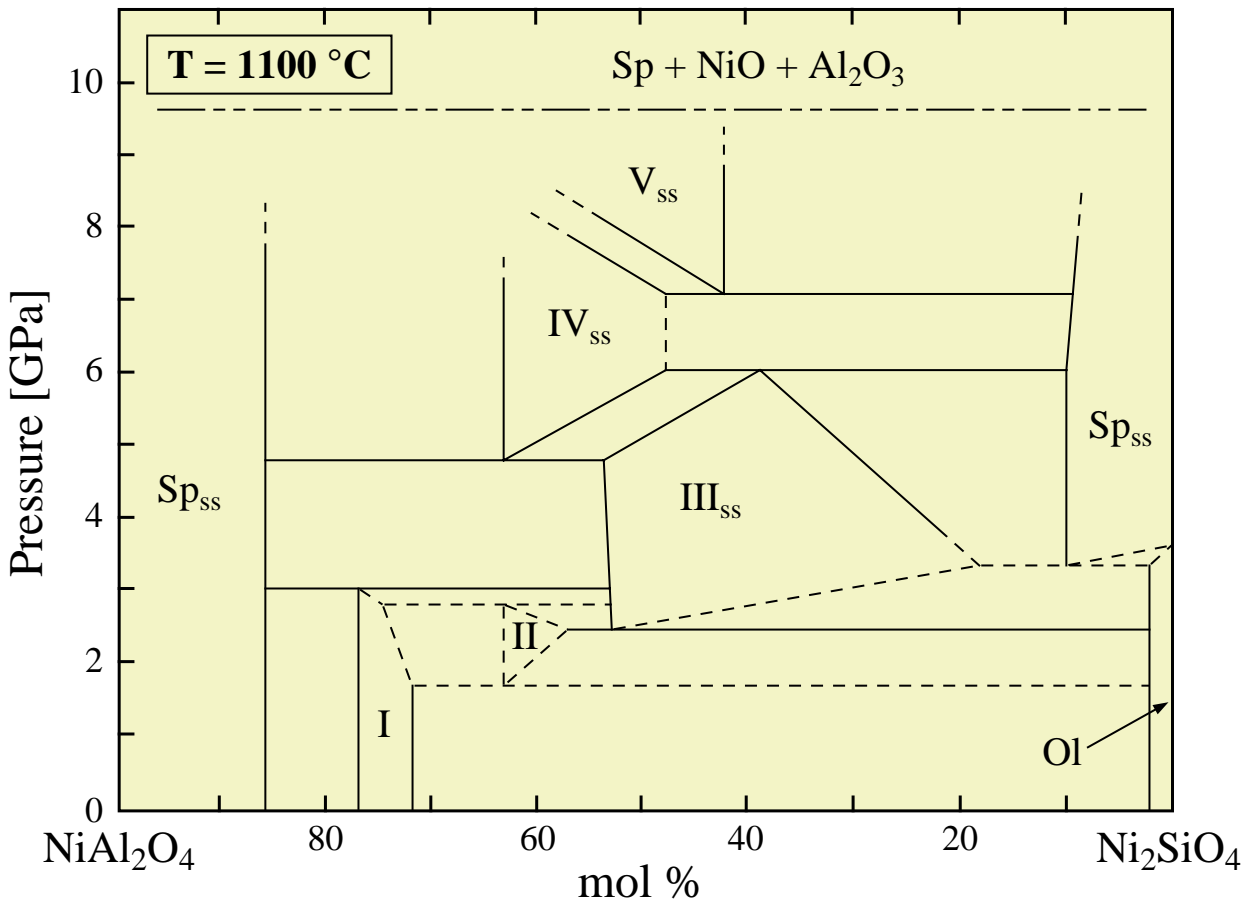
Fig. 1.4: Phase relations in the binary system $NiAl_2O_4$–Ni_2SiO_4 as a function of pressure at 1100 °C modified after Akaogi et al. (1982). In this system, five intermediate phases (I to V) have been synthesised.

Therefore the term "spinelloids" was introduced to indicate their close structural relationships with spinel (Horiuchi et al. 1980). Various spinelloid polytypes are known to exist in a number of different chemical systems such as $NiGa_2O_4$–Ni_2SiO_4, $MgGa_2O_4$–Mg_2GeO_4, $MgFe_2O_4$–Mg_2GeO_4, Fe_3O_4–Fe_2SiO_4 and Fe_3O_4–$(Mg,Fe)_2SiO_4$ (Hammond & Barbier 1991; Barbier 1989; Woodland & Angel 1998, 2000; Angel & Woodland 1998; Ross et al. 1992; Koch et al. 2003). From theoretical considerations based on free energy calculations more than 37 structures have been proposed to potentially exist (Price 1983; Horiuchi et al. 1982). However only six, including spinel, have been found to be stable.

These phases have a general M_2TO_4 stoichiometry and can occur in a variety of crystal structures. Here, the M atoms occupy octahedral sites and the T atoms the tetrahedral sites. Spinel has a cubic closest packed structure (cubic, Fd3m SG, isolated tetrahedra) whereas the spinelloids are based on a slightly distorted cubic closest packing (orthorhombic, Pmma or Imma SG, bridging and non-silicate

oxygens, Si_2O_7 groups, can be protonated). The major difference between spinel and the spinelloid structures lies in the arrangement of the TO_4 polyhedra, which are isolated in the spinel structure, but may be coupled in the spinelloids (Horiuchi et al. 1982). From the spinel structure a "basic structural unit" can be derived which is stacked in different ways along the *b*-axis to produce all the spinelloid structures (Fig. 1.5, Table 1.1). The "basic structural unit" can be denoted as an oriented arrow, which allows for a one-dimensional representation of the stacking of this unit (Fig. 1.5, Table 1.1).
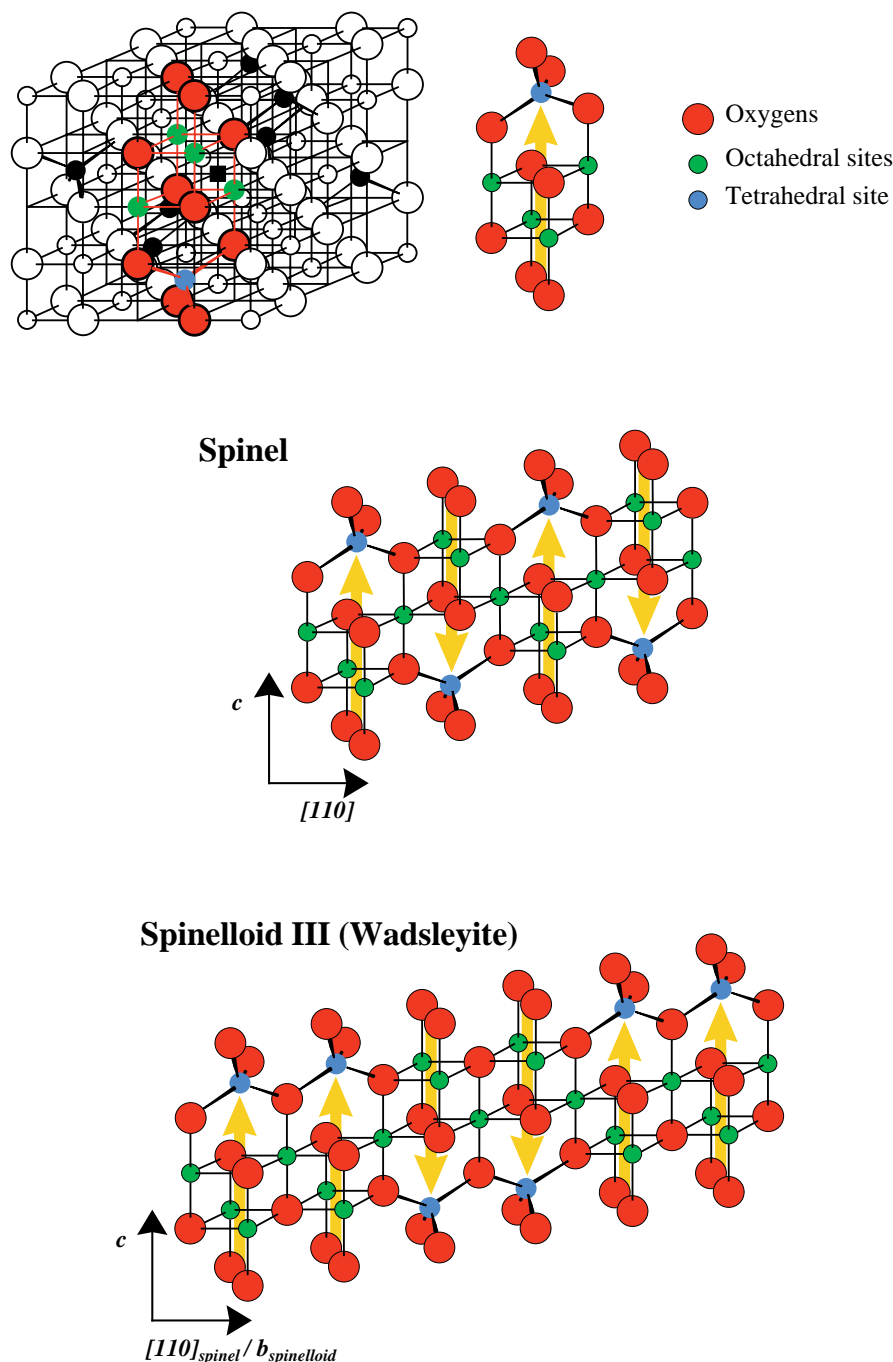
Fig. 1.5: From the spinel unit cell (top left), oriented to emphasize the (111) planes (modified after Lindsley 1976), the basic structural unit (top right) from Horiuchi et al. (1982) can be derived from which the stuctures of all spinelloid polytypes as well as spinel can be constructed. This is accomplished by characteristic stacking of this unit along the *b*-direction, such as illustrated here for spinel (center) and spinelloid III (bottom; see Table 1.1). For clarity, yellow arrows are drawn pointing towards the tetrahedral site in this structural unit to indicate the relative orientation of these units in the different stacking sequences. The *a*-direction points out of the paper.

Within the group of spinelloids there exist structures with T_2O_7 and T_3O_{10} tetrahedral groups (denoted by ↑↑ and ↑↑↑ sequences in Table 1.1). Spinelloids I, IV and V additionally contain isolated TO_4 groups alternating in the stacking sequence. Wadsleyite is isostructural with the spinelloid III polytype found in the $NiAl_2O_4$–Ni_2SiO_4 system by Ma (1974).

Table 1.1: Existing spinelloid minerals. Stacking sequence is illustrated in the *b*-direction.

Name	Polyhedra	Stacking sequence	Mineral
Spinel	TO_4 groups	... ↑↓↑↓ ...	Ringwoodite
Spinelloid I	T_3O_{10} & TO_4 groups	... ↑↑↑↓ ...	-
Spinelloid II	T_3O_{10} groups	... ↑↑↑↓↓↓ ...	Manganostibite [1]
Spinelloid III	T_2O_7 groups	... ↑↑↓↓ ...	Wadsleyite
Spinelloid IV	T_2O_7 & TO_4 groups	... ↑↑↓↓↑↓↓↑↑↓ ...	-
Spinelloid V	T_2O_7 & TO_4 groups	... ↑↑↓↑↑↓ ...	-

[1] Manganostibite = $(Mn,Fe^{2+})_7Sb^{5+}As^{5+}O_{12}$

1.3. Fe^{3+} in the Earth's mantle

Since wadsleyite and silicate spinel (both $(Mg,Fe)_2SiO_4$) are generally considered to be the major mineralogical constituents of the transition zone, the possible incorporation of Fe^{3+} into these phases will influence their stabilities and this could cause a shift in the depth at which the 410 km, 520 km and 660 km seismic discontinuities occur (Fig. 1.2). In addition, the presence of Fe^{3+} has ramifications for the oxidation state and the electrical conductivity of this part of the Earth's mantle.

The substitution of Fe^{3+} in silicate spinel or wadsleyite must occur via a coupled substitution in order to maintain charge balance. Recent experiments indicate a complete solid solution between magnetite and Fe_2SiO_4-spinel that is stable at temperatures of 1100-1200 °C and pressures above 8.0 GPa (Ohtaka et al. 1997; Woodland & Angel 2000). At lower pressures in the Fe_2SiO_4–Fe_3O_4 binary system, the phase relations are rather complex as compared to the Fe^{3+}-free system (compare Figs. 1.6, 1.3). Three different intermediate phases have been found that correspond to the spinelloid polytypes II, III and V (Akaogi et al. 1982; Woodland & Angel 1998, 2000; Angel & Woodland 1998; Ohtaka et al. 1997; Canil et al. 1991). The stability of a Fe^{3+}-rich spinelloid III polytype in this system is of particular petrologic importance since this phase is isostructural with wadsleyite (Woodland & Angel 1998). This contrasts with the $(Mg,Fe)_2SiO_4$ binary system where the stability field of wadsleyite is restricted to Mg-rich compositions with $Fe^{2+}/(Fe^{2+}+Mg) \leq 0.25$ (Bina & Wood 1987; Katsura & Ito 1989; Fei et al. 1991; Fig. 1.3). Thus, the presence of Fe^{2+} appears to destabilise the wadsleyite structure, while Fe^{3+} appears to stabilise it. In fact, Fe^{3+}-wadsleyite is stable along the Fe_2SiO_4–Fe_3O_4 binary at much lower pressures than "true" $(Mg,Fe)_2SiO_4$ wadsleyite (compare Figs. 1.6, 1.3; see also Woodland & Angel 2000). At higher pressures, spinelloid V is stable over a wide compositional range and can coexist with magnetite-rich spinel or Fe^{3+}-bearing silicate spinel or spinelloid III (Fig. 1.6). Although spinelloid V has never been found in nature, this phase still has potential relevance as an additional Fe^{3+}-bearing phase in the transition zone.
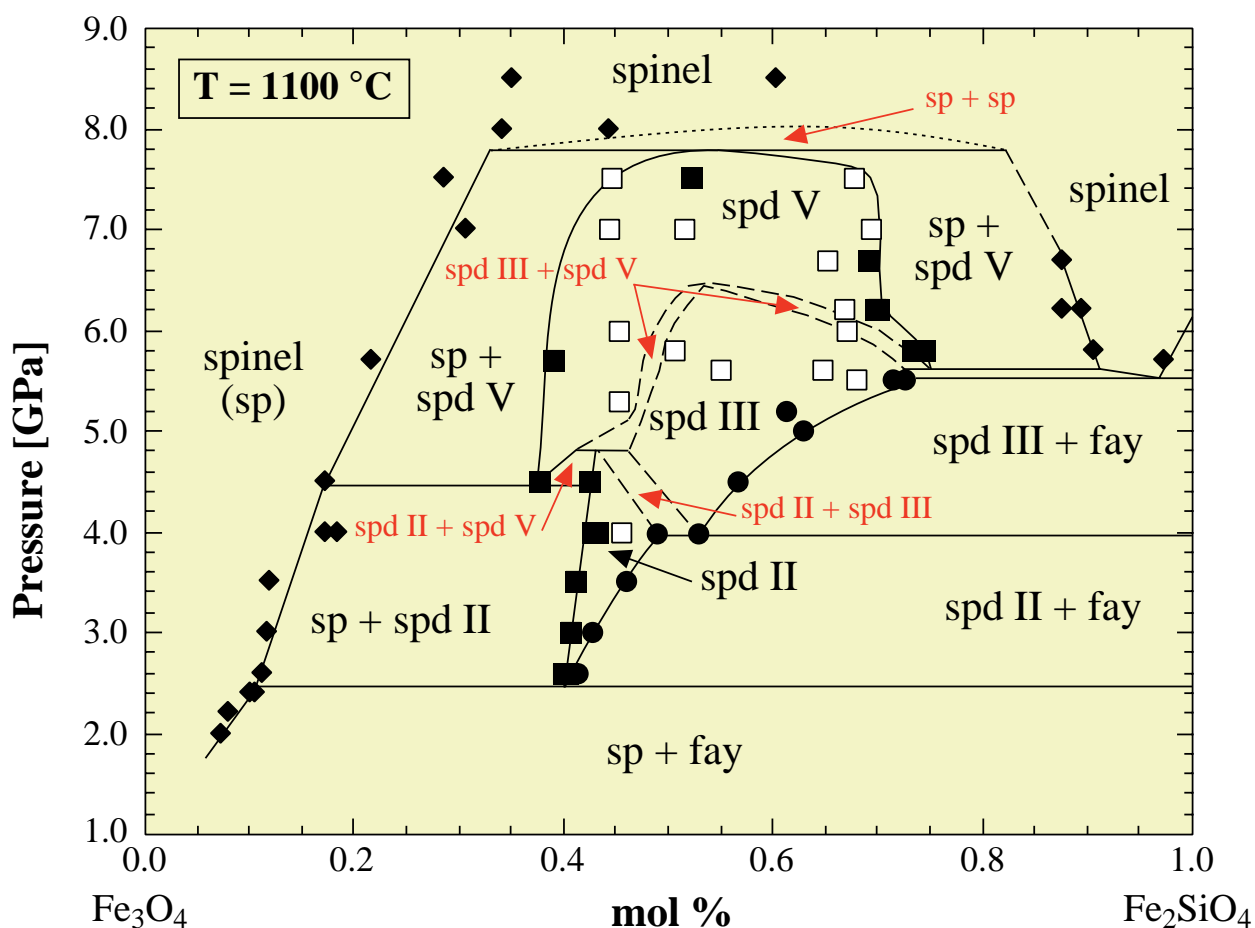
Fig. 1.6: Phase relations in the binary system Fe_3O_4–Fe_2SiO_4 as a function of pressure at 1100 °C modified after Woodland and Angel (2000). The solid squares and circles indicate spinelloid compositions in equilibrium with spinel or fayalite respectively. The open squares denote spinelloid samples that are either single phase or samples that do not coexist with either spinel or fayalite. The "sp + sp" two phase field represents the possible coexistence of a magnetite-rich spinel and a Si-rich spinel, before a complete spinel solid solution becomes stable at higher pressure.

1.4. Goals of this Study

In order to understand the phase relations and stabilities of the various spinelloid polytypes in more petrologically relevant compositions containing Fe^{3+}, experiments were conducted between 3.0 and 16.0 GPa at 1100 and 1200 °C in the Mg_2SiO_4–Fe_2SiO_4–Fe_3O_4 ternary system. Particular attention was paid to the compositional range in which spinelloid III (Fe^{3+}-wadsleyite) is stable, with the interest of whether complete solid solution occurs between this phase and $(Mg,Fe)_2SiO_4$-wadsleyite. Phase relations in the Fe_2SiO_4–Fe_3O_4 and Mg_2SiO_4–Fe_2SiO_4 binary sub-systems (Figs. 1.3, 1.6) were used as a guide for investigating the ternary system. In addition, this work has laid emphasis on the Fe^{2+}-Mg partitioning between olivine and Fe^{3+}-bearing spinel and spinelloid solid solutions as well as on the determination of molar volumes and thermodynamic mixing models for spinel and spinelloid solid solutions. Last but not least, this study might provide some insights into the effects of Fe^{3+} and Mg substitution on the mineralogy of the transition zone as well as the on the shape and position of the 410 km seismic discontinuity.

2. Experimental Methods

2.1. Starting material synthesis

The starting materials for all experiments were stoichiometric mixtures of olivine$_{ss}$ and magnetite (ground under acetone and dried), with olivine having X_{fa} = 0.1, 0.3, 0.5, 0.8 or 0.9 (Fig. 2.1). Magnetite was synthesised from high purity Fe_2O_3 (99.99%) in a 1-atm CO-CO_2 gas-mixing furnace at 1100 °C and a log fO_2 = -9.1 and drop quenched into distilled water. Olivine solid solutions were prepared in an analogous way. First pure fayalite and forsterite were synthesised from stoichiometric mixtures of high-purity SiO_2 (99.999%), Fe_2O_3 and MgO (99.99%) at 1100 °C and a log fO_2 = -13.0 (slightly above the Fe wüstite oxygen buffer of O'Neill and Pownceby 1993) and at 1350 °C in air, respectively. In a second step the actual olivine compositions were prepared from stoichiometric mixtures of the two endmembers at various temperatures and oxygen fugacities corresponding to redox conditions slightly above the Fe wüstite oxygen buffer (Table 2.1). Several cycles of grinding and firing were necessary to achieve homogeneity. Microprobe analyses confirmed the homogeneity and nominal composition (± 1 mol %) of the olivine$_{ss}$.

Table 2.1: Synthesis conditions for all olivine solid solutions.

Olivine$_{ss}$	Fa10	Fa30	Fa50	Fa80	Fa90
T [°C]	1350	1300	1300	1200	1100
log fO_2	-10.2	-10.2	-10.2	-11.7	-13.0
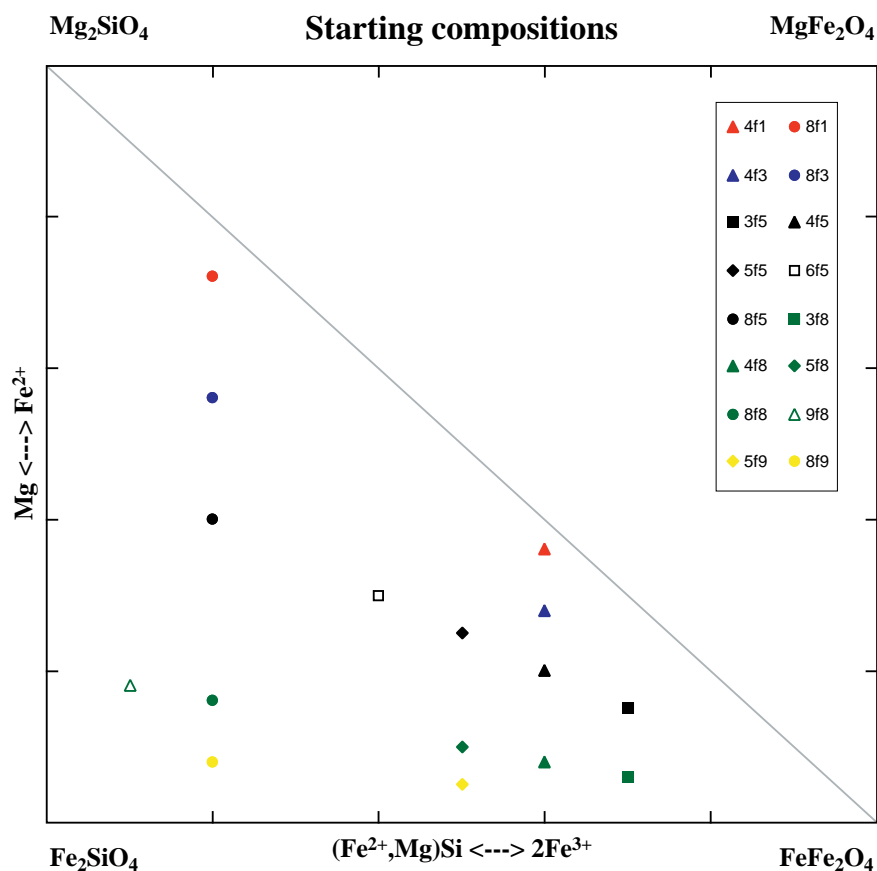
Fig. 2.1: All different starting compositions used, plotted in the same phase diagram as it will be seen in section 4.1.1. The notation refers to the sample mix and olivine composition: 4f1 is a 40% olivine - 60% magnetite mixture, with olivine having a composition of X_{fa} = 0.1 (see also section 2.2.2).

2.2. High pressure experiments

2.2.1. Multianvil apparatus

Experiments above 6.0 GPa were performed in three different multianvil presses at the Bayerisches Geoinstitut, Universität Bayreuth, Germany (Figs. 2.2, 2.3). Following the standard procedure for the Voggenreiter and Haymag presses, Toshiba F grade tungsten carbide cubes were used with an 11.0 mm truncated edge-length along with a Cr_2O_3-doped MgO octahedra 18.0 mm (18M) on edge (Figs. 2.4, 2.5, 2.6, 2.7). The assembly was heated by a graphite resistance heater and temperature was monitored by axially placed Pt-$Pt_{90}Rh_{10}$ thermocouples with no correction made for the pressure effect on emf. Alternatively, a $LaCrO_3$ heater, along with a $W_{97}Re_3$-$W_{75}Re_{25}$ thermocouple was used in some experiments (see Fig. 2.8). For experiments exceeding 10.5 GPa, either the 5000 t Zwick press with bigger tungsten carbide cubes but still 18M pressure cell assemblies or the Hymag and Voggenreiter presses were used applying 14M assemblies with a $LaCrO_3$ heater and $W_{97}Re_3$-$W_{75}Re_{25}$ thermocouples (Fig. 2.8). Pressure and temperature calibrations were made using several different phase changes to cover the whole operational P-T range of each individual press (i.e. Woodland & Angel 1997; Woodland & O'Neill 1993). The accuracy in pressure is on the order of $\pm$ 0.3 GPa and the temperature gradient across the sample is considered to be < 25 °C (c.f. Canil 1994).

Fig. 2.2: Multianvil lab at the Bayerisches Geoinstitut, Bayreuth. From front to rear Sumitomo press (blue), Hymag press (green) and the big 5000 t Zwick press (grey). People in the lab are Christine Gessmann, Dan Frost and myself.

Fig. 2.3: Deformation lab at the Bayerisches Geoinstitut, Bayreuth. Walker-type multianvil press (Voggenreiter) on which most experiments were done.

The starting materials for 18M assemblies were loaded into 2.0 mm Ag tubing, with the ends sealed by inserting a Ag disc prior to crimping and hammering into a die to produce a cold weld. For experiments in 14M assemblies starting materials were packed into rhenium foil, folded to a diameter of 1.6 mm and 2.7 mm in height with the ends also closed by a cold weld.
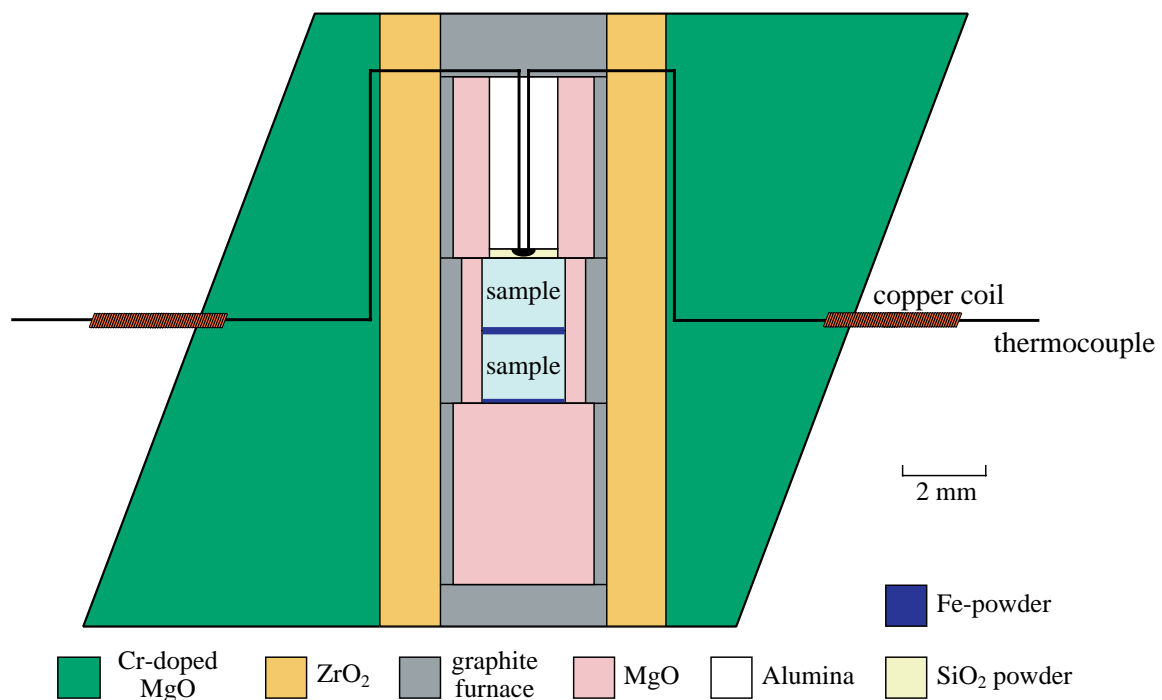
Fig. 2.4: Schematic drawing of the multi-anvil pressure cell octahedron. For a more detailed view of the inner parts of the octahedron see Fig. 2.5 and Fig. 2.8 below. The hole in the upper graphite piece (compare Fig. 2.5) as well as the cut slits for the thermocouples are being closed by a fireproof cement kit (see also Figs. 2.6, 2.7).
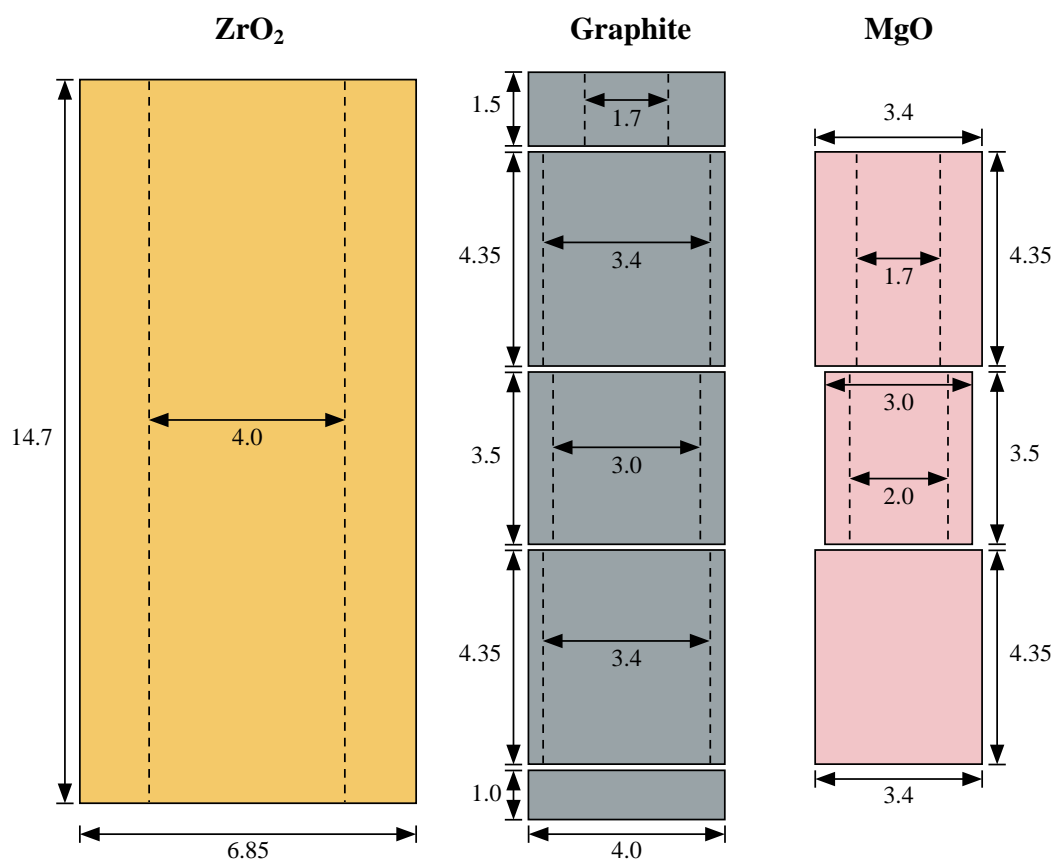
Fig. 2.5: Detailed diagramm of the interior parts of the pressure cell used in experiments up to 10.5 GPa (18M, with Pt-Rh thermocouple (TC)). Distances are given in millimeters. Color codes correspond to the legend in Fig. 2.4.

Fig. 2.6: From left to right: Raw MgO octahedra, fired and cut to provide space for the thermocouple (above); stepped graphite heater; double silver capsules; MgO octahedra after the run (note size difference); copper coils to protect the thermocouples from flowing pyrophyllite gaskets (compare Figs. 2.4, 2.7). Scale bar in centimeters.

Using the two-capsule configuration with capsule heights of about 1.7 mm each (18M assembly, compare Fig. 2.5), it is possible to run two different starting mixtures in one experiment, which was not possible for experiments using the 14M assembly, since there is much less space for the capsules.
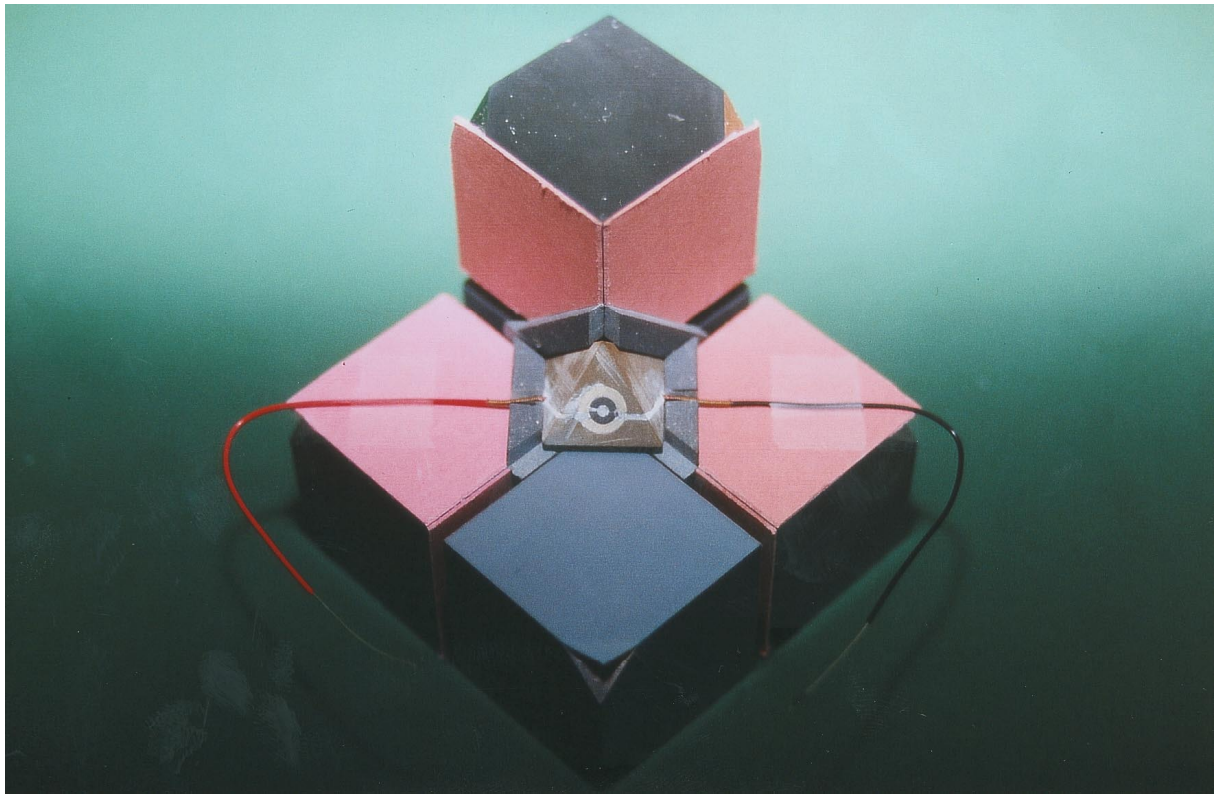
Fig. 2.7: Completly prepared pressure-octahedra sitting within pyrophyllite gaskets and a total of eight WC cubes.
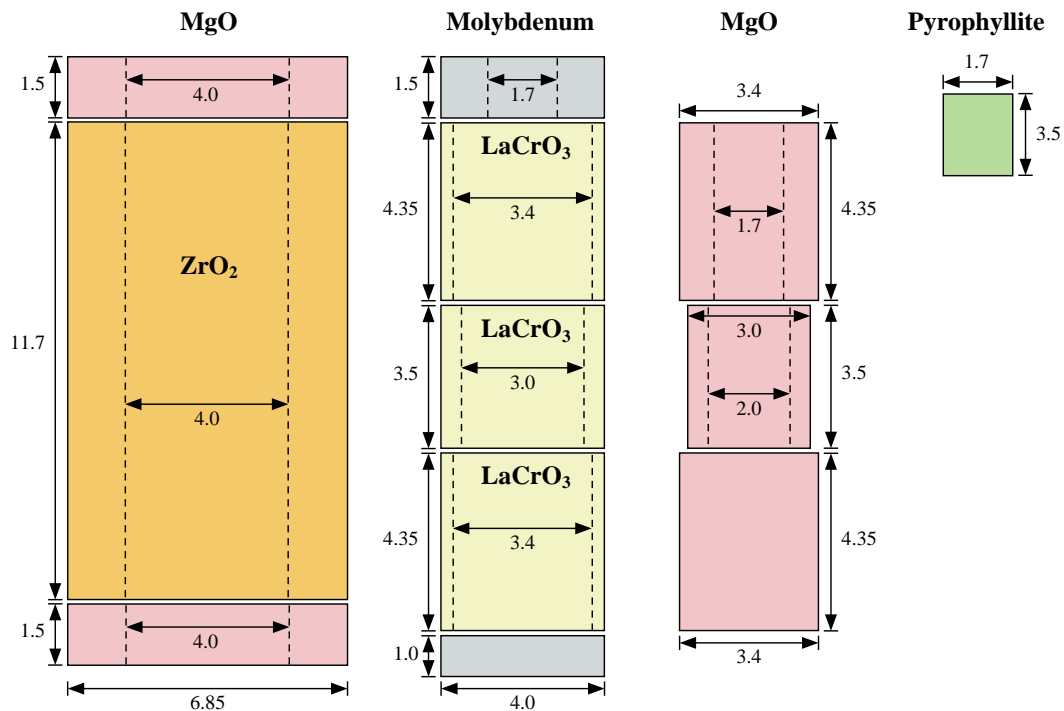
Fig. 2.8: Detailed diagramm of the interior parts of the pressure cell used in experiments above 10.5 GPa (18M, with W-Re thermocouple). For 14M assemblies the same basic setup was used but scaled down to fit the 8.0 mm truncated edge-length on the tungsten carbide cubes. Distances are given in millimeters.

2.2.2. Belt apparatus

Experiments from 3.0 to 5.0 GPa were performed in a belt apparatus (Fig. 2.9) at the Institut für Mineralogie, Universität Frankfurt, Germany (Fig. 2.10). Starting materials for all experiments were packed into 4.4 mm diameter Ag capsules with 0.5 mm thick walls and sealed with a friction-fitting lid. The two-capsule configuration described above was used in all belt experiments as well. A full description of the CaF_2-pressure assembly can be found in Brey et al. (1990) (Figs. 2.11, 2.12). Pressure and temperature calibrations have an accuracy of ± (1% nominal pressure + 0.05 GPa) and ± 7 °C (Brey et al. 1990).

The sluggishness of reaction in this system made it necessary to increase the run times significantly in order to obtain homogeneous run products. The experiments had a duration of 44-97 h in the belt apparatus and 12-37 h in the multi-anvil press. Due to the impracticalities of controlling the fO_2 in the experiments, we relied on a closed system approach, whereby the bulk $Fe^{3+}/\Sigma Fe$ was fixed by stoichiometric proportions of magnetite and olivine$_{ss}$. This approach has proven successful in previous studies involving Fe in multiple valence states (e.g. Woodland & O'Neill 1993; Woodland & Angel 2000). Some experiments in the early stages of this study produced extensive pyroxene, indicating oxidation during the experiment. This problem was successfully minimised by packing fine-grained Fe-powder around the outside of the capsules to serve an "oxygen-getter" during the experiment (see Fig. 2.4).

Experiments are labeled according to the composition and mixture of their starting material as well as which press was used for the experiment. For example "4f8b1200" would be a mixture of 40% olivine (with X_{fa} = 0.8) and 60% magnetite run in the belt apparatus ("b") as successive experiment number 1200 ("h" stands for the Hymag press, "z" for the Zwick press and "v"or the Voggenreiter press all located at the BGI in Bayreuth).
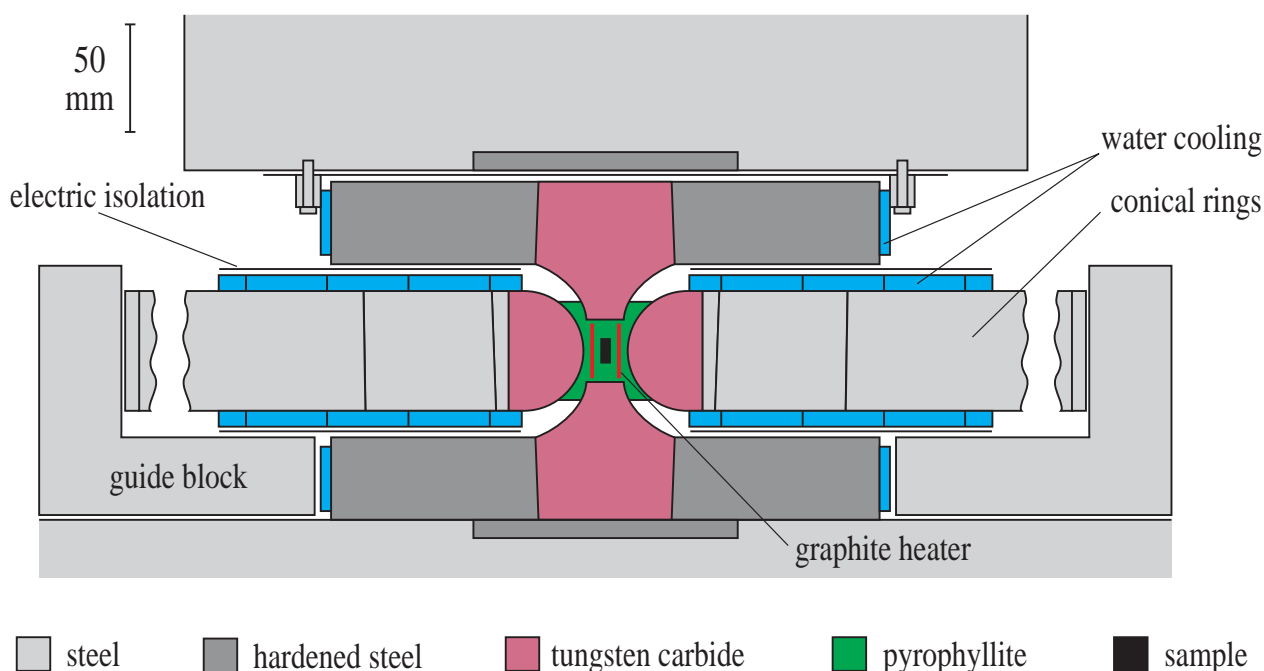
Fig. 2.9: Schematic drawing of the belt apparatus setup.

Fig. 2.10: Belt lab at the Institut für Mineralogie, Frankfurt. This belt-type press consists of a smaller 300 t press to the left and a bigger 500 t press to the right which can be independantly run. Newest feature is a spindle (atop) to make pressurizing much smoother on the 300 t press.
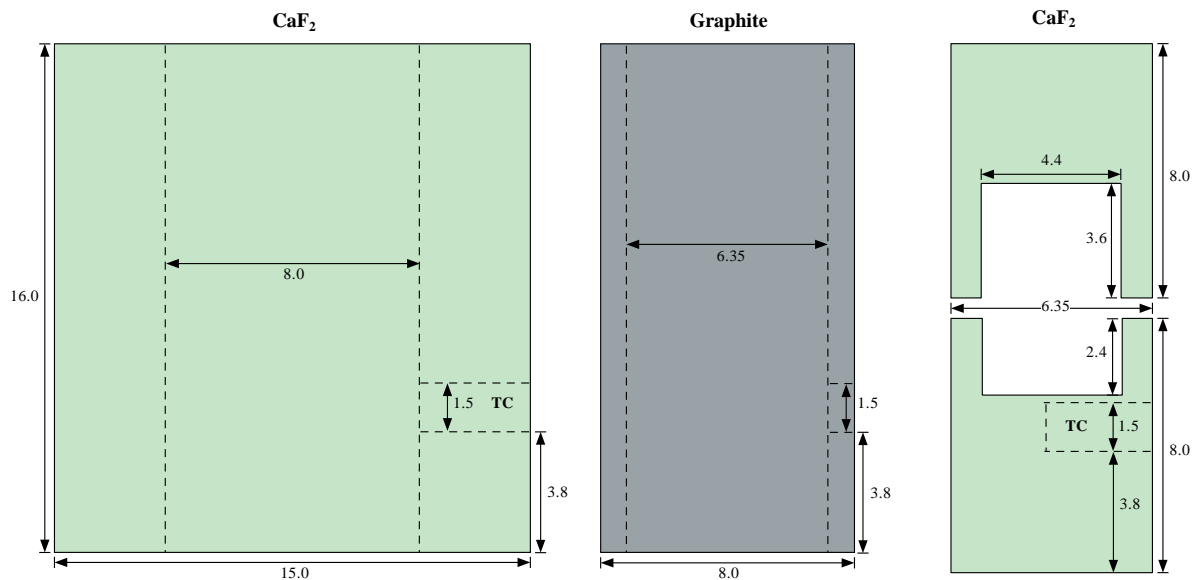
Fig. 2.11: Detailed diagramm of the interior parts of the pressure cell used in all belt apparatus experiments. Distances are given in millimeters. TC stands for thermocouple and indicates where the alumina rod is being placed within the setup (compare Fig. 2.12).
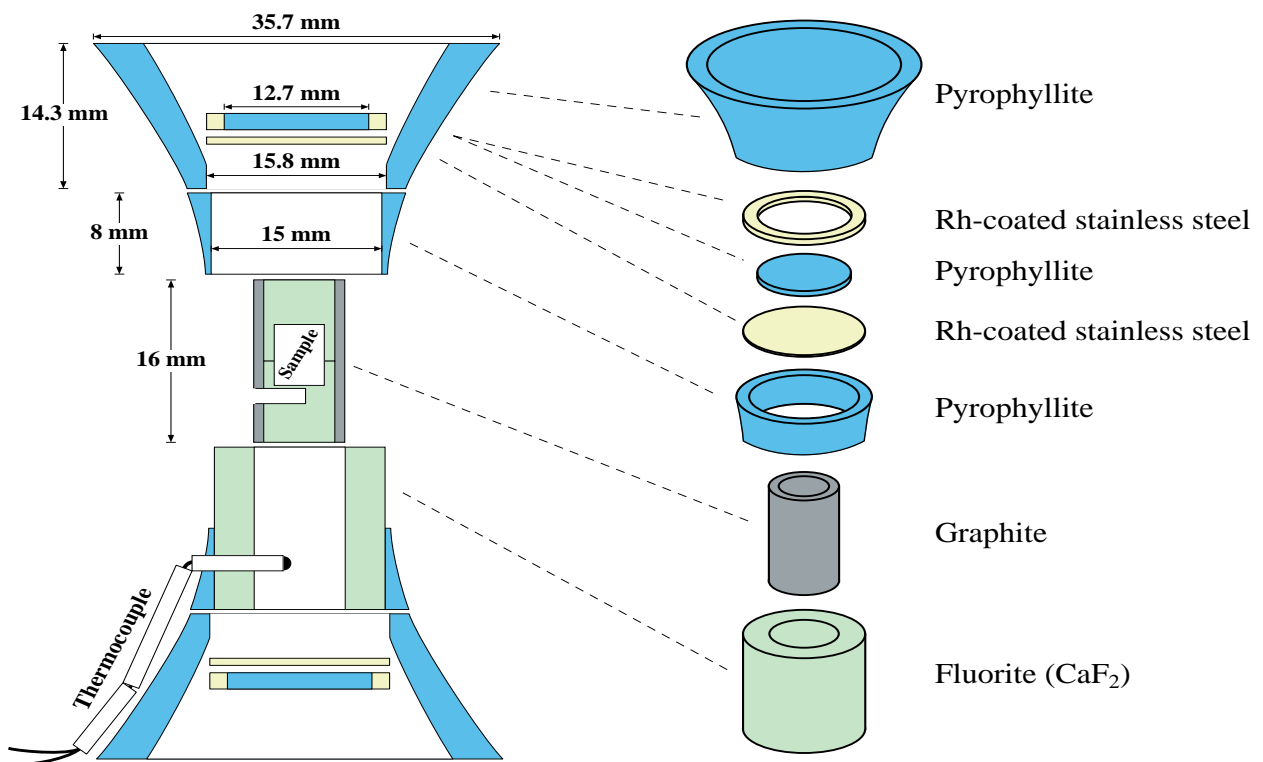
Fig. 2.12: Detailed diagramm of the furnace assembly used in belt apparatus experiments.

3. Analytical Methods

3.1. Electron microprobe and scanning electron microscope

The chemical composition of the experimental products were determined by an electron microprobe (Cameca SX-51) equipped with five wavelength-dispersive spectrometers (Fig. 3.1). Operating conditions were 20 nA beam current and 15 kV accelerating voltage with a beam diameter of about 1 μm and 20 s counting times on the peak and background. Wollastonite, Fe_2O_3 and MgO were used as standards for Si, Fe and Mg, respectively. The raw counts were recalculated using the PAP correction procedure (Pouchou & Pichoir 1985) supplied by Cameca. The composition of the phases encountered in the ternary system were calculated assuming an ideal stoichiometry based on four oxygens per formula unit and charge balance (see Appendix 9.1).

High resolution back-scattered electron (BSE) images were obtained from a LEO 440 scanning electron microscope, equipped with an Oxford semiconductor detector using an accelerating voltage of 20 kV and a beam current in the range of 1.5 to 4.7 nA. This imaging was used to provide detailed textural information which is important in assessing the stable coexistence of phases and identifying relict starting materials.

Further technical details on these two electron beam techniques can be found in Gill (1997).

Fig. 3.1: Electron microprobe lab at the Mineralogisches Institut, Heidelberg.

3.2. X-Ray powder diffraction

Phase identification of all experimental products was performed by X-ray powder diffraction (e.g. Krischner & Koppelhuber-Bitschnau 1994). Diffraction patterns from 30 to 120° 2Θ were collected on a STOE STADI-P diffractometer with monochromatic Co K_{α_1} radiation and a small-aperture linear PSD (Fig. 3.2).

Fig. 3.2: Experimental setup of a STOE XRD measurement at the Bayerisches Geoinstitut, Bayreuth. From right to left: Co X-ray source, monochromator and slits, rotating sample, beamstop and detector.

Operating conditions were 40 kV and 30 mA with counting times of 60 s per 0.5° step. Si metal (NBS 640) was added to each sample as an internal standard and the 2Θ scale was corrected, with the software package provided by STOE, by using the Si peak positions calculated for a = 5.4309 Å. The corrections to 2Θ, which never amounted to more than 0.10° 2Θ, account for diffractometer aberrations, specimen displacement and absorption, and inhomogeneities and variations in the detector calibration. Unit-cell parameters of the run product phases were then determined from the corrected patterns by full-pattern Rietveld refinements with the GSAS software package (Larson & von Dreele 1988) driven with the EXPGUI interface (Toby 2001) in which the structural parameters of each phase were held constant and the scale, unit-cell parameters and profile parameters of each phase, plus sufficient background terms, were refined. The atomic occupancies of the different sites were fixed from the composition as determined by microprobe analysis with the assumption that only Fe^{3+} and Si are

present on tetrahedral sites. Where necessary the peak cut-off values were adjusted to produce a better overall fit to regions with extensive peak overlapping. The goodness of fit of the diffraction patterns is reflected by the magnitude of the uncertainties (esd) obtained for each of the refined structural parameters, which are generally on the order of 0.0001-0.0004 Å.

4. Results

4.1. Chemical data

4.1.1. Phase relations

The coexisting phases produced in all experiments are summarized in Table 4.1, as are the compositions of spinel, spinelloid and olivine. The construction of the phase diagrams presented here as a function of pressure relied not only on chemical analyses, but also on X-ray diffraction for phase identification. In the course of this project it turned out that spinels in some run products have Si < Mg/2, indicating a decoupling of Mg from Si and implying the presence of a Mg-ferrite component (see Fig. 4.1). Therefore, the phase relations are presented in the four-component system Mg_2SiO_4–Fe_2SiO_4–Fe_3O_4–$MgFe_2O_4$. Note that in the following discussion, the term Mg-ferrite is used to distinguish those spinels that contain this component, even if magnetite is the dominant component present.

At low pressures of 3.0 to 3.5 GPa, olivine coexists with a spinel that usually incorporates more Si than Mg. However, in very Mg-rich compositions (i.e. olivine with $X_{fo} > 0.70$) the opposite chemical behaviour is observed with the spinel sometimes containing a considerable Mg-ferrite component (Fig. 4.1). Since it is not known if Mg-ferrite incorporates any Si the phase boundary terminates short of the Mg-ferrite component corner (Fig. 4.1).
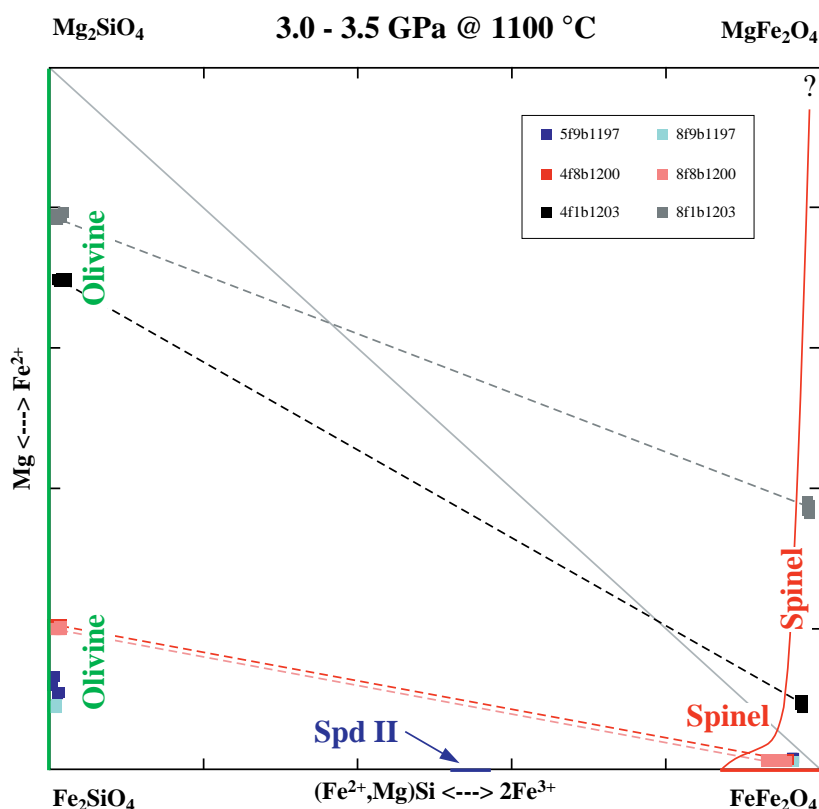
Fig. 4.1: Phase relations in the system Mg_2SiO_4–Fe_2SiO_4–Fe_3O_4–$MgFe_2O_4$ at 1100 °C and 3.0-3.5 GPa. Dashed lines connect phases that are in local equilibrium; if there is no dashed line drawn, as for the two blue experiments, the phases are, on textural grounds, not in equilibrium. The thin grey diagonal line represents compositions with Si = Mg/2. Spinels plotting above this line have Si < Mg/2, which implies a Mg-ferrite component. Coloured solid lines indicate stability fields and incorporate data from the literature for the Fe_2SiO_4–Fe_3O_4 and Mg_2SiO_4–Fe_2SiO_4 binary subsystems from Woodland and Angel (2000) and Fei et al. (1991), respectively (lines along the eges of the diagram).

Table 4.1: Results of all experiments performed at 1100 and 1200 °C.

Experimen	T [°C]	P [GPa]	t [h]	Stable phases present *	sp nSi#	nMg	nFe^{2+}	nFe^{3+}	spd nSi	nMg	nFe^{2+}	nFe^{3+}	ol X$_{fo}$
5f9b1197	1100	3.0	88.0	isc + (ol + sp)									0.11
8f9b1197	1100	3.0	88.0	ol + isc + (sp)									0.09
4f8b1200	1100	3.0	68.8	sp + ol + (isc)	0.06	0.02	1.05	1.87					0.20
8f8b1200	1100	3.0	68.8	ol + sp	0.06	0.02	1.04	1.88					0.20
4f1b1203	1100	3.5	70.0	Mg-ferrite + ol	0.02	0.12	0.91	1.95					0.70
8f1b1203	1100	3.5	70.0	ol + Mg-ferrite	0.01	0.38	0.64	1.97					0.79
4f8b0271	1100	4.0	44.0	sp + spd II + ol	0.12	0.04	1.08	1.76	0.42	0.10	1.32	1.16	0.28
8f8b0271	1100	4.0	44.0	ol + spd II + (opx + sp)					0.47	0.03	1.44	1.06	0.08
4f5b0272	1100	4.0	44.0	ol + sp	0.06	0.12	0.95	1.87					0.46
8f5b0272	1100	4.0	44.0	ol + Mg-ferrite	0.05	0.12	0.92	1.91					0.47
5f9b1196	1100	4.0	70.5	spd II + ol + (sp)					0.43	0.07	1.35	1.15	0.19
8f9b1196	1100	4.0	70.5	spd II + ol + (opx)					0.46	0.04	1.42	1.08	0.12
4f5b1180	1100	5.0	92.0	sp + ol	0.07	0.06	0.98	1.89					0.49
8f5b1180	1100	5.0	92.0	ol + sp + (opx)	0.07	0.06	1.01	1.86					0.49
5f9b1194	1100	5.0	68.0	spd II + isc + (ol)					0.45	0.06	1.40	1.09	0.17
8f9b1194	1100	5.0	68.0	spd II + ol + (isc)					0.48	0.04	1.44	1.04	0.11
4f8b1195	1100	5.0	97.0	spd II + (sp + ol)					0.43	0.09	1.34	1.14	0.25
8f8b1195	1100	5.0	97.0	spd II + ol + (sp)					0.44	0.08	1.37	1.11	0.21
4f1b1199	1100	5.0	68.0	Mg-ferrite + ol	0.02	0.13	0.89	1.96					0.76
8f1b1199	1100	5.0	68.0	ol + Mg-ferrite	0.01	0.19	0.83	1.97					0.83
3f5h1360	1100	6.0	35.7	sp + ol + (Mg-ferrite)	0.11	0.07	1.03	1.79					0.51
8f5h1360	1100	6.0	35.7	ol + sp	0.13	0.07	1.06	1.74					0.49
4f8v0095	1100	6.0	33.6	spd II + (sp + ol)					0.45	0.17	1.27	1.11	0.41
8f8v0095	1100	6.0	33.6	spd III + ol + (opx)					0.54	0.11	1.42	0.93	0.25
3f8v0082	1100	6.5	34.2	sp + (opx)	0.13	0.04	1.09	1.74					
8f8v0082	1100	6.5	34.2	spd III + ol + opx + (spd V + sp)					0.54	0.12	1.42	0.92	0.27
4f5v0094	1100	6.5	34.3	sp + ol + (opx)	0.16	0.10	1.06	1.68					0.55
8f5v0094	1100	6.5	34.3	ol + spd V + sp + (opx)	0.18	0.10	1.09	1.63	0.41	0.19	1.21	1.19	0.53
4f8v0126	1100	6.5	34.0	spd V + (sp)					0.42	0.16	1.26	1.16	
8f8v0126	1100	6.5	34.0	spd III + ol + opx + (spd V + sp)					0.63	0.15	1.48	0.74	0.29
3f5h1136	1200	7.0	12.7	sp + opx	0.09	0.14	0.94	1.83					
8f5h1136	1200	7.0	12.7	ol + spd II + sp + opx	0.15	0.10	1.05	1.70	0.45	0.26	1.18	1.11	0.54
3f8h1137	1200	7.0	12.3	sp + opx	0.15	0.05	1.10	1.70					
8f8h1137	1200	7.0	12.3	spd III + opx + (spd V + ol + sp)					0.66	0.20	1.46	0.68	0.34
4f8v0083	1100	7.0	34.5	spd V + sp + (opx)	0.17	0.07	1.10	1.66	0.41	0.14	1.27	1.18	
8f8v0083	1100	7.0	34.5	spd III + ol + (opx + sp + spd V)					0.64	0.16	1.47	0.73	0.30
4f5v0084	1100	7.0	34.0	sp + ol + (opx)	0.15	0.12	1.04	1.69					0.60
8f5v0084	1100	7.0	34.0	ol + spd V + (opx + sp)					0.41	0.21	1.21	1.17	0.55
4f1v0097	1100	7.0	33.7	ol + Mg-ferrite	0.06	0.19	0.87	1.88					0.79
8f1v0097	1100	7.0	33.7	ol + Mg-ferrite	0.04	0.23	0.81	1.92					0.84
4f3v0130	1100	7.0	34.3	ol + Mg-ferrite	0.08	0.21	0.86	1.85					0.65
8f3v0130	1100	7.0	34.3	ol + Mg-ferrite + (opx)	0.07	0.21	0.86	1.86					0.63
5f9v0180	1100	7.0	34.5	spd V + (opx + sp)					0.45	0.08	1.36	1.11	
8f9v0180	1100	7.0	34.5	spd III + opx + (spd V + sp)					0.66	0.11	1.55	0.68	
4f5v0096	1100	7.5	34.5	sp + ol + (opx)	0.15	0.13	1.03	1.69					0.64
5f5v0096	1100	7.5	34.5	sp + ol + (opx)	0.15	0.13	1.00	1.72					0.65
8f5v0128	1100	7.5	33.0	ol + spd III + (opx + sp)					0.53	0.31	1.22	0.94	0.58
8f8v0128	1100	7.5	33.0	spd V + (opx + sp)					0.73	0.27	1.48	0.52	
4f8v0080	1100	8.0	33.3	spd V + sp	0.23	0.07	1.15	1.55	0.48	0.16	1.31	1.05	
8f8v0080	1100	8.0	33.3	spd V + ol + Si-sp + (sp)	0.95	0.25	1.69	0.11	0.70	0.21	1.50	0.59	0.64
4f5v0081	1100	8.0	32.7	sp + ol + spd V + (cpx)	0.18	0.13	1.06	1.63	0.45	0.28	1.18	1.09	0.59
8f5v0081	1100	8.0	32.7	ol + spd V + (cpx)					0.52	0.28	1.24	0.96	0.38
5f8v0125	1100	8.0	34.0	spd V + sp	0.28	0.10	1.18	1.44	0.49	0.19	1.30	1.02	
9f8v0125	1100	8.0	34.0	Si-sp + (Mg-ferrite)	0.93	0.35	1.58	0.14					
4f3v0182	1100	8.0	33.5	Mg-ferrite + ol + (sp)	0.11	0.23	0.87	1.79					0.66
8f3v0182	1100	8.0	33.5	ol + Mg-ferrite	0.10	0.20	0.89	1.81					0.63

Table 4.1: Continued.

Experimen	T [°C]	P [GPa]	t [h]	Stable phases present *	sp nSi#	nMg	nFe^{2+}	nFe^{3+}	spd nSi	nMg	nFe^{2+}	nFe^{3+}	ol X$_{fo}$
5f9v0231	1100	8.0	32.9	spd V + (sp + cpx)					0.52	0.08	1.44	0.96	
8f9v0231	1100	8.0	32.9	Si-sp + spd V + (sp)	0.87	0.15	1.71	0.27	0.58	0.11	1.48	0.83	
3f5h0998	1100	9.0	12.5	sp + cpx	0.10	0.14	0.96	1.80					
8f5h0998	1100	9.0	12.5	ol + spd V + cpx + ? + (Mg-ferrite)					0.57	0.34	1.23	0.86	0.62
4f8v0053	1100	9.0	36.7	sp + (cpx)	0.25	0.06	1.20	1.49					
8f8v0053	1100	9.0	36.7	Si-sp + (Mg-ferrite + cpx + ?)	0.73	0.22	1.50	0.55					
4f1v0098	1100	9.0	34.3	Mg-ferrite + ol + (cpx)	0.06	0.26	0.80	1.88					0.88
8f1v0098	1100	9.0	34.3	ol + Mg-ferrite	0.08	0.26	0.81	1.85					0.88
5f8v0099	1100	9.0	33.3	sp + (cpx)	0.30	0.08	1.22	1.40					
9f8v0099	1100	9.0	33.3	Si-sp + spd V + (cpx)	0.91	0.32	1.59	0.18	0.66	0.25	1.41	0.68	
5f8v0124	1100	9.0	23.6	spd V + sp	0.40	0.13	1.27	1.20	0.55	0.23	1.32	0.90	
9f8v0124	1100	9.0	23.6	Si-sp + (sp)	0.93	0.35	1.59	0.13					
4f5v0129	1100	9.0	32.0	spd V + Mg-ferrite + cpx + ?	0.00	0.13	0.87	2.00	0.52	0.43	1.09	0.96	
6f5v0129	1100	9.0	32.0	spd V + ol + (Mg-ferrite)					0.76	0.56	1.20	0.48	0.68
4f3v0131	1100	9.0	34.0	spd V + ol + Mg-ferrite + ?	0.00	0.14	0.86	2.00	0.54	0.45	1.09	0.92	0.72
8f3v0131	1100	9.0	34.0	ol + (spd V + Mg-ferrite)									0.66
5f9v0181	1100	9.0	33.7	spd V + sp	0.37	0.06	1.30	1.27	0.51	0.10	1.41	0.98	
8f9v0181	1100	9.0	33.7	spd V + Si-sp	0.85	0.15	1.70	0.30	0.67	0.14	1.54	0.66	
4f5v0055	1100	10.5	37.3	Mg-ferrite + cpx + (sp)	0.00	0.10	0.90	2.00					
8f5v0055	1100	10.5	37.3	Si-sp + (cpx + Mg-ferrite)	0.99	0.96	1.03	0.02					
4f8v0085	1100	10.5	34.0	sp + (cpx + Mg-ferrite)	0.34	0.11	1.22	1.33					
8f8v0085	1100	10.5	34.0	Si-sp + (cpx + Mg-ferrite)	0.82	0.29	1.53	0.36					
5f5v0100	1100	10.5	33.7	Mg-ferrite + ? + (cpx)	0.00	0.13	0.88	1.99					
8f5v0100	1100	10.5	33.7	Si-sp + (Mg-ferrite + cpx + ?)	0.90	0.88	1.02	0.20					
4f1v0127	1100	10.5	34.3	Mg-ferrite + ol + ? + (cpx)	0.00	0.32	0.68	2.00					0.91
8f1v0127	1100	10.5	34.3	ol + Mg-ferrite + ? + (cpx)	0.00	0.29	0.72	1.99					0.90
5f9v0232	1100	10.5	32.5	sp + ? + (Mg-ferrite)	0.56	0.11	1.44	0.89					
9f8v0232	1100	10.5	32.5	Si-sp + (? + Mg-ferrite)	0.94	0.35	1.58	0.13					
4f1v0233	1100	12.0	32.9	? + Mg-ferrite + wads + (cpx)	0.00	0.27	0.74	1.99	0.97	1.44	0.53	0.06	
8f1v0238	1100	12.0	32.8	wads + ? + Mg-ferrite	0.00	0.36	0.64	2.00	0.98	1.63	0.35	0.04	
4f5z0133	1100	14.0	29.5	Mg-ferrite + cpx + (?)	0.00	0.13	0.88	1.99					
8f5z0133	1100	14.0	29.5	Si-sp + cpx + (? + Mg-ferrite)	0.98	0.95	1.04	0.03					
4f1h1645	1100	14.0	33.5	? + wads + Mg-ferrite + (cpx)	0.01	0.28	0.72	1.99	0.99	1.64	0.35	0.02	
8f1h1646	1100	14.0	34.7	wads + ? + Mg-ferrite + (cpx)	0.00	0.37	0.64	1.99	0.98	1.65	0.34	0.03	
4f1h1844	1100	16.0	32.8	? + cpx + Mg-ferrite	0.01	0.23	0.77	1.99					
8f1h1845	1100	16.0	31.6	ringw + ? + (Mg-ferrite)	0.99	1.66	0.34	0.01					

* Stable phases produced are listed in the order of abundance, minor phases in parentheses. $^{\#}$ n = number of Si, Mg, Fe^{2+} and Fe^{3+} cations per formula unit based upon 4 oxygens and assuming perfect stoichiometry. sp denotes a mt-rich spinel; Mg-ferrite a mt-rich spinel but with Si < Mg/2; isc = iscorite; ol = olivine; Si-sp = silica-spinel; ringw = ringwoodite; spd = spinelloid; II, III & V denote the spinelloid polytypes; X$_{fo}$ = X$_{Mg_2SiO_4}$ in olivine; ? = unknown phase.

The pressure at which an intermediate phase first appears significantly increases in the presence of Mg. Spinelloid II, which is stable at 2.6 GPa in the Mg-free system (Fig. 1.6), first becomes stable at 4.0 GPa, even though it only contains a maximum of ~5 mol % Mg$_2$SiO$_4$ component (Fig. 4.2). Between 4.0 and 5.0 GPa, Spinelloid II has a limited compositional range of X$_{Fe_3O_4}$ = 0.50 to 0.59, which is similar in extent to the width of the stability field of Mg-free spinelloid II portrayed in Figure 1.6. Depending on composition, spinelloid II can coexist with either olivine, a Si-bearing magnetite-rich spinel or both. In Mg-rich bulk compositions that crystallised olivine with X$_{fo}$ > 0.46, spinelloid II is no longer stable and olivine coexists with a magnetite-rich spinel (Fig. 4.2). The Si content of spinel decreases with progressive incorporation of Mg. In extrem Mg-rich bulk compositions, olivine coexists with a magnetite-rich spinel (Mg-ferrite) that incorporates more Mg than Si (Figs. 4.2, 4.3).

Fig. 4.2: Phase relations at 1100 °C and pressures between 4.0-5.0 GPa. In this pressure range spinelloid II is the only stable intermediate phase.

Fig. 4.3: Sample 8f1b1199 shows coexisting Mg-ferrite (white) and olivine (grey) as the main mass, with some darker spots that are relicts from the starting material synthesis that have not reacted with or affected the run products in any way.

A very well crystallized experiment with a run time of 97 hours at pressure and temperature is illustrated in Figure 4.4, showing mainly spinelloid II with minor amounts of starting materials remaining.
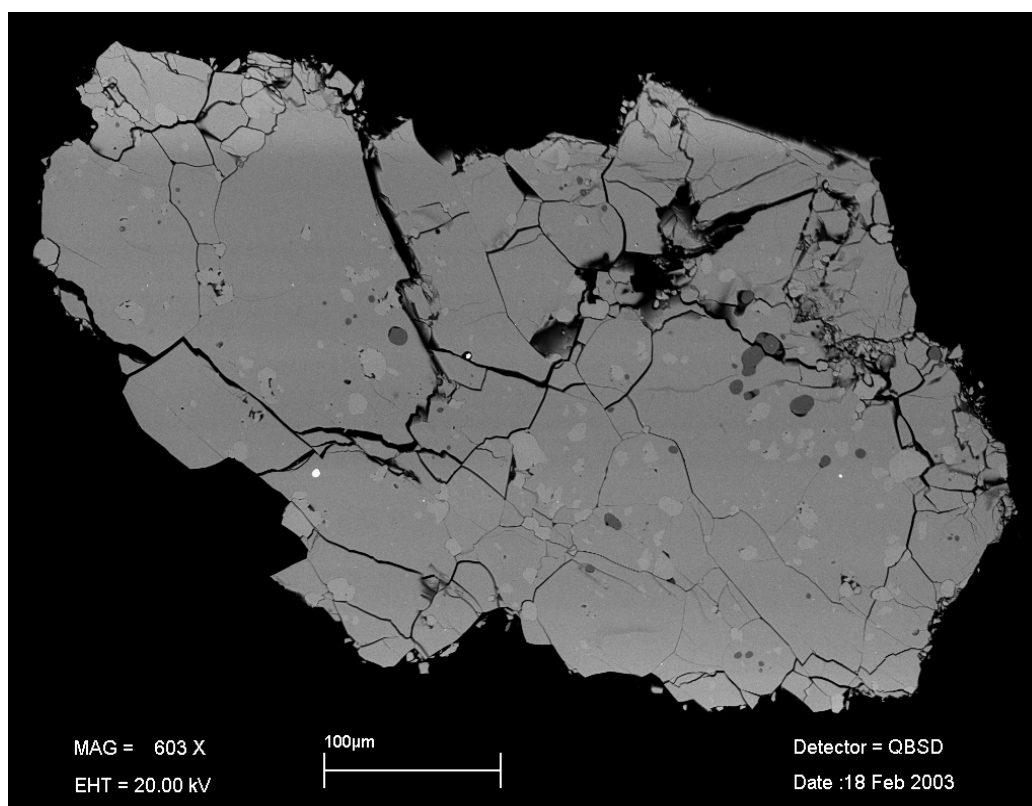
Fig. 4.4: Sample 4f8b1195 showing spinelloid II (grey) as the main mass with some typical darker (olivine) and lighter (magnetite) spots that are remnants of the starting materials.

Spinelloid III first appears at 6.0 GPa in the Mg-bearing system. As with spinelloid II, the stability field of spinelloid III is shifted upwards by ~2.0 GPa due to the incorporation of only small amounts of Mg (compare Figs. 4.5, 1.6). Spinelloid III is always richer in Si than the coexisiting spinelloid II. Between 6.0 and 6.5 GPa spinelloid II is effectively replaced by spinelloid V, emphasising the polytypic nature of these two phases (Fig. 4.6). This isochemical change in the spinelloid structure can also be observed very well in the Mg-free system (Fig. 1.6), but again at pressures that are about 2.0 GPa lower (Woodland & Angel 2000). However, spinelloid II was also produced in a reconnaissance experiment at 7.0 GPa and 1200 °C (8f5h1136) demonstrating that an increase in temperature can stabilise the individual intermediate phases to even higher pressures (Fig. 4.7, also compare Table 4.1). This phenomenon was also observed in the Mg-free system (Woodland & Angel 2000) where experiments performed at 900 °C only produced the spinelloid V polytype, whereas at higher temperatures all three polymorphs are stable. Depending on pressure, spinelloid III can coexist with either spinelloid II or spinelloid V along with olivine. Spinelloid III can accomodate up to 0.94 cations per formula unit (c.p.f.u.) Fe^{3+}, but is always poorer in Fe^{3+} compared to either coexisting polytype. Figure 4.8 shows a BSE image of sample 8f8v0095 that produced spinelloid III coexisting with olivine and orthopyroxene (compare Fig. 4.5).
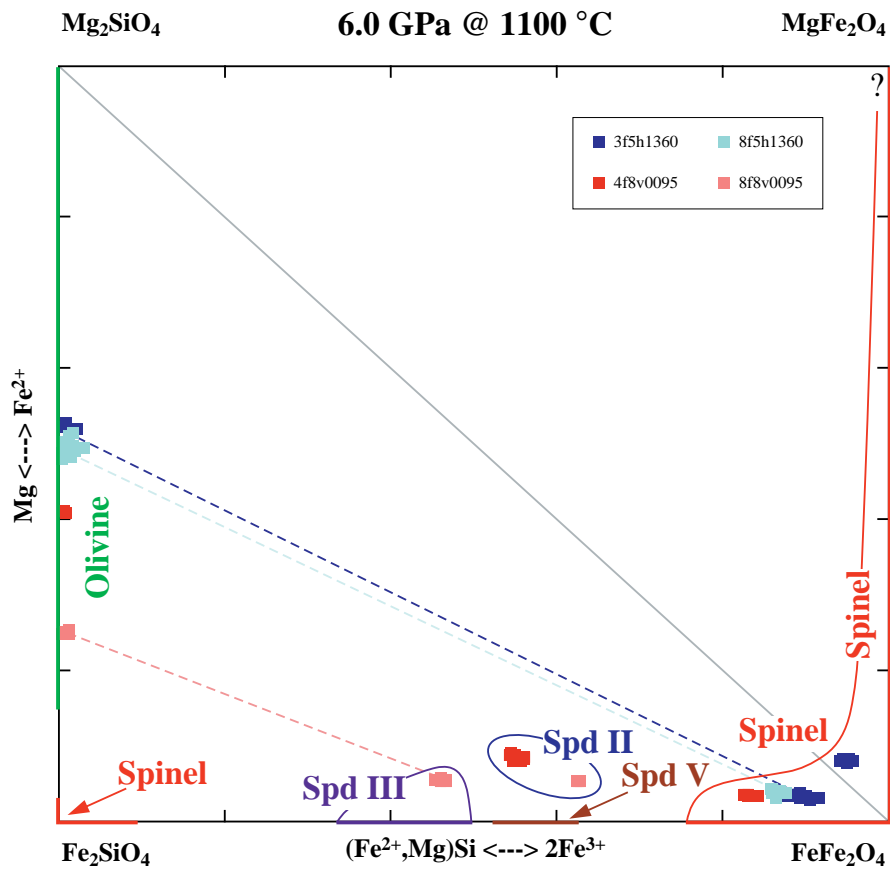
Fig. 4.5: Phase relations at 1100 °C and 6.0 GPa. First appearance of spinelloid III together with spinelloid II. Spinelloid III is always more Si-rich than any other intermediate phase at these pressures.
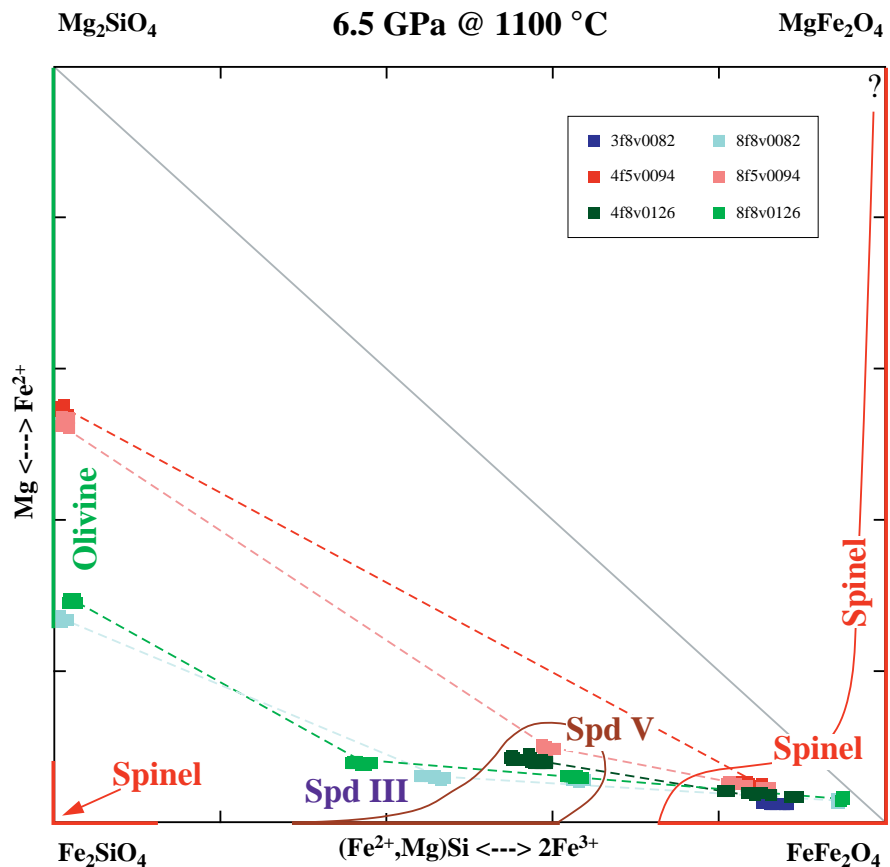
Fig. 4.6: Phase relations at 1100 °C and 6.5 GPa. Spinelloid V replaces the isochemical polytype II.
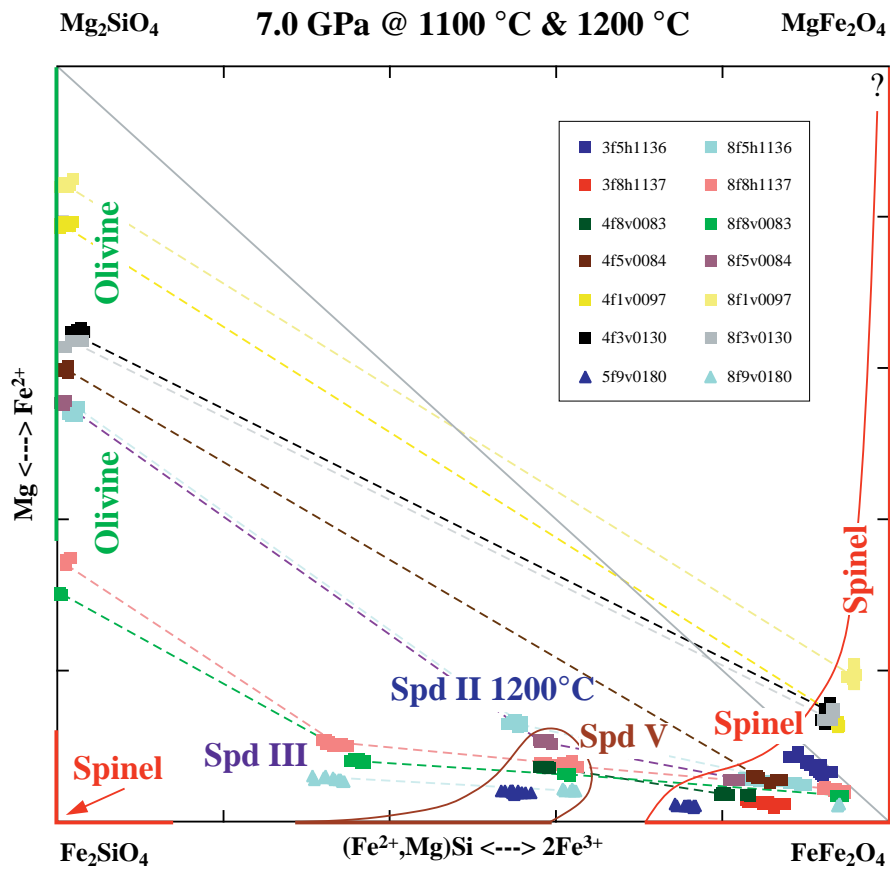
Fig. 4.7: Phase relations at 1100 to 1200 °C and 7.0 GPa. Spinelloid V coexists with spinelloid III. With increasing temperature, the stability of all intermediate phases shift to significantly higher pressures as illustrated here with spinelloid II.
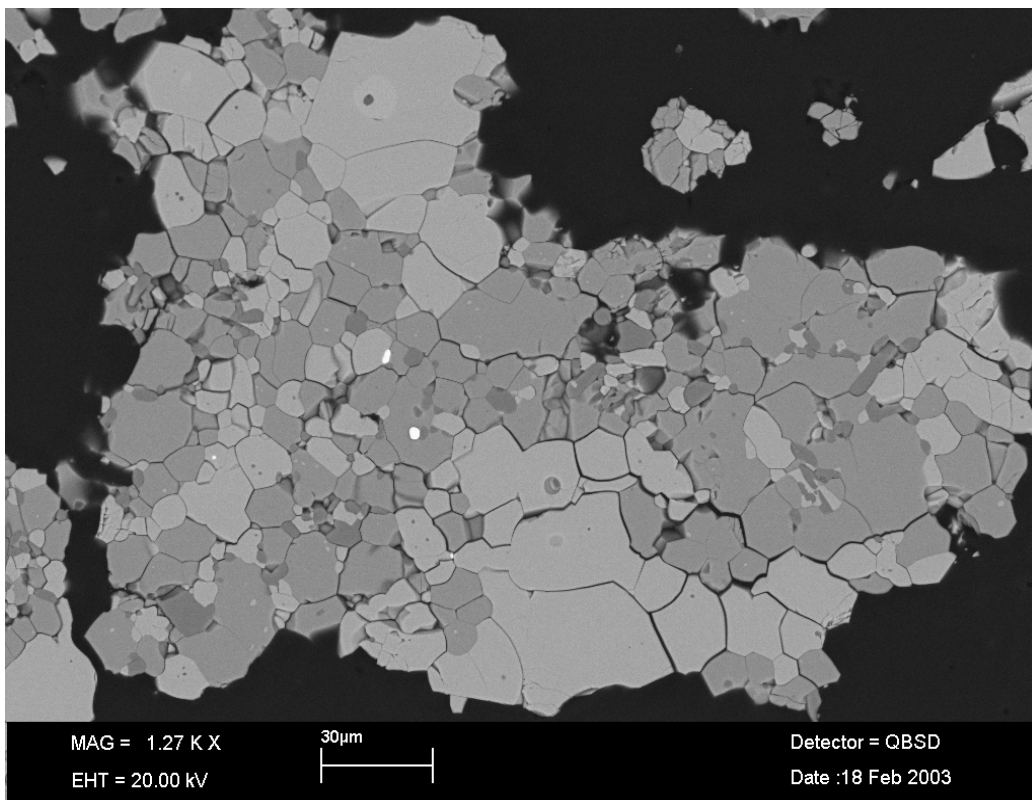
Fig. 4.8: Sample 8f8v0095 showing mainly spinelloid III (light) along with some larger quantities of olivine (grey). Associated with olivine are some dark grey grains that are orthopyroxene.

The stability field of spinelloid III is limited in P-T-composition space by the stability of the assemblage olivine + spinelloid V. At 7.5 GPa, the stability field of spinelloid III is compositionally limited by the stability field of spinelloid V (Fig. 4.9) in the same way as in the Mg-free system (Fig. 1.6) with increasing pressure (Woodland & Angel 2000). At 1100 °C, spinelloid III finally gives way to the assemblage olivine + spinelloid V between 7.5 and 8.0 GPa (Fig. 4.10). In terms of composition, the maximum Mg content of spinelloid III is limited to ~10 mol % Mg_2SiO_4 at 7.0 GPa, increasing to somewhat more than 15 mol % Mg_2SiO_4 at 7.5 GPa. This maximum Mg content is reached in a bulk composition where the olivine has a X_{fo} between 0.34 and 0.55 (Figs. 4.7, 4.9).
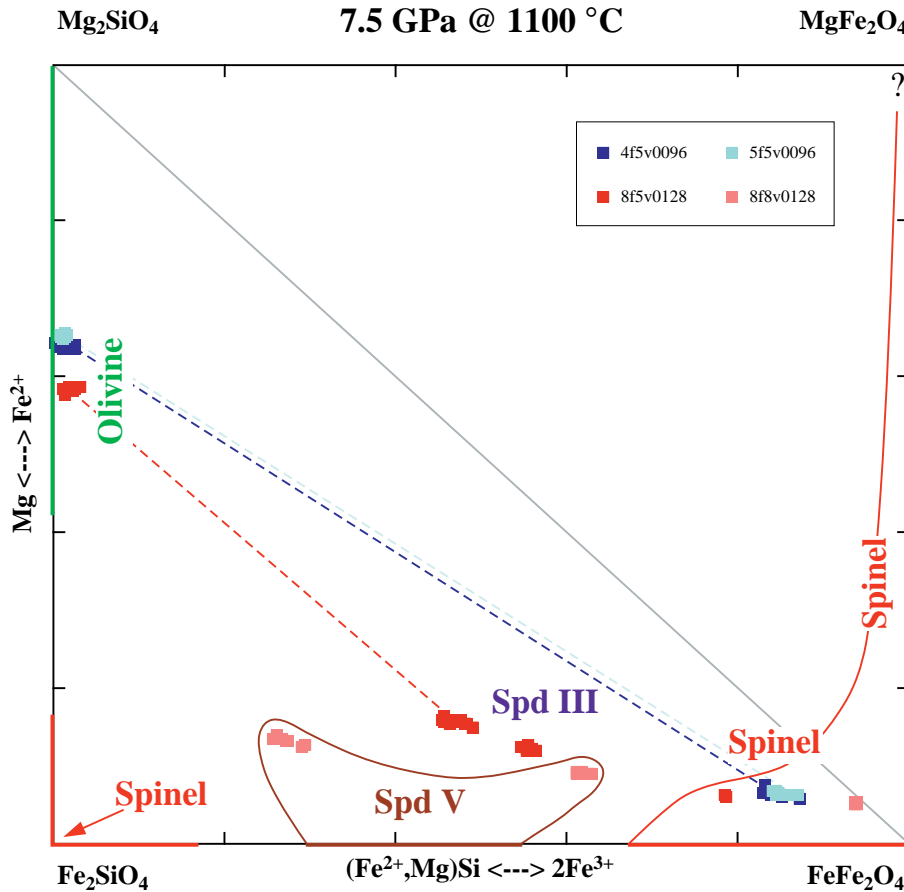
Fig. 4.9: Phase relations at 1100 °C and 7.5 GPa. Spinelloid III has nearly reached its upper pressure limit, while being compositionally limited by spinelloid V, which is the only stable intermediate phase at higher pressures.

At pressures ≥ 8.0 GPa, the only stable intermediate phase is spinelloid V, which spans a large compositional range from $X_{Fe_3O_4} = 0.25$ to 0.62 (Fig. 4.10). Si-spinel appears for the first time in the Mg-bearing system, whereas in the Mg-free and Fe^{3+}-free system Si-spinel is stable at much lower pressures of ~6.0 GPa (see Figs. 1.3, 1.6, 4.5, 4.10). In an analogous way to spinelloid III, the stability field of spinelloid V is limited in terms of Mg content by the appearance of another assemblage, olivine + spinel, which occurs when olivine has a composition of $X_{fo} > 0.58$ or > 0.75 at 7.0 GPa and 9.0 GPa, respectively (Figs. 4.7, 4.11). The maximum Mg content of spinelloid V also increases with pressure, reaching ~30 mol % Mg_2SiO_4 at 9.0 GPa (Fig. 4.11). At the same time, the stability field of spinelloid V is considerably reduced at low Mg contents by the increasing extent of solid solution between Fe_2SiO_4-spinel and magnetite, which can also contain minor amounts of Mg.
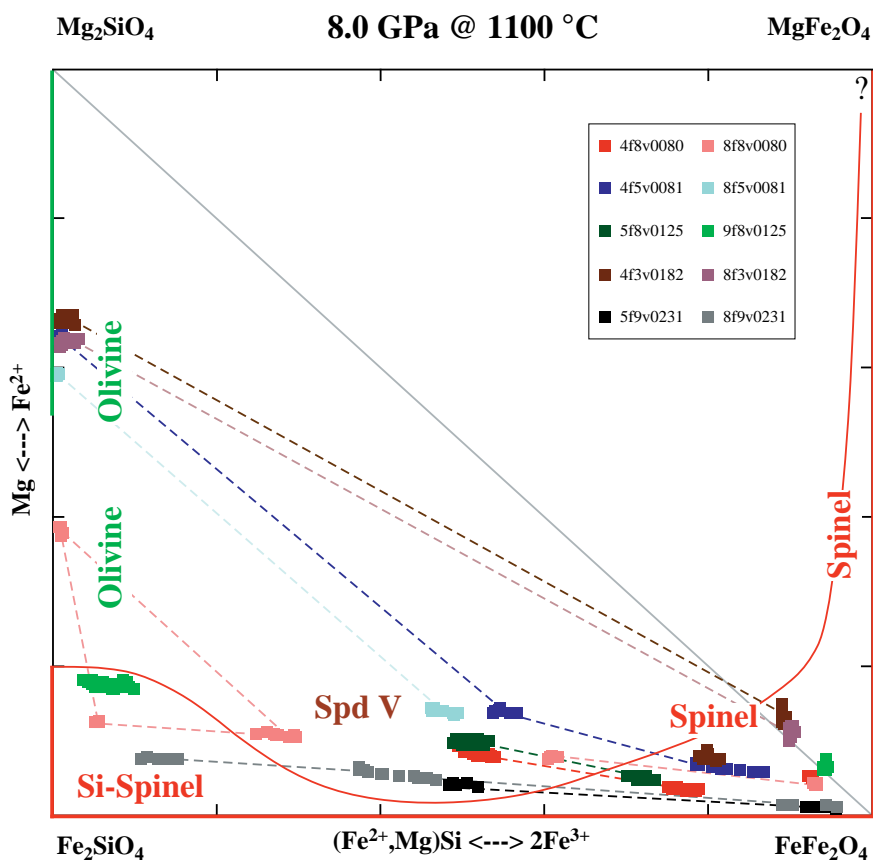
Fig. 4.10: Phase relations at 1100 °C and 8.0 GPa. Spinelloid V is the only stable intermediate phase. It has a very large compositional range, which is partially limited by the stability field of spinel solid solutions. The red solid line approximates the position of the narrow two-phase field between spinel solid solution and spinelloid V.
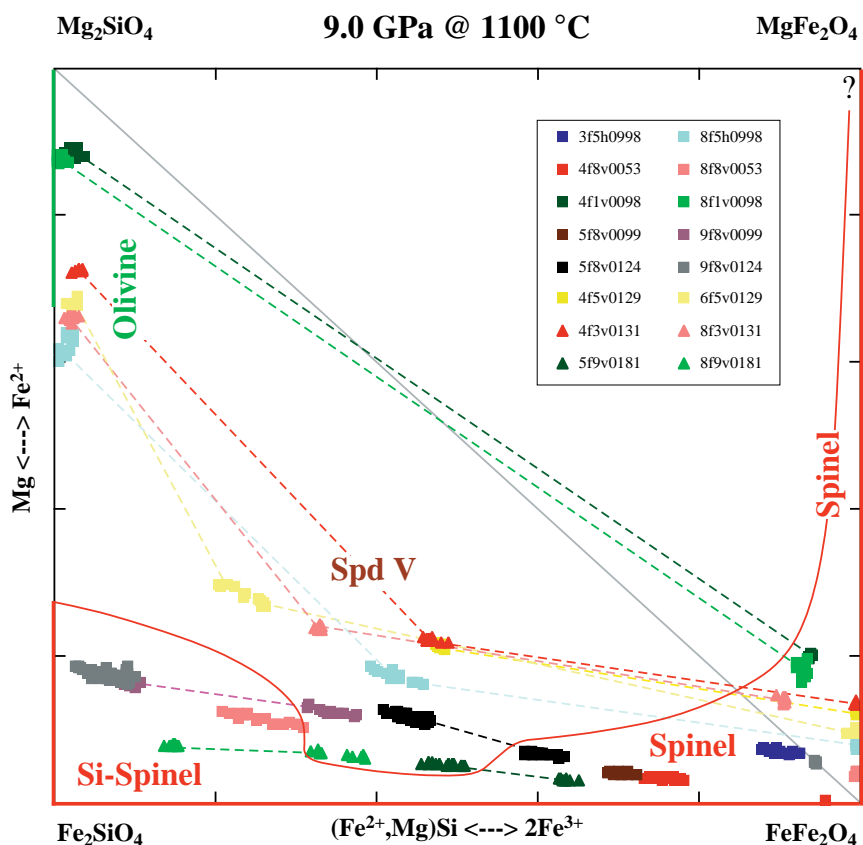
Fig. 4.11: Phase relations at 1100 °C and 9.0 GPa. At low Mg-content, the stability field of spinelloid V gets narrowed, whereas at higher Mg-content, it shifts to a more Si-rich composition.

A complete spinel solid solution is stable between Fe_3O_4 and Fe_2SiO_4 at P > 7.5 GPa (Fig. 1.6). At 9.0 GPa, the minimum Mg content of spinelloid V is 5 mol % Mg_2SiO_4. Thus, although spinelloid V, which is also illustrated in Figure 4.12, is stable over a fairly wide range of Fe^{3+}/Si ratio, the compositional range, in terms of Mg content, is rather limited (Figs. 4.10, 4.11). At low Mg contents the stability field of spinelloid V appears to terminate in an analogous fashion to that observed with respect to pressure in the Fe_3O_4–Fe_2SiO_4 system (compare Figs. 4.10, 4.11 with Fig. 1.6).

The phase boundary drawn along the Fe_3O_4–$MgFe_2O_4$ join is schematic in so much as the Si content of $MgFe_2O_4$-rich spinels is unknown, but assumed to be very minor. It has been shown by Andrault and Bolfan-Casanova (2001) that the Mg-ferrite endmember spinel does not undergo any phase transformation at least up to 25.0 GPa. Several two-phase fields must be present in Figures 4.10 and 4.11, separating the primary phase fields of spinel and the spinelloids. As these two-phase fields are expected to be extremely narrow (see Fig. 1.6) and their geometry is very poorly constrained, these fields have been omitted from the phase diagrams for the sake of clarity.
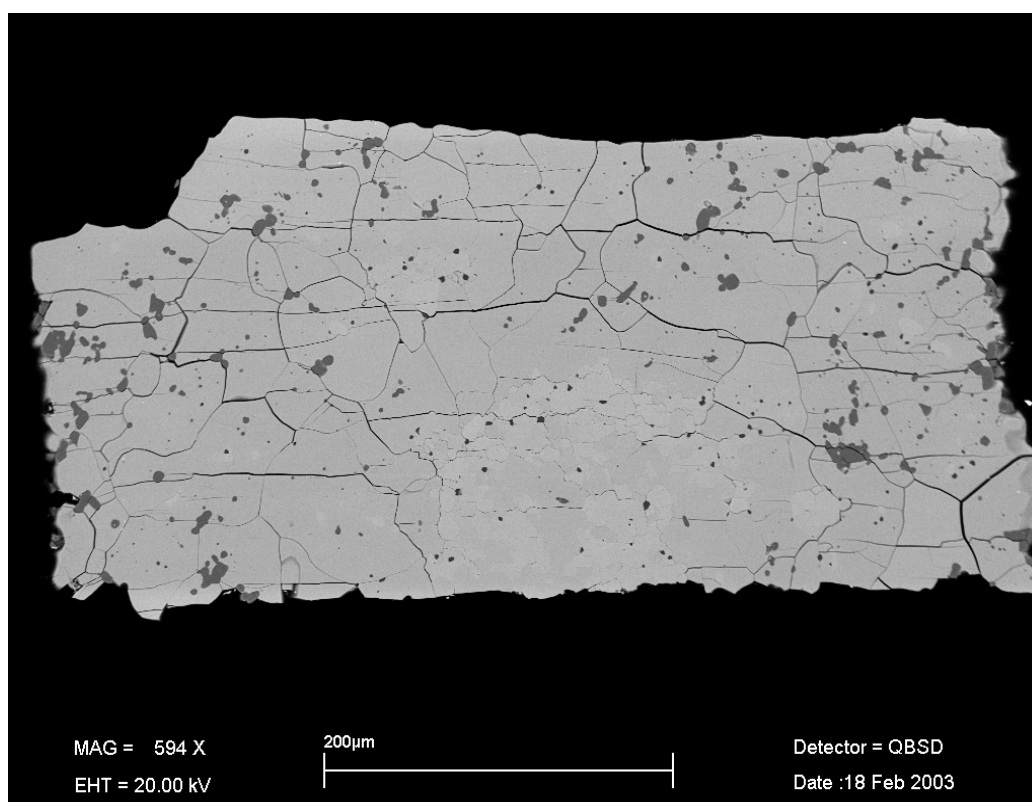
Fig. 4.12: BSE image of sample 5f9v0180 showing spinelloid V (grey) along with some orthopyroxene (dark) and magnetite (light) spots still left. Olivine from the starting material has been completely used up.

At 10.5 GPa, spinelloid V is no longer stable. In its place the stability field of spinel solid solution extends further into the four-component composition space from the Fe_2SiO_4–Fe_3O_4, Fe_2SiO_4–Mg_2SiO_4 and $MgFe_2O_4$–Fe_3O_4 joins (Fig 4.13). At Mg-rich bulk compositions, olivine is still stable and coexists with a Fe^{3+}-rich spinel containing a significant $MgFe_2O_4$ component. This spinel is essentially Si-free, supporting the interpretation that Si is effectively excluded from spinels

containing a $MgFe_2O_4$ component. In an analogous fashion, Si-rich spinel incorporates progressively less Fe^{3+} with increasing Mg content (Figs. 4.13, 4.14).
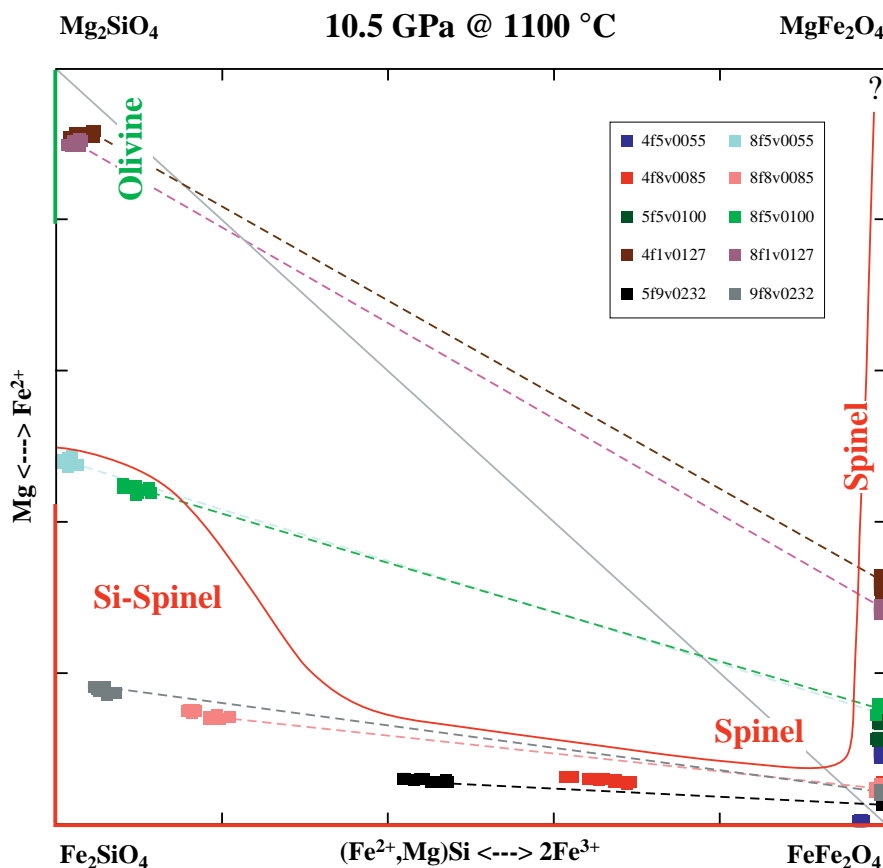
Fig. 4.13: Phase relations at 1100 °C and 10.5 GPa. No intermediate phases are stable at this pressure and a complete spinel solid solution has developed in Fe^{2+}-rich compositions.

At 12.0 GPa, olivine has been replaced by wadsleyite (Figs. 4.14, 4.15) coexisting with a spinel that has a large $MgFe_2O_4$ component. The compositional range of wadsleyite is rather narrow but corresponds very well with the results from Fei et al. (1991). Clearly no continuous solid solution exists between wadsleyite and the isotructural spinelloid III, since their stability fields are well separated in terms of pressure, as well as composition. Furthermore, the assemblage olivine + spinelloid V lies compositionally between the stability fields of spinelloid III and wadsleyite.

Experiments at 16.0 GPa did not produce any wadsleyite, but in the case of experiment 8f1h1845 ringwoodite (Si-rich spinel) appeared coexisting with a $MgFe_2O_4$-rich spinel (see Table 4.1). The chemical composition of ringwoodite is very similar to that of wadsleyite in experiments 4f1h1645 and 8f1h1646 performed at 14.0 GPa, indicating that the wadsleyite-ringwoodite two-phase field has been traversed at 16.0 GPa and 1100 °C, for a composition of $X_{Fe} = 0.17$. Thus, the two-phase region must be < 2.0 GPa wide at this point. This is in accord with the model of Fei et al. (1991) for the Mg_2SiO_4–Fe_2SiO_4 binary and suggests that Fe^{3+} has little influence on the pressure interval over which the wadsleyite to ringwoodite phase transition occurs.
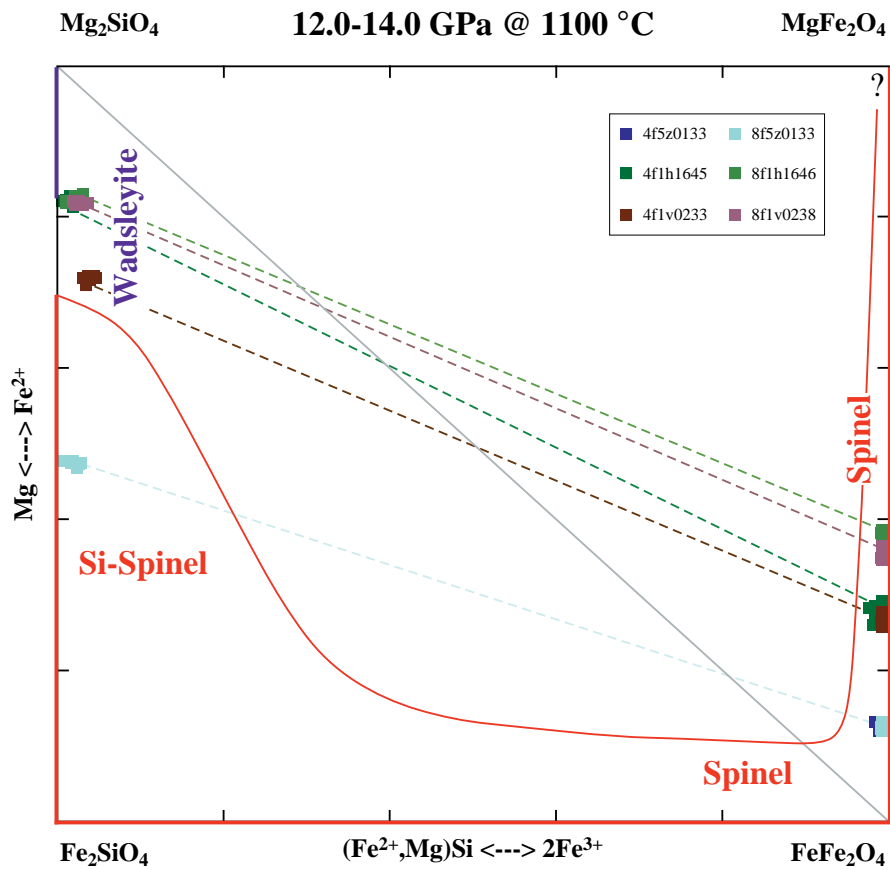
Fig. 4.14: Phase relations at 1100 °C and 12.0-14.0 GPa. Olivine has been replaced by wadsleyite, which coexists mainly with a $MgFe_2O_4$-bearing spinel.
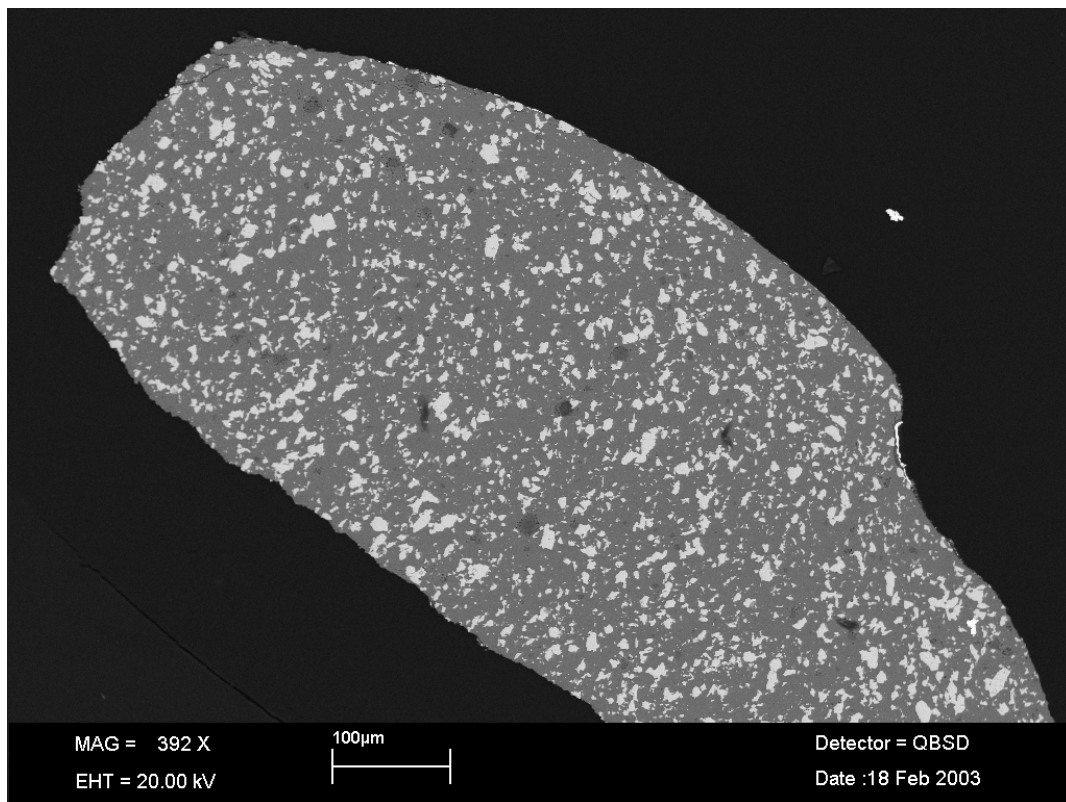
Fig. 4.15: Sample 8f1v0238 showing wadsleyite as the main mass in grey along with some Mg-ferrite (white). The rare dark grey spots are relict starting materials (compare Fig. 4.3).

4.1.2. Stability of spinelloid III and wadsleyite

The stability field of spinelloid III is restricted to the Fe^{2+}-rich part of the Mg_2SiO_4–Fe_2SiO_4–Fe_3O_4 ternary system. Of the three spinelloid polytypes found to be stable in this system, spinelloid III has the highest Si content and can coexist with either olivine or Si-rich spinel at pressures between 6.0 and 7.5 GPa at 1100 °C. Although solid solution of a Mg component shifts the stability of spinelloid III to higher pressures, as compared to the Mg-free system (Woodland & Angel 2000), this effect is rather limited. The incorporation of Fe^{3+} in wadsleyite appears to be quite minor and this phase was only found in experiments conducted at 12.0 and 14.0 GPa and 1100 °C (see Fig. 4.14).

4.1.3. Stability of spinel

Magnetite-rich spinel can incorporate significant amounts of Si and Mg when coexisting with the various spinelloid polytypes (up to 0.42 and 0.17 c.p.f.u., respectively). Such behaviour is particularly apparent in the Mg-free system (Fig. 1.6). In terms of Si incorporation, a steady increase with pressure can be observed up to a maximum between 7.0 and 8.5 GPa, followed by a decrease in Si solubility at even higher pressures, suggesting a phase change. In Mg-rich bulk compositions or at pressures > 10.0 GPa, where olivine coexists directly with spinel solid solutions, Si appears to become excluded from the spinel (e.g. Fig. 4.13). This causes a shift in the spinel composition to include a Mg-ferrite component, since Si is not present in sufficient quantities to balance all the Mg as a Mg_2SiO_4 component.

Si-rich spinel forms a complete solid solution with magnetite-rich spinel along the Fe_2SiO_4–Fe_3O_4 binary above 8.0 GPa (Fig. 1.6) and extends into the quaternary system at higher pressures. This phase can incorporate significant amounts of Mg and Fe^{3+} (up to 0.97 and 0.62 c.p.f.u., respectively) when coexisting with a magnetite-rich spinel (see Figs. 4.11, 4.13). However, complete solid solution between Si-rich and Fe^{3+}-rich spinel is rather limited in the presence of Mg. In Mg-rich bulk compositions, silicate spinel first becomes stable at pressures ≥ 16.0 GPa and apparently incorporates only very small amounts of Fe^{3+} (up to 0.04 c.p.f.u.).

4.1.4. Occurrence of additional phases

Additional phases appeared in some of our experiments that cannot be plotted in composition diagrams such as Figure 4.1. The most common extra phase was pyroxene (orthopyroxene or clinopyroxene depending on pressure). Several other experiments between 3.0 and 5.0 GPa produced a mixed valence phase informally referred to as "iscorite" (Nell & van den Berg 1988; Smuts et al. 1969), in addition to the expected phases. Run products from some of the experiments performed at pressures ≥ 9.0 GPa contain an additional phase as revealed by a number of extra peaks in their XRD patterns. These reflections could not be indexed by any high pressure phase known in our chemical system and so the identity of this phase currently remains unknown (phase labelled "?" in Table 4.1).

4.2. Structural data

Since most experimental products contain multiple phases, the X-ray powder diffraction patterns are generally rather complex, often with a number of overlapping reflections. However, pattern refinements using the Rietveld method were successful in obtaining an acceptable overall fit to the patterns, as well yielding accurate determinations of the structural parameters of the major phases present in each sample. Refinements of representative samples containing spinelloid polytypes II, III and V and spinel are illustrated in Figures 4.16, 4.17 and 4.18. The presence of additional phases in these samples is indicated in the individual Figures. As is apparent in these representative refinements, a difference in peak intensity between the observed and calculated patterns (a residual) sometimes occurs. Such differences can have a number of causes, including preferred orientation in the sample mount or differences between the actual cation distribution and the model distribution adopted for a given phase in the refinement. Although the structural models for spinel and the spinelloid phases were fixed using compositional data from microprobe analyses, the models assumed that Fe^{3+} can be tetrahedrally, as well as octahedrally coordinated (e.g. Angel & Woodland 1998), but the exact cation distribution on the various crystallographic sites could not be uniquely constrained. However, the residual is generally symmetric with respect to a given reflection, indicating that the peak positions have been reliably located and this is what is essential for the accurate determination of the cell parameters and molar volume of the phases.
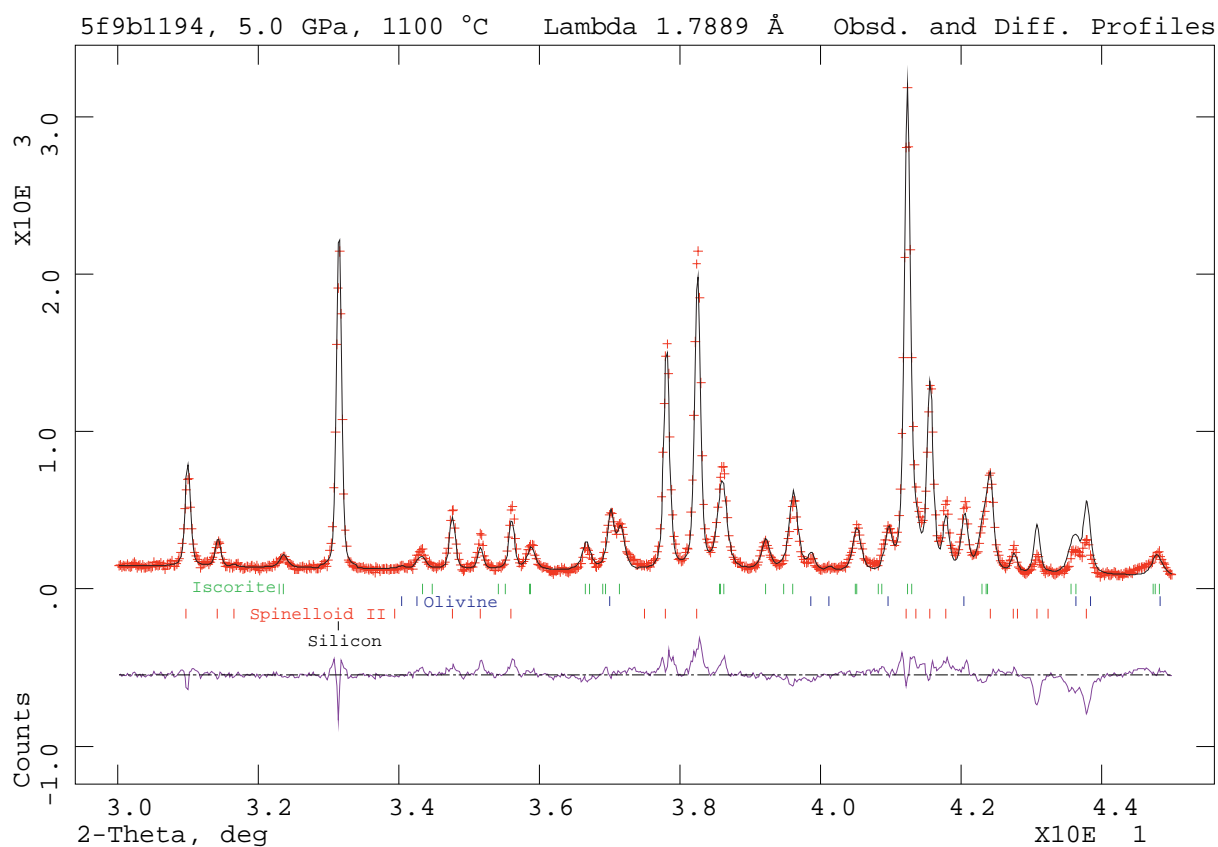
Fig. 4.16: Refinement of sample 5f9b1194 showing the observed (measured) pattern as red crosses and the calculated pattern (black solid line) in the range of 30 to 45° 2Θ. Reflection markers included in the fit belong to silicon (black), spinelloid II (red), olivine (blue) and iscorite (green). The purple pattern represents the difference between the observed and calculated pattern.
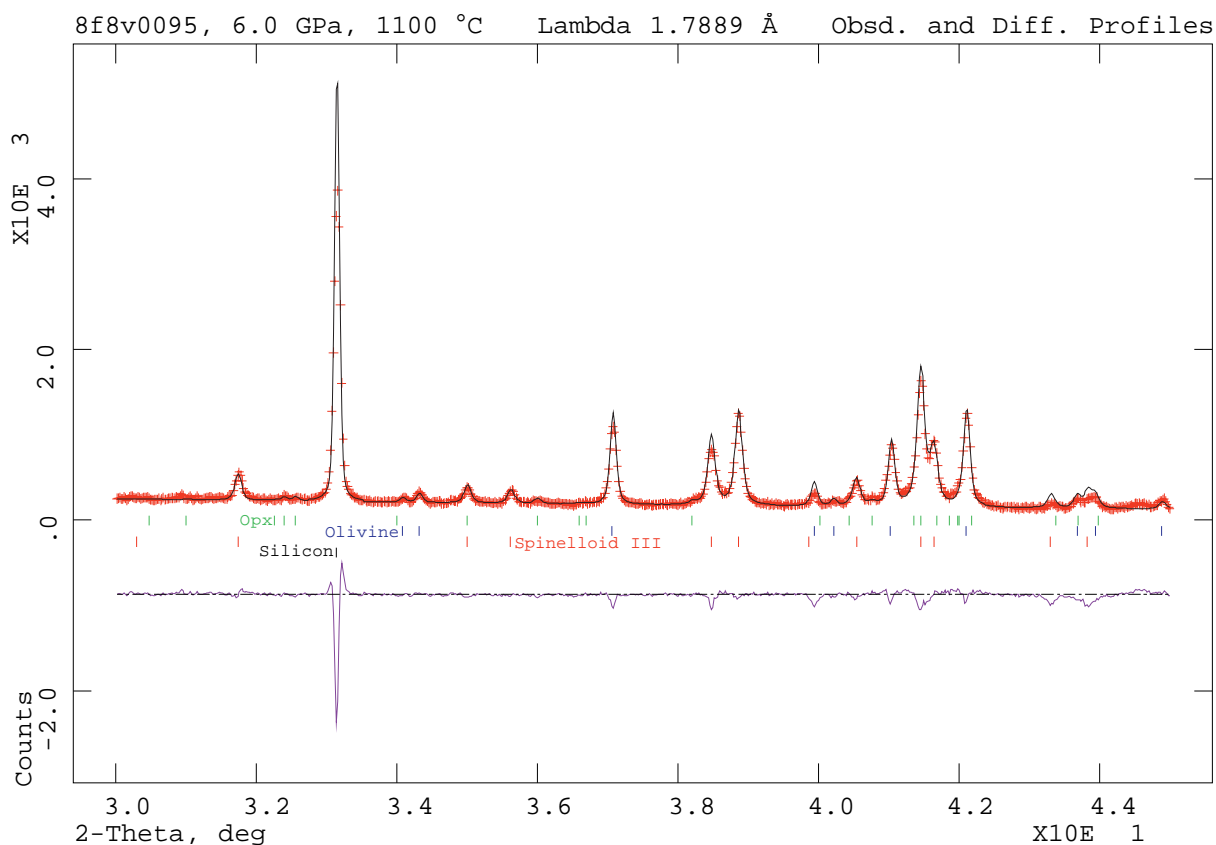
Fig. 4.17: Refinement of sample 8f8v0095 in the range of 30 to 45° 2Θ. Reflection markers included in the fit belong to silicon (black), spinelloid III (red), olivine (blue) and orthopyroxene (green).
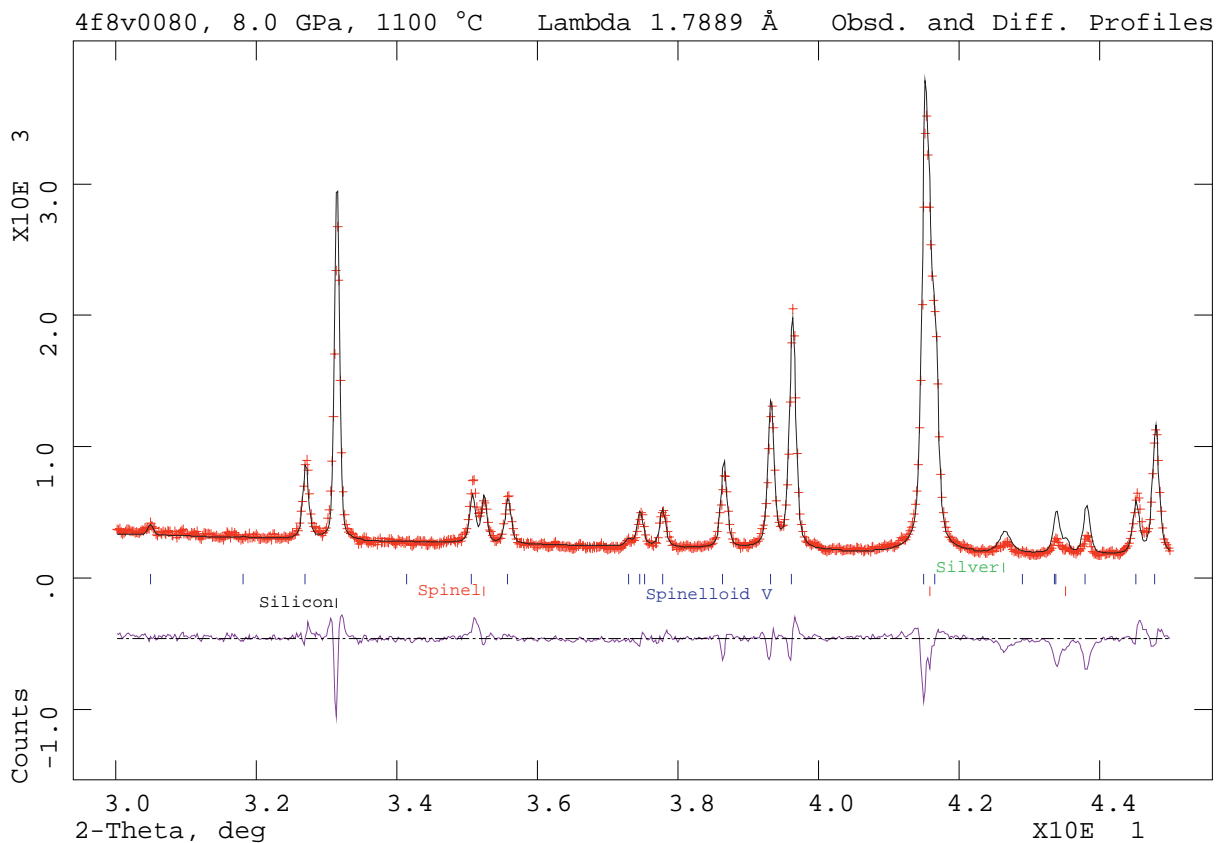
Fig. 4.18: Refinement of sample 4f8v0080 in the range of 30 to 45° 2Θ. Reflection markers included in the fit belong to silicon (black), spinel (red), spinelloid V (blue) and silver (green).

The rather large residual associated with the Si peak in the Figures results from the fact that the peak shape for this phase was not refined. After being used as an internal standard to correct the raw diffraction data, Si plays no particular role in the Rietveld refinement except for being an added phase to be accounted for in the fitting procedure (see section 3.2).

4.2.1. Unit-cell parameters and cell volumes of spinel solid solutions

The unit-cell parameters and volumes of the spinel solid solutions are summarised in Table 4.2 where they have been subdivided depending on whether they contain a magnesioferrite component or not. This subdivision has no thermodynamic or particular crystal chemical significance, but is made for convenience since structural data for compositions with a magnesioferrite component need to be treated differently than the Si-bearing spinels (see Appendix 9.1).

Table 4.2: Unit-cell parameters and volumes of synthesised spinels. See text and Appendix 9.3 for the derivation of the reduced parameters. Uncertainties (esd) are given in parenthesis.

Sample	$X_{Fe_3O_4}$	$nMg^{\#}$	a [Å]	reduced-b [Å]	V [Å³]	reduced-V [Å³]
8f1h1845	0.01(1)	1.66	8.0996(3)	5.7273	531.36(5)	265.678
8f5z0133	0.02	0.95	8.1580(2)	5.7686	542.933(39)	271.466
8f5v0055	0.02	0.96	8.1620(2)	5.7714	543.730(30)	271.864
8f8v0080	0.06	0.25	8.2251(2)	5.8160	556.439(35)	278.219
9f8v0232	0.06(1)	0.35	8.2128(1)	5.8073	553.950(29)	276.975
9f8v0124	0.07(2)	0.35	8.2170(1)	5.8103	554.804(17)	277.401
9f8v0125	0.07(2)	0.35	8.2180(1)	5.8110	555.007(29)	277.503
9f8v0099	0.09(1)	0.32	8.2255(1)	5.8163	556.526(12)	278.262
8f9v0231	0.13(1)	0.15	8.2389(1)	5.8258	559.256(23)	279.628
8f9v0181	0.15	0.15	8.2420(1)	5.8280	559.881(12)	279.940
8f8v0085	0.17	0.29	8.2342(1)	5.8225	558.300(18)	279.150
5f9v0232	0.44(2)	0.11	8.2966(1)	5.8665	571.074(27)	285.537
5f8v0124	0.60(2)	0.13	8.3251(1)	5.8868	576.999(16)	288.499
5f9v0181	0.64(1)	0.06	8.3344(2)	5.8933	578.932(43)	289.465
5f8v0099	0.70(1)	0.08	8.3429(1)	5.8993	580.710(10)	290.353
5f8v0125	0.72(2)	0.10	8.3450(12)	5.9008	581.14(26)	290.572
4f8v0053	0.75(1)	0.06	8.3503(1)	5.9045	582.236(7)	291.118
4f8v0080	0.77(1)	0.07	8.3565(2)	5.9089	583.550(40)	291.773
4f5v0081	0.80(2)	0.13	8.3609(1)	5.9120	584.456(11)	292.227
4f8v0083	0.82(2)	0.07	8.3627(1)	5.9133	584.839(17)	292.419
8f5v0094	0.82(2)	0.10	8.3643(4)	5.9145	585.18(8)	292.592
4f5v0094	0.84(1)	0.10	8.3680(1)	5.9171	585.954(12)	292.977
4f8b0271	0.85(1)	0.04	8.3756(1)	5.9225	587.558(18)	293.779
3f8h1137	0.85(1)	0.05	8.3701(1)	5.9185	586.387(7)	293.193
4f5v0084	0.85(1)	0.12	8.3678(1)	5.9169	585.912(8)	292.955
4f5v0096	0.85(2)	0.13	8.3671(1)	5.9164	585.760(10)	292.879
5f5v0096	0.85(2)	0.13	8.3676(1)	5.9168	585.882(11)	292.941
8f5h1360	0.86(1)	0.07	8.3731(1)	5.9207	587.034(15)	293.516
8f5h1136	0.86(3)	0.10	8.3688(2)	5.9176	586.127(47)	293.063
3f8v0082	0.88(1)	0.04	8.3732(1)	5.9208	587.051(7)	293.525
3f5h1360	0.89(1)	0.07	8.3767(1)	5.9232	587.792(7)	293.896
3f5h0998	0.90(1)	0.14	8.3751(1)	5.9221	587.441(7)	293.720
3f5h1136	0.92	0.14	8.3805(1)	5.9259	588.584(7)	294.291
8f8b1200	0.93	0.02	8.3851(1)	5.9292	589.562(12)	294.780
8f5b1180	0.93	0.06	8.3808(1)	5.9261	588.644(15)	294.322
4f5b1180	0.93(1)	0.06	8.3835(1)	5.9280	589.212(6)	294.606
4f8b1200	0.94(1)	0.02	8.3877(1)	5.9310	590.102(7)	295.051

Table 4.2: Continued.

Sample	$X_{Fe_3O_4}$	nMg[#]	a [Å]	reduced-b [Å]	V [Å³]	reduced-V [Å³]
MgFe₂O₄-bearing spinel						
8f1b1203	0.63	0.38	8.4007(10)	5.9402	592.85(22)	296.424
4f1v0098	0.80	0.26	8.3805(1)	5.9259	588.579(13)	294.289
8f1v0097	0.81(1)	0.23	8.3859(1)	5.9298	589.734(16)	294.866
8f1v0098	0.82	0.26	8.3790(1)	5.9249	588.279(12)	294.139
8f1b1199	0.83	0.19	8.3894(1)	5.9322	590.469(12)	295.234
4f3v0130	0.86(1)	0.21	8.3690(1)	5.9178	586.171(17)	293.085
8f3v0130	0.86(1)	0.21	8.3952(16)	5.9363	591.68 (33)	295.840
4f3v0131	0.87	0.14	8.3731(9)	5.9207	587.03 (19)	293.515
4f1v0097	0.87	0.19	8.3832(1)	5.9278	589.160(12)	294.580
4f3v0182	0.87	0.23	8.3603(1)	5.9116	584.340(7)	292.170
4f5v0129	0.88	0.13	8.3517(4)	5.9056	582.54(9)	291.270
4f1b1199	0.89	0.13	8.3898(1)	5.9325	590.538(8)	295.268
8f3v0182	0.89(1)	0.20	8.3771(5)	5.9235	587.87(9)	293.934
4f1b1203	0.91	0.12	8.3905(1)	5.9330	590.696(13)	295.347
8f5b0272	0.92	0.12	8.3991(20)	5.9390	592.51(42)	296.252

[#] n = number of Mg cations per formula unit based upon 4 oxygens and assuming perfect stoichiometry. Uncertainties in nMg are < 0.01 c.p.f.u..

4.2.2. Unit-cell parameters and cell volumes of the spinelloids

The unit-cell parameters and volumes for the Fe_3O_4–Fe_2SiO_4–Mg_2SiO_4 spinelloids synthesised in this study are listed in Table 4.3. The main difference between the various spinelloid polytypes is in their *b*-parameter, which is directly attributable to the different stacking sequences of the basic structural unit along the *b*-direction in the three polytypes (see section 1.2). In four experiments that produced wadsleyite it was only possible to retrieve reliable cell parameters from two of these samples due to extensive peak overlap with the unknown phase (mentioned in section 4.1.4).

Table 4.3: Unit-cell parameters and volumes of spinelloids II, III and V. For details on the reduced *b*-parameter and reduced volume see text and Appendix 9.3. Uncertainties (esd) are given in parenthesis.

Sample	$X_{Fe_3O_4}$	nMg[#]	a [Å]	b [Å]	reduced-b [Å]	c [Å]	V [Å³]	reduced-V [Å³]
spinelloid II								
8f9b1194	0.52	0.04	5.8509(1)	17.9529(3)	5.9843	8.3817(1)	880.418(19)	293.472
8f8b0271	0.54(2)	0.03	5.8518(1)	17.9758(4)	5.9919	8.3801(2)	881.504(25)	293.834
8f9b1196	0.54(1)	0.04	5.8507(1)	17.9568(4)	5.9856	8.3798(2)	880.383(22)	293.461
5f9b1194	0.55	0.06	5.8507(1)	17.9641(3)	5.9880	8.3811(1)	880.871(14)	293.623
4f8v0095	0.55(1)	0.17	5.8448(1)	17.9749(3)	5.9916	8.3771(1)	880.104(17)	293.368
8f5h1136	0.55	0.26	5.8356(2)	17.9635(7)	5.9878	8.3713(3)	877.559(41)	292.519
8f8b1195	0.56	0.08	5.8501(1)	17.9707(3)	5.9902	8.3790(1)	880.889(18)	293.629
5f9b1196	0.57(1)	0.07	5.8531(1)	17.9755(3)	5.9918	8.3816(2)	881.843(19)	293.947
4f8b1195	0.57	0.09	5.8506(1)	17.9793(3)	5.9931	8.3779(2)	881.268(21)	293.755
4f8b0271	0.58	0.10	5.8523(2)	17.9858(5)	5.9953	8.3791(3)	881.967(31)	293.988
spinelloid III								
8f8h1137	0.34(2)	0.20	5.8324(2)	11.8150(5)	5.9075	8.3715(3)	576.881(27)	288.440
8f8v0083	0.36(1)	0.16	5.8372(1)	11.8415(3)	5.9208	8.3685(2)	578.440(13)	289.219
8f8v0126	0.37(1)	0.15	5.8369(1)	11.8353(3)	5.9177	8.3697(2)	578.191(17)	289.095
8f8v0095	0.46(1)	0.11	5.8472(2)	11.8961(3)	5.9481	8.3634(2)	581.750(21)	290.875
8f8v0082	0.46(1)	0.12	5.8456(1)	11.8874(2)	5.9437	8.3633(1)	581.160(10)	290.579
8f5v0128	0.47(1)	0.31	5.8319(3)	11.8873(5)	5.9437	8.3522(3)	579.026(31)	289.512

Table 4.3: Continued.

Sample	$X_{Fe_3O_4}$	nMg[#]	a [Å]	b [Å]	reduced-b [Å]	c [Å]	V [Å³]	reduced-V [Å³]
wadsleyite								
8f1h1646	0.01(1)	1.65	5.7163(8)	11.4924(16)	5.7462	8.2780(10)	543.82(9)	271.907
8f1v0238	0.02(1)	1.63	5.7179(7)	11.4938(14)	5.7469	8.2827(8)	544.35(8)	272.173
spinelloid V								
6f5v0129	0.24(2)	0.56	5.8016(2)	8.7897(4)	5.8598	8.3201(3)	424.280(19)	282.853
8f8v0128	0.27(1)	0.27	5.8222(1)	8.8021(2)	5.8681	8.3388(2)	427.344(12)	284.896
8f8v0080	0.29(2)	0.21	5.8292(2)	8.8157(2)	5.8771	8.3418(2)	428.676(13)	285.784
8f9v0181	0.33(1)	0.14	5.8339(3)	8.8278(5)	5.8852	8.3410(4)	429.562(23)	286.374
9f8v0099	0.33(1)	0.25	5.8240(3)	8.8145(4)	5.8763	8.3343(4)	427.845(22)	285.230
8f9v0231	0.39(1)	0.11	5.8411(5)	8.8464(8)	5.8976	8.3482(7)	431.371(39)	287.580
5f8v0124	0.45(1)	0.23	5.8367(1)	8.8776(2)	5.9184	8.3419(2)	432.236(12)	288.157
4f3v0131	0.47(1)	0.45	5.8281(3)	8.8769(6)	5.9179	8.3381(4)	431.380(30)	287.584
8f5v0081	0.48(2)	0.28	5.8393(1)	8.8842(2)	5.9228	8.3461(2)	432.971(12)	288.647
5f9v0231	0.49	0.08	5.8504(2)	8.8812(4)	5.9208	8.3516(3)	433.937(19)	289.291
5f9v0181	0.49(1)	0.10	5.8483(1)	8.8907(2)	5.9272	8.3492(2)	434.119(12)	289.412
5f8v0125	0.51(1)	0.19	5.8446(1)	8.8937(2)	5.9291	8.3481(1)	433.937(9)	289.291
4f8v0080	0.53(1)	0.16	5.8541(1)	8.9040(2)	5.9360	8.3554(1)	435.524(9)	290.349
5f9v0180	0.55(1)	0.08	5.8576(1)	8.9080(1)	5.9387	8.3573(1)	436.079(7)	290.719
4f5v0081	0.55(1)	0.28	5.8468(8)	8.9182(16)	5.9455	8.3543(4)	435.62(9)	290.412
4f8v0126	0.58(1)	0.16	5.8571(1)	8.9145(2)	5.9430	8.3580(2)	436.395(11)	290.930
4f8v0083	0.59(1)	0.14	5.8602(1)	8.9198(2)	5.9466	8.3604(2)	437.011(11)	291.340
8f5v0094	0.59	0.19	5.8575(2)	8.9214(4)	5.9476	8.3587(3)	436.80(2)	291.199
8f5v0084	0.59	0.21	5.8555(1)	8.9165(2)	5.9443	8.3568(2)	436.31(1)	290.873

[#] n = number of Mg cations per formula unit based upon 4 oxygens and assuming perfect stoichiometry. Uncertainties in nMg are < 0.01 c.p.f.u..

4.2.3. Olivine

Olivine solid solutions were produced in experiments over a wide range of pressures from 3.0 to 10.5 GPa (see Table 4.1). Their unit-cell parameters and volumes have been provided in Table 4.4. The cell volumes vary systematically with composition, decreasing with increasing forsterite content.

Table 4.4: Unit-cell parameters and volumes of synthesised olivine solid solutions. Uncertainties (esd) are given in parenthesis.

Sample	X_{fo}	a [Å]	b [Å]	c [Å]	V [Å³]
8f9b1197	0.09	4.8158(1)	10.4506(1)	6.0786(1)	305.921(4)
8f9b1194	0.11	4.8150(1)	10.4452(1)	6.0766(1)	305.613(5)
5f9b1197	0.11(1)	4.8149(2)	10.4458(4)	6.0774(2)	305.663(13)
8f9b1196	0.12	4.8139(2)	10.4422(2)	6.0746(2)	305.359(9)
5f9b1194	0.17	4.8125(5)	10.4276(8)	6.0709(4)	304.655(26)
5f9b1196	0.19	4.8125(9)	10.4267(14)	6.0689(8)	304.529(48)
4f8b1200	0.20	4.8108(2)	10.4213(3)	6.0685(2)	304.239(9)
8f8b1200	0.20	4.8101(1)	10.4210(1)	6.0674(1)	304.131(4)
8f8b1195	0.21	4.8094(1)	10.4148(1)	6.0651(1)	303.797(5)
8f8v0095	0.25	4.8084(2)	10.4060(3)	6.0618(2)	303.312(12)
4f8b1195	0.25(1)	4.8058(5)	10.3942(8)	6.0575(5)	302.587(30)
8f8v0082	0.27	4.8075(1)	10.4013(2)	6.0603(1)	303.040(6)
4f8b0271	0.28	4.8066(3)	10.3998(6)	6.0596(3)	302.906(20)
8f8v0126	0.29	4.8062(2)	10.3934(4)	6.0572(2)	302.576(14)
8f8v0083	0.30	4.8054(2)	10.3906(4)	6.0567(2)	302.416(14)

Table 4.4: Continued.

Sample	X_{fo}	a [Å]	b [Å]	c [Å]	V [Å^3]
8f8v0080	0.38	4.8010(3)	10.3699(4)	6.0489(3)	301.148(17)
4f5b0272	0.46	4.7961(3)	10.3485(4)	6.0405(3)	299.799(15)
8f5b0272	0.47(1)	4.7957(1)	10.3520(2)	6.0419(1)	299.945(6)
4f5b1180	0.49	4.7932(1)	10.3395(3)	6.0373(2)	299.202(9)
8f5b1180	0.49	4.7923(1)	10.3376(1)	6.0358(1)	299.016(5)
8f5h1360	0.50(1)	4.7932(1)	10.3389(1)	6.0364(1)	299.140(3)
3f5h1360	0.51(2)	4.7905(2)	10.3285(4)	6.0331(2)	298.506(14)
8f5v0094	0.53	4.7910(1)	10.3280(2)	6.0325(1)	298.495(7)
8f5h1136	0.54	4.7898(1)	10.3227(2)	6.0306(1)	298.170(7)
8f5v0084	0.55	4.7893(1)	10.3207(1)	6.0299(1)	298.051(5)
4f5v0094	0.55(1)	4.7903(4)	10.3226(6)	6.0308(4)	298.212(21)
8f5v0128	0.58	4.7876(2)	10.3139(4)	6.0271(2)	297.611(14)
8f5v0081	0.59	4.7867(1)	10.3105(2)	6.0258(1)	297.396(7)
4f5v0084	0.60	4.7866(3)	10.3094(5)	6.0258(3)	297.355(17)
8f5h0998	0.62(1)	4.7826(3)	10.2950(5)	6.0198(3)	296.390(16)
8f3v0130	0.63	4.7834(1)	10.2999(2)	6.0219(1)	296.690(6)
8f3v0182	0.63	4.7837(1)	10.2999(1)	6.0217(1)	296.698(4)
4f5v0081	0.64	4.7830(4)	10.2968(7)	6.0199(4)	296.480(23)
4f5v0096	0.64	4.7831(4)	10.2986(6)	6.0210(4)	296.586(21)
5f5v0096	0.65	4.7813(4)	10.2924(7)	6.0186(4)	296.185(22)
4f3v0130	0.65	4.7825(4)	10.2975(7)	6.0206(4)	296.500(23)
4f3v0182	0.66	4.7811(3)	10.2914(5)	6.0184(3)	296.128(16)
8f3v0131	0.66	4.7817(2)	10.2926(3)	6.0187(2)	296.217(9)
6f5v0129	0.68(1)	4.7794(7)	10.2881(11)	6.0162(8)	295.821(39)
4f1b1203	0.70	4.7776(2)	10.2804(3)	6.0150(2)	295.432(10)
4f3v0131	0.72	4.7787(7)	10.2765(13)	6.0123(7)	295.257(43)
4f1b1199	0.76	4.7732(1)	10.2635(2)	6.0082(1)	294.336(8)
8f1b1203	0.79	4.7715(1)	10.2576(1)	6.0062(1)	293.972(4)
4f1v0097	0.79	4.7712(3)	10.2564(6)	6.0056(3)	293.883(18)
8f1b1199	0.83	4.7668(1)	10.2424(1)	5.9997(1)	292.925(4)
8f1v0097	0.84	4.7672(1)	10.2408(2)	5.9994(1)	292.891(6)
8f1v0098	0.88	4.7645(1)	10.2315(2)	5.9953(1)	292.255(7)
4f1v0098	0.88(1)	4.7635(5	10.2288(9)	5.9944(5)	292.074(28)
8f1v0127	0.90	4.7630(3)	10.2266(5)	5.9933(3)	291.930(17)
4f1v0127	0.91	4.7615(14)	10.2268(25)	5.9931(15)	291.83(8)

5. Discussion

5.1. Phase relations

5.1.1. Spinelloids and spinel

The sequence of stability of the spinelloid intermediate phases with increasing pressure is the same as that observed in the Mg-free system (Woodland & Angel 2000): spinelloid II → spinelloid III → spinelloid V (see Figs. 4.2, 4.6, 4.10). However, the addition of Mg acts to shift the stability fields of the spinelloids towards higher pressures. These phases tend to become richer in Mg and Si with increasing pressure as well as temperature when they coexist with olivine. For example, the spinelloid II present in a reconnaissance experiment at 1200 °C had the highest Mg content of any spinelloid II synthesised (see Fig. 4.7). However, stability fields of the spinelloids are generally restricted to quite Fe-rich compositions (see Figs. 4.2, 4.7). At high bulk Mg contents, olivine coexists with a Fe^{3+}-rich spinel containing a Mg-ferrite component. There is clearly a large gap between the stability fields of "true" $(Mg,Fe)_2SiO_4$-wadsleyite (e.g. Katsura & Ito 1989; Fei et al. 1991) and the isostructural spinelloid III (Fe^{3+}-wadsleyite), both in terms of composition space as well as pressure. It is currently unclear what thermodynamic relationship there is between these two phases.

In Mg-rich bulk compositions and at pressures above 16.0 GPa a ringwoodite is produced that incorporates only very small amounts of Fe^{3+} (up to 0.04 c.p.f.u.). Frost et al. (2001) performed experiments under relatively "oxidising" conditions (Re-metal was used as a capsule) and also produced Mg-rich ringwoodites with negligible Fe^{3+}. In their experiments spinel was in equilibrium with magnesiowüstite. In contrast, the experiments described here contained coexisting $MgFe_2O_4$-rich spinel, which has a much higher Fe^{3+} content than magnesiowüstite, and thus suggests even more oxidising conditions. It might be expected that the ringwoodites synthesised under such conditions would have higher Fe^{3+} contents than those reported by Frost et al. (2001). The fact that only minor amounts of Fe^{3+} are observed, reinforces the contention that solid solution between silicate and Fe^{3+}-rich spinels is strongly influenced by the presence of Mg. Furthermore, the apparent mutual exclusivity of Mg and Si in magnetite-rich spinels argues against significant solid solution along the Mg_2SiO_4–$MgFe_2O_4$ binary join and suggests complex activity-composition behaviour in $(Mg,Fe^{2+})Fe^{3+}_2O_4$–$(Mg,Fe^{2+})_2SiO_4$ spinel solid solutions.

5.1.2. Additional phases

Depending on pressure, orthopyroxene or clinopyroxene is the most common extra phase that appeared in some of our experiments. Slight oxidation during the experiment shifts the original Fe^{3+}/Fe^{2+} ratio so that excess Si becomes available for producing pyroxene along with spinel, spinelloid or olivine. As such, pyroxene acts as a sink for Si compensating for the presence of excess Fe^{3+} that can be incorporated in spinel or spinelloid. The orthorhombic to high-P monoclinic phase transition was observed to occur between 7.5 and 8.0 GPa (Table 4.1), which is in excellent agreement with experiments of Woodland (1998) on $(Mg,Fe)SiO_3$ pyroxenes. However, due to the unquenchable nature of the high-P monoclinic polymorph (e.g. Hugh-Jones et al. 1994), the recovered clinopyroxene

always had the low-P $P2_1/c$ structure. Pyroxenes only incorporate minor amounts of Fe^{3+} up to about 0.1 cations per formula unit. This is due to the fact that there is no Al in the system and apparently the Fe^{3+}-Tschermaks type substitution is not favoured. Selected mean mineral analysis are provided in Appendix 9.2.1.

Between 3.0 and 5.0 GPa, a mixed valence phase, informally referred to as "iscorite" (Nell & van den Berg 1988; Smuts et al. 1969), was produced in several experiments. This phase has a nominal composition of Fe_7SiO_{10} and a limited substitution of Mg, from 0.66 - 1.25 wt% MgO. The low $Fe^{3+}/(Fe^{2+}+Mg)$ ratio indicates that this phase lies on the reduced side of the chemical system investigated (see Woodland & Angel 2000). Thus, slight reduction of the starting materials is observed in some experiments while some oxidation occurred in others. Therefore, iscorite will never coexist with orthopyroxene and shows a rather uniform chemical composition (see Appendix 9.2.2), even over a pressure range of 2.0 GPa.

At pressures ≥ 9.0 GPa, some run products have additional peaks in their XRD patterns that cannot be indexed by any high pressure phase known in our chemical system (the phase labelled "?" in Table 4.1). The positions of the most apparent reflections have d-spacings of 2.708(28), 2.643(100), 2.444(24), 2.236(15), 2.133(33), 2.046(54), 1.672(9), 1.570(15), 1.512(11), 1.507(12) and 1.448(20) whereby the values in parentheses denote the approximate relative intensities. Unfortunately, investigation of these samples with the microprobe and SEM revealed no additional phase that could be correlated with the XRD data. Numerous attempts to fit this unknown phase have been made by including additional structure models for stable phases in related and analog systems. Apart from the phases listed in Table 4.1, hematite, (Fe,Mg)O, "skiagite" garnet (e.g. Woodland & O'Neill 1993; Woodland & Ross 1994), laihunite (Tamada et al. 1983), anhydrous Phase B (e.g. Hazen et al. 1992) and even model spinelloid I, spinelloid IV and iwakiite (e.g. Ma et al. 1975; Horioka et al. 1981a; Matsubara & Kato 1979) structures were considered. In addition, perovskite and the high-P $CaMn_2O_4$-structure type (e.g. Fei et al. 1999) of magnetite and endmember Mg-ferrite, phases that are stable at much higher pressures, could not explain the additional peaks in the patterns. The unknown phase which can be a major phase in some experiments (compare Table 4.1) must have a composition like that of coexisting spinel, otherwise it would have been detected by microprobe or SEM imaging. Since there are virtually no peaks at very low angles (10 - 30° 2Θ) and taking into account the number of unindexed peaks, the unknown phase should have a small unit-cell and should be at least orthorhombic, rather than cubic. If these unindexed peaks should for some reason not belong to a new separate phase, the only other feasible explanation would be the occurrence of superstructure reflections of one of the already identified phases, most likely spinel. Further investigations with Raman spectroscopy and TEM are planned to try to shed more light on this mysterious phase.

5.1.3. Equilibrium and Mg-Fe^{2+} partitioning

The aforementioned slight oxidation or reduction in some experiments could lead one to question whether the run products represent equilibrium assemblages or not. However, there are a number of lines of evidence that indicate that local equilibrium was attained in the experiments. Many experiments

contained two samples which had the same starting olivine composition, but differed in their magnetite/olivine ratio (i.e. variable bulk Fe^{3+} content). In some cases, these samples produced different assemblages, which is not unexpected. However, when the phase relations were such that the same assemblage was produced in the two samples, the mineral compositions were virtually identical to each other, indicating approach to equilibrium from two different bulk Fe^{3+} contents (see Table 4.1). When olivine was a part of the run product assemblage, its composition was usually different from that of the starting material, demonstrating that this phase recrystallised and adjusted its composition during the experiment.

The partitioning of Fe^{2+} and Mg between phases can also be used as a test of whether chemical equilibrium was attained between any two phases in the assemblage. For example, partitioning between orthopyroxene and olivine in our samples is consistent with the experimental data of von Seckendorff and O'Neill (1993), providing evidence of local equilibrium even in the experiments that experienced some oxidation (Fig. 5.1a). It seems likely that the slight oxidation occurred at the onset of the experiment and that the sample assemblage had adequate time to chemically adjust to this small shift in bulk composition. Pyroxene is always the phase richest in Mg and olivine is always richer in Mg compared to any coexisting spinelloid phase or spinel as can be seen in the Roozeboom diagrams of Figures 5.1b and 5.1c. The Fe^{2+}-Mg partitioning between olivine and the spinelloid polymorphs as well as between olivine and spinel varies systematically with composition (Figs. 5.1b, 5.1c). Such systematic behaviour also supports our contention that local equilibrium was easily attained during our relatively long-duration experiments.
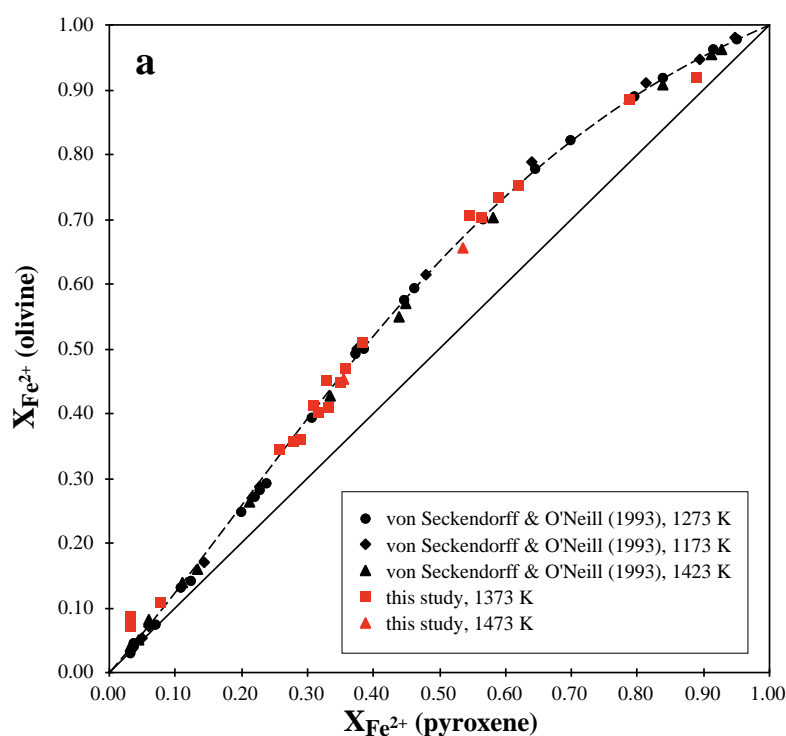
Fig. 5.1a: Roozeboom diagram for olivine coexisting with pyroxene. Experimental data from von Seckendorff and O'Neill (1993) have been included for reference. Dashed lines are drawn by hand.
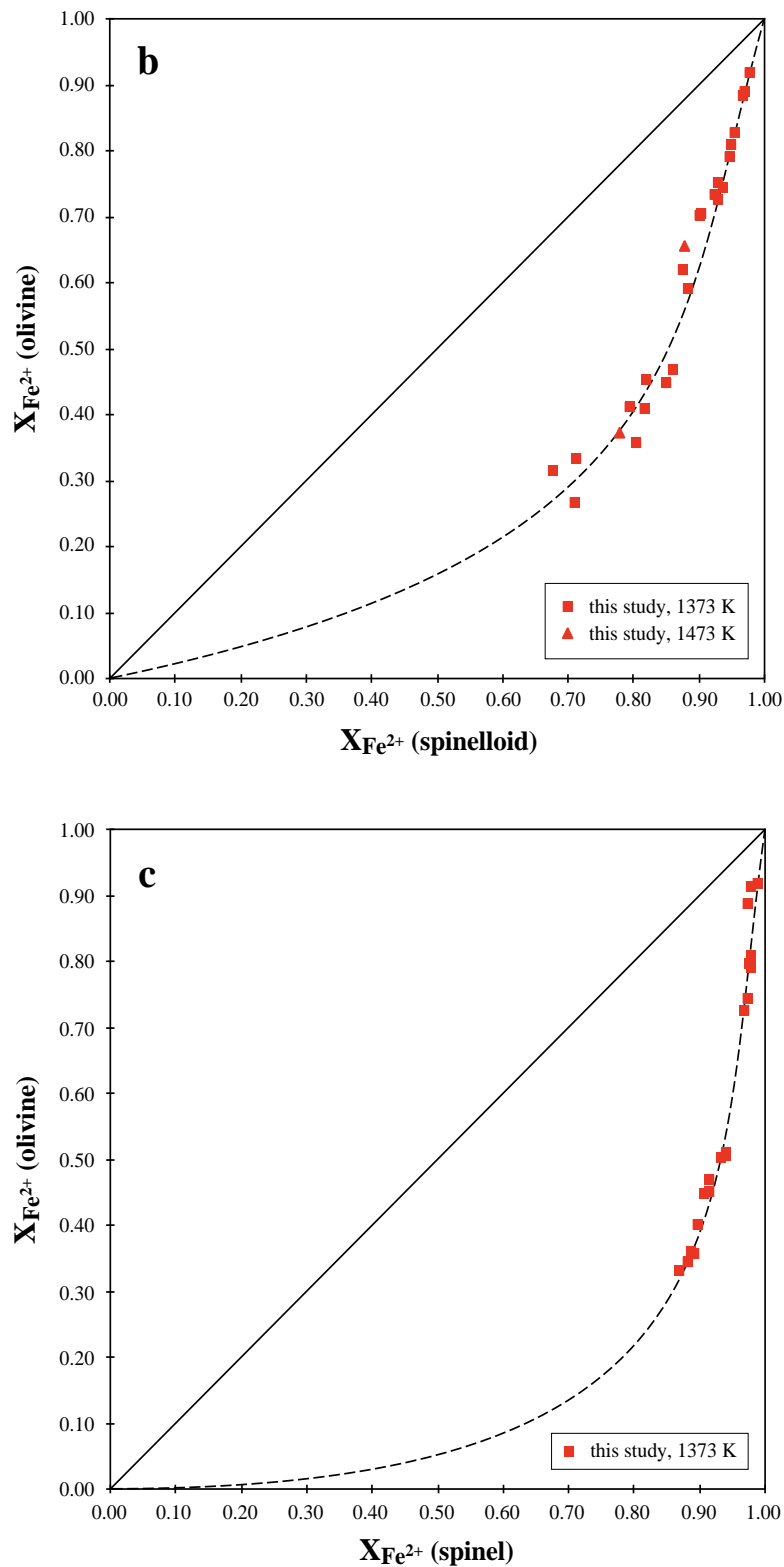
Fig. 5.1b,c: Roozeboom diagrams for olivine coexisting with (b) the spinelloids and (c) spinel. Similar trends are observed if olivine is substituted by pyroxene. All spinelloid polytypes have been plotted together since their Fe^{2+} values are very similar. Only mt-rich spinels with $Si > Mg/2$ have been plotted in (c). Dashed lines are drawn by hand.

Partitioning between olivine and the spinelloids II, III and V is esssentially identical, thus we plotted all three spinelloids together in Figure 5.1b. In all cases there is no noticeable pressure dependence on Fe^{2+}-Mg partitioning between these phases, implying that the spinelloid phases and spinel have a negligible excess volumes of mixing.

5.2. Structural data and molar volumes

5.2.1. Spinel

The cell parameter and molar volume decrease systematically with decreasing magnetite content in spinel (Figs. 5.2, 5.3). This behaviour is expected since magnetite has a larger molar volume (and cell parameter) than any of the other endmember components: magnetite = 44.528 cm^3 (Hill et al. 1979), Fe_2SiO_4-spinel = 41.981 cm^3 (Woodland & Angel 2000), Mg_2SiO_4-spinel = 39.49 cm^3 (Sasaki et al. 1982), and magnesioferrite = 43.989 cm^3 (Hill et al. 1979).
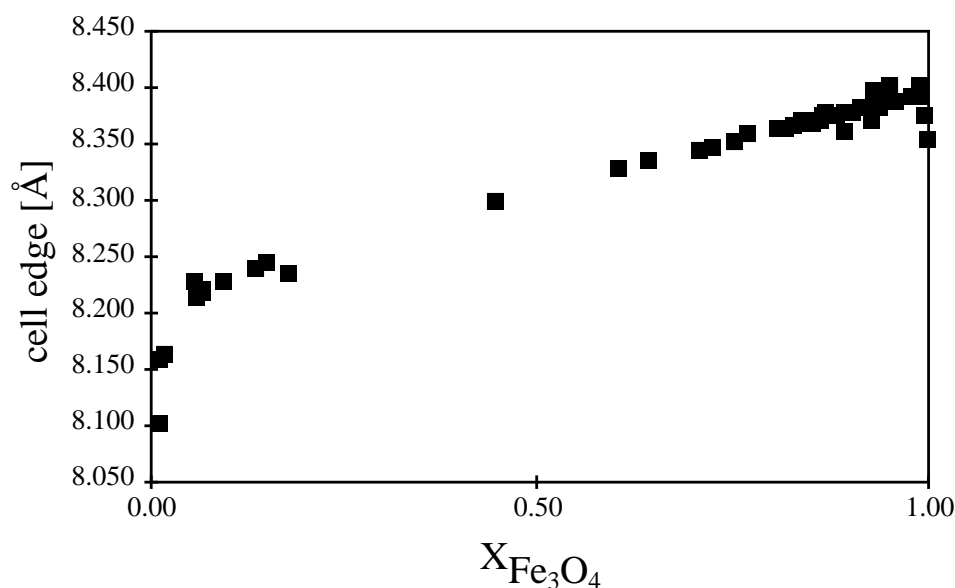
Fig. 5.2: Variation of the unit-cell parameter in spinel solid solutions plotted as a function of magnetite content. The scatter is due to variable Fe_2SiO_4 and Mg_2SiO_4 contents, which also influence the cell parameter. $MgFe_2O_4$-bearing spinels have been plotted as $1-X_{Fe_2SiO_4}$, which represents a $ZFe^{3+}_2O_4$ component, where Z = Fe^{2+} or Mg.
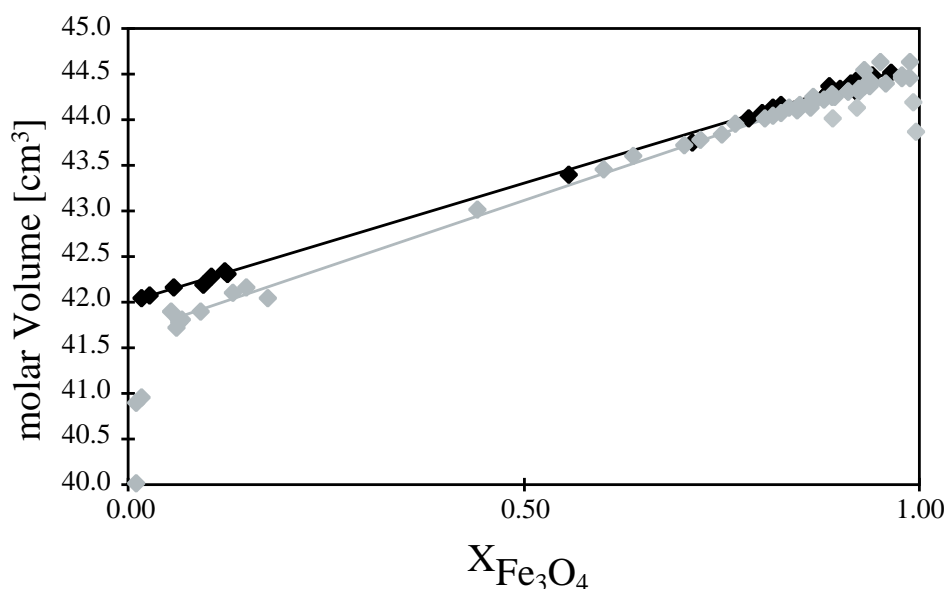
Fig. 5.3: Variation of the molar volume in spinel solid solutions plotted as a function of magnetite content. The darker coloured data points are samples from the Mg-free system (Woodland & Angel 2000) and the lighter coloured data are from the Mg-bearing system (this study). The scatter is due to variable Fe_2SiO_4 and Mg_2SiO_4 contents, which also influence the molar volume. $MgFe_2O_4$-bearing spinels have been plotted as $1 - X_{Fe_2SiO_4}$, which represents a $ZFe^{3+}_2O_4$ component, where Z = Fe^{2+} or Mg. The lines are not fits to the data, but are meant to provide a visual guide for the effect of substitution of a Si-bearing component in a Fe^{3+}-bearing spinel.

The scatter in the figures is mostly due to variable Mg/Fe^{2+} ratios in the different samples, which also influences the structural parameters. In addition, for those spinels that contain a magnesioferrite component, this component is combined with the magnetite component. Therefore, the composition parameter for these spinels actually represents the substitution of a Si-component in a Fe^{3+}-bearing spinel independent of whether Fe^{2+} or Mg is present.

The systematics of the molar volume in these compositionally complex spinels can be evaluated in several ways. Spinels along the Fe_2SiO_4–Fe_3O_4 binary exhibit close to ideal mixing behaviour in terms of their molar volumes (Woodland & Angel 2000), suggesting that ideal mixing might also be a good first-order assumption for the Mg-bearing spinels. If this is the case, then the molar volume of a given solid solution can be determined from the following relationship:

$$V_{ss} = (X_{Fe_3O_4} * V°_{Fe_3O_4}) + (X_{Fe_2SiO_4} * V°_{Fe_2SiO_4}) + (X_{Mg_2SiO_4} * V°_{Mg_2SiO_4}), \tag{5.2.1}$$

at least for those spinels that do not contain a magnesioferrite component. Using the best-fit values for $V°_{Fe_3O_4}$ and $V°_{Fe_2SiO_4}$ from Woodland and Angel (2000) and rearranging equation 5.2.1, a value for $V°_{Mg_2SiO_4}$ can be derived from the volume and composition data for each spinel listed in Table 4.2. The resulting values for $V°_{Mg_2SiO_4}$ are quite consistent among the 37 spinels used in this analysis and yield $V°_{Mg_2SiO_4} = 40.21(44)$ cm^3 (Table 5.1). For the spinels containing a magnesioferrite component a different component set is required. Using Fe_3O_4, Fe_2SiO_4 and $MgFe_2O_4$ to describe their composition, a relation analogous to 5.2.1 can be employed to calculate molar volumes under the assumption of ideal mixing:

$$V_{ss} = (X_{Fe_3O_4} * V°_{Fe_3O_4}) + (X_{Fe_2SiO_4} * V°_{Fe_2SiO_4}) + (X_{MgFe_2O_4} * V°_{MgFe_2O_4}) \tag{5.2.2}$$

This relation can also be applied to many Si-bearing spinels listed in Table 4.2, which allows magnesioferrite-bearing and Fe-Si-rich spinels to be considered together. In this case, values for $V°_{MgFe_2O_4}$ can be calculated following a similar approach to that described previously for deriving $V°_{Mg_2SiO_4}$. A total of 40 spinels yield a very consistent $V°_{MgFe_2O_4} = 43.80(19)$ cm^3 (Table 5.1). Comparison of these results with literature data for $V°_{Mg_2SiO_4}$ and $V°_{MgFe_2O_4}$ permits an assessment of the assumption of ideal mixing behaviour for the spinel solid solutions (Table 5.1). The close agreement in values of $V°_{MgFe_2O_4}$ leads to the conclusion that ideal mixing is indeed a very good approximation for the thermodynamic behaviour of Fe_3O_4–Fe_2SiO_4–$MgFe_2O_4$ spinels. On the other hand, the molar volume of the Mg_2SiO_4 endmember derived here is ~0.7 cm^3 larger than that reported by Sasaki et al. (1982), suggesting more significant non-ideal behaviour in Mg_2SiO_4-bearing spinels.

Table 5.1: Molar volumes of spinel endmembers derived assuming ideal mixing in the spinel solid solutions produced in this study along with values reported in the literature.

Component	V° [cm^3]	Reference
Fe_3O_4	44.58	Woodland & Angel (2000)
Fe_2SiO_4	41.981(14)	Woodland & Angel (2000)
Mg_2SiO_4	40.21(44)	this study
$MgFe_2O_4$	43.80(19)	this study

Table 5.1: Continued.

Component	V° [cm³]	Reference
literature data		
Fe_3O_4	44.52	Fabrichnaya (1998)
Fe_3O_4	44.53	Hill et al. (1979)
Fe_2SiO_4	41.86	Frost et al. (2001)
Fe_2SiO_4	42.01	Akaogi et al. (1989)
Fe_2SiO_4	42.02	Jeanloz & Thompson (1983)
Fe_2SiO_4	42.02	Fabrichnaya (1998)
Fe_2SiO_4	42.02	Fei et al. (1991)
Fe_2SiO_4	42.03	Ringwood & Major (1970)
Fe_2SiO_4	42.03	Yagi et al. (1974)
Fe_2SiO_4	42.04	Marumo et al. (1977)
Mg_2SiO_4	39.49	Ito & Yamada (1982)
Mg_2SiO_4	39.49	Frost et al. (2001)
Mg_2SiO_4	39.49	Sasaki et al. (1982)
Mg_2SiO_4	39.53	Akaogi et al. (1989)
Mg_2SiO_4	39.58	Ringwood & Major (1970)
Mg_2SiO_4	39.65	Fabrichnaya (1998)
Mg_2SiO_4	39.65	Fei et al. (1991)
Mg_2SiO_4	39.65	Jeanloz & Thompson (1983)
$MgFe_2O_4$	43.99	Hill et al. (1979)
$MgFe_2O_4$	44.57	Fabrichnaya (1998)

An alternative approach is to explicitly account for potential non-ideality in the spinel solid solutions by using the published data for the endmember molar volumes and the observed V_{ss}. In the case of a ternary regular solution involving the Fe_3O_4, Fe_2SiO_4 and Mg_2SiO_4 endmembers the molar volume can be expressed as follows:

$$V_{ss} = V^{ideal} + V^{ex}, \tag{5.2.3}$$

where V^{ideal} is obtained from equation 5.2.1 and the excess volume, V^{ex}, is given by:

$$V^{ex} = (X_{Fe_3O_4} * X_{Fe_2SiO_4} * W_{V(mt\text{-}FeSi)}) + (X_{Fe_2SiO_4} * X_{Mg_2SiO_4} * W_{V(FeSi\text{-}MgSi)}) +$$
$$(X_{Fe_3O_4} * X_{Mg_2SiO_4} * W_{V(mt\text{-}MgSi)}) \tag{5.2.4}$$

Here, the W_V terms are the Margules parameters that describe regular solution behaviour along each of the three binary joins that form part of the ternary system. For the Fe_3O_4–Fe_2SiO_4 binary, Woodland and Angel (2000) report $W_{V(mt\text{-}FeSi)} = -0.15(6)$ cm³. The two remaining parameters, $W_{V(FeSi\text{-}MgSi)}$ and $W_{V(mt\text{-}MgSi)}$, can be evaluated from the structural data presented in Table 4.2. A weighted least squares regression of 37 spinels yielded $W_{V(FeSi\text{-}MgSi)} = 0.25(5)$ cm³ and $W_{V(mt\text{-}MgSi)} = 1.6(5)$ cm³. Thus, the Fe_3O_4–Mg_2SiO_4 binary exhibits the greatest degree of non-ideal behaviour. This result is consistent with the observed phase relations described in section 4.1, which indicate that the incorporation of Mg reduces the extent of solid solution between Si-rich and Fe^{3+}-rich spinel components.

The analogous formulation using the $MgFe_2O_4$ component instead of Mg_2SiO_4 permits the magnesioferrite-bearing spinels to be considered along with many of the Si-rich spinels and allows evaluation of the $W_{V(FeSi-mf)}$ and $W_{V(mt-mf)}$ Margules parameters through the following relationship:

$$V^{ex} = (X_{Fe_3O_4} * X_{Fe_2SiO_4} * W_{V(mt-FeSi)}) + (X_{Fe_2SiO_4} * X_{MgFe_2O_4} * W_{V(FeSi-mf)}) +$$

$$(X_{Fe_3O_4} * X_{MgFe_2O_4} * W_{V(mt-mf)}) \tag{5.2.5}$$

A least squares fit to 40 spinels whose composition can be described using Fe_3O_4, Fe_2SiO_4 and $MgFe_2O_4$ as components yielded $W_{V (mt-mf)} = -0.09(23)$ cm^3 and $W_{V (FeSi-mf)} = 10(43)$ cm^3, indicating that mixing along the magnetite-magnesioferrite join is essentially ideal. The calculated value of $W_{V(FeSi-mf)}$ is extremely (unrealistically?) large. However, the previous assessment of molar volumes using equation 5.2.2 suggests that near ideal behaviour is expected for Fe_3O_4–Fe_2SiO_4–$MgFe_2O_4$ spinels and this large value should be viewed with scepticism, especially since the uncertainty attached to this value is so large. The very large uncertainty in $W_{V(FeSi-mf)}$ is due to the fact that many spinels in the dataset lie near to the magnetite endmember in composition and thus provide very little constraint on the properties of Fe_2SiO_4–$MgFe_2O_4$ binary spinels.

5.2.2. Spinelloids

Structural parameters available in the literature for spinelloids along the $NiAl_2O_4$–Ni_2SiO_4 and Fe_3O_4–Fe_2SiO_4 binary joins provide a starting point for analysing and interpreting the structural data for the spinelloids in the more complex Mg–Fe system studied here (see summary in Table 5.2).

Table 5.2: Summary of published unit-cell parameters for spinelloids stable in the $NiAl_2O_4$–Ni_2SiO_4 and Fe_3O_4–Fe_2SiO_4 systems based upon single crystal and powder diffraction (*) measurements. SG stands for space group.

Ni-Al-Si System							
Phase	X_{NiAl_2O}	SG	a [Å]	b [Å]	c [Å]	V [Å^3]	Reference
Spinelloid I	0.71	Pmma	5.6664(5)	11.496(2)	8.0983(7)	527.530	Ma et al. (1975)
Spinelloid II	0.58	Imma	5.6603(7)	17.298(2)	8.110(1)	794.065	Ma & Tillmanns (1975)
Spinelloid III	0.44	Imma	5.6646(4)	11.455(2)	8.1007(7)	525.638	Ma & Sahl (1975)
Spinelloid III	0.50	Imma	5.665(2)	11.483(2)	8.100(2)	526.915	Akaogi et al. (1982)
Spinelloid IV	0.50	Imma	5.665(2)	28.646(9)	8.091(3)	1313.004	Horioka et al. (1981a)
Spinelloid V	0.50	Pmma	5.665(1)	8.590(1)	8.097(2)	394.019	Horioka et al. (1981b)
Fe^{3+}-Fe^{2+} System							
Phase	$X_{Fe_3O_4}$	SG	a [Å]	b [Å]	c [Å]	V [Å^3]	Reference
Spinelloid I		-	-	-	-	-	has not been found
Spinelloid II	0.57	Imma	5.85928(10)	17.9801(3)	8.38395(14)	883.252(17)	Angel & Woodland (1998)
Spinelloid II*	0.55	Imma	5.8576(1)	17.9702(2)	8.3835(1)	882.458(12)	Woodland & Angel (2000)
Spinelloid III	0.45	Imma	5.8559(2)	11.8936(4)	8.3684(2)	582.84(2)	Woodland & Angel (1998)
Spinelloid III*	0.46	Imma	5.8559(2)	11.8989(4)	8.3669(2)	582.990(21)	Woodland & Angel (2000)
Spinelloid IV		-	-	-	-	-	has not been found
Spinelloid V	0.68	Pmma	5.867(1)	8.917(1)	8.362(1)	437.2(1)	Ross II et al. (1992)
Spinelloid V*	0.55	Pmma	5.8664(4)	8.9132(5)	8.3641(5)	437.347(37)	Woodland & Angel (2000)

The spinelloid polytypes I and IV, which are stable in the Ni-aluminosilicate system, have not been found in either the Fe_3O_4–Fe_2SiO_4 system or in the Mg–Fe system. For the other stable polytypes II, III and V, the unit-cell parameters and volumes are smaller in the Ni-aluminosilicate spinelloids compared to their analogues in the Fe_3O_4–Fe_2SiO_4–Mg_2SiO_4 system. This is expected since Ni has a smaller ionic radius than either Fe^{2+} or Mg and Al is always smaller than Fe^{3+} in the same coordination (Shannon 1976).

Spinelloids are related to the spinel structure by different stacking sequences of a basic structural unit as described in section 1.2. The variation in this stacking sequence results in different degrees of condensation of the tetrahedral sites. Spinelloid II contains T_3O_{10} groups with a central T2 site bonded to two adjacent T1 sites (Angel & Woodland 1998). Spinelloid III has symmetrically equivalent tetrahedral sites that form T_2O_7 groups (Woodland & Angel 1998). The structure of spinelloid V is intermediate to those of spinelloid III and spinel in as much as both T_2O_7 and isolated TO_4 groups are present in equal numbers (Ross et al. 1992). Since stacking of the basic structural unit is parallel to [010], the greatest difference in the unit-cell parameters between the spinelloid polytypes is in the *b*-parameter (Table 5.2).

The systematics of spinelloid II are difficult to assess given the narrow compositional range over which this phase is stable. This makes it difficult to make extrapolations with confidence. In fact the *a*-parameter is very similar for all three polytypes (Tables 4.3, 5.2), even if a small systematic decrease in *a* is apparent with decreasing Fe_3O_4 content (Fig. 5.4a). The *c*-parameter of spinelloid V exhibits similar behaviour with composition, but the *c*-parameter of spinelloid III varies in the opposite manner, increasing with decreasing Fe_3O_4 content (Fig. 5.4b). This contrasting behaviour was also observed in the Mg-free system by Woodland and Angel (2000) and is attributable to the different crystal structures of the two spinelloid polytypes. In spinelloid III the octahedral site occupancy has the greatest influence on the *c*-parameter (Ma & Sahl 1975; Woodland & Angel 1998). With increasing $(Mg,Fe)_2SiO_4$ content the octahedral sites become progressively filled with Fe^{2+} and Mg^{2+},which have larger ionic radii than octahedrally coordinated Fe^{3+}, leading to the observed increase in the *c*-parameter with decreasing $X_{Fe_3O_4}$. In the spinelloid V structure, an alternation of layers containing the T_2O_7 and TO_4 groups in the *c*-direction means that the tetrahedral site occupancy plays a greater role in determining the systematics of the *c*-parameter. Substitution of the smaller Si cation for Fe^{3+} in the tetrahedral sites with decreasing $X_{Fe_3O_4}$ leads to a progressive reduction of the *c*-parameter.
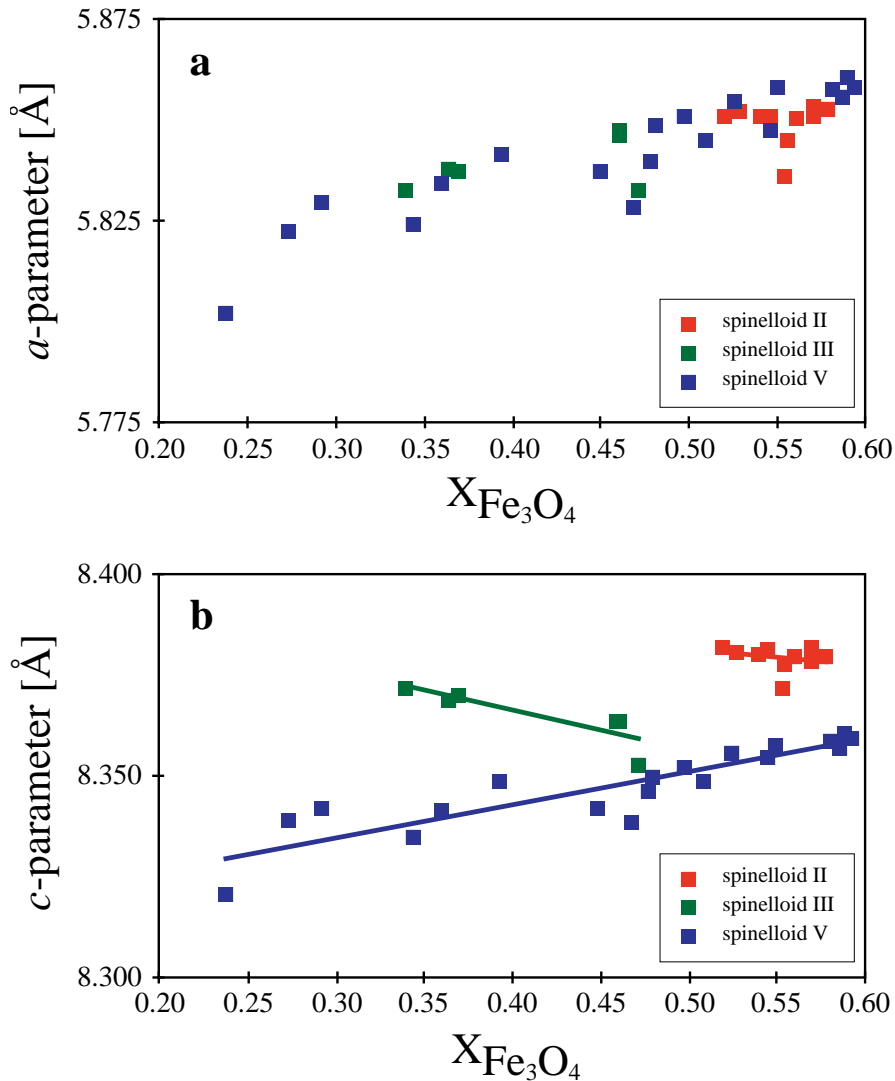
Fig. 5.4: Variation in the a) *a*- and b) *c*-parameter of spinelloids II, III and V as a function of $X_{Fe_3O_4}$. The scatter is due to variable Fe_2SiO_4 and Mg_2SiO_4 contents, which also influence the cell parameter. The lines are not fits to the data, but are meant to provide a visual guide for the compositional effects on the cell parameter.

As previously mentioned, due to the different stacking sequences, the greatest difference in the unit-cell parameters between the spinelloid polytypes is in the *b*-parameter. As a way to better compare the *b*-parameters of the different spinelloids, a reduced *b*-parameter is introduced that is normalised on the basis of the number of slabs per unit-cell (see Appendix 9.3). Therefore, this reduced parameter represents the average dimensions of the structural slabs in each phase. A further benefit of this reduced parameter is that an analogous value for spinel can also be derived, which permits direct comparison of the structural systematics between spinel and the three spinelloid polytypes. The reduced *b*-parameter of all three spinelloid polytypes, as well as for spinel, decreases progressively with decreasing Fe_3O_4 content (Fig. 5.5). The values plotted in Figure 5.5 are on a basis of two slabs. In addition, for a given composition, the reduced *b*-parameter becomes smaller in the following order of phases: spinelloid II → spinelloid III → spinelloid V → spinel, reflecting progressively compacter structures as the number of tetrahedral bridging oxygen bonds is reduced; the bridging oxygen bonds are generally longer than non-bridging oxygen bonds (Ross et al. 1992; Angel & Woodland 1998; Woodland & Angel 1998).
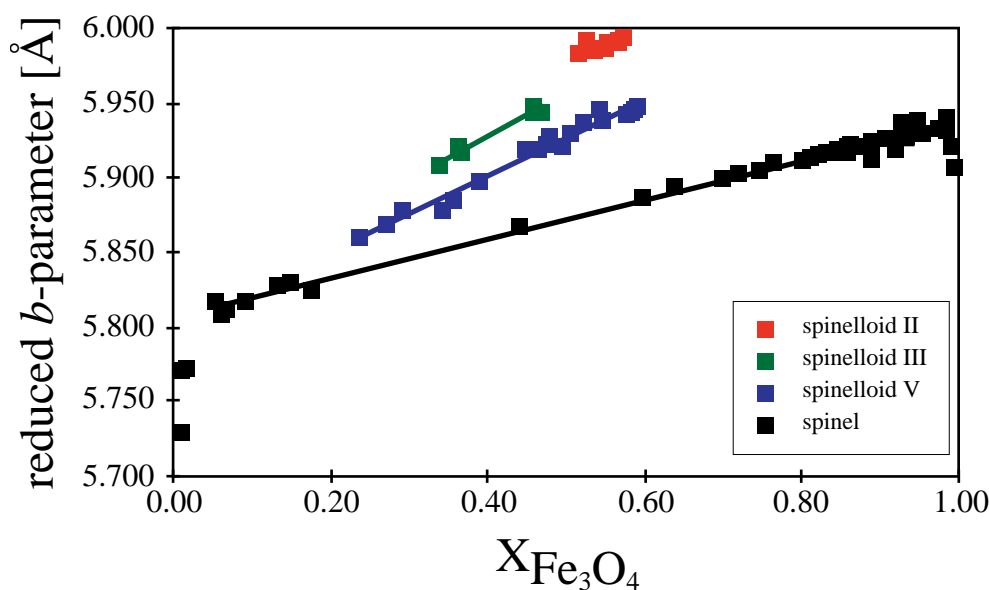
Fig. 5.5: Variation in the reduced *b*-parameter of spinel and all three spinelloid polytypes with $X_{Fe_3O_4}$. The scatter is due to variable Fe_2SiO_4 and Mg_2SiO_4 contents, which also influence the cell parameter. The lines are not fits to the data, but are meant to provide a visual guide for the compositional effects on the cell parameter. See text and Appendix 9.3 for details on the derivation of the reduced cell parameter.

The molar volumes of all three spinelloid polytypes decrease with decreasing Fe_3O_4 content (Fig. 5.6). The different behaviour observed in the *c*-parameter with $X_{Fe_3O_4}$ between spinelloids III and V is apparently more than compensated by the simultaneous decrease in the *b*-parameter (Fig. 5.5), leading to an overall reduction in molar volume with decreasing Fe_3O_4 content for both spinelloid polytypes. In addition, the incorporation of Mg in these phases leads to a significant reduction in unit-cell volume compared to spinelloids in the Mg-free system (Fig. 5.6). This is expected from the smaller ionic radius of Mg versus Fe^{2+} in octahedral coordination (Shannon 1976). The scatter in the data is attributable to variations in the Mg/Fe^{2+} ratios between the individual data points.

A detailed evaluation of the molar volume systematics of the three spinelloid polymorphs like that performed for spinel is hampered by a lack of sufficient data. However, combination of structural data from this study and from Woodland and Angel (2000) does allow a limited assessment, in particular the extraction of molar volumes for the hypothetical Fe_3O_4, Fe_2SiO_4 and Mg_2SiO_4 endmembers for spinelloids II, III and V under the assumption of ideal mixing in these phases. The first step in this analysis was to perform linear regressions of the volume data from Woodland and Angel (2000) for spinelloids in the Fe_3O_4–Fe_2SiO_4 subsystem to derive molar volumes for the hypothetical Fe_3O_4 and Fe_2SiO_4 endmembers. Then, in the same manner as done for spinel, application of equation 5.2.1 to volume data for the Mg-bearing spinelloids determined in this study give an estimate of $V°_{Mg_2SiO_4}$. The results of this procedure are summarised in Table 5.3. The very limited compositional range of spinelloid II in both the Fe_3O_4–Fe_2SiO_4 subsystem and in Mg-bearing compositions (see section 4.1) means that the estimation of the molar volumes of the hypothetical endmembers is subject to a large uncertainty for this phase.
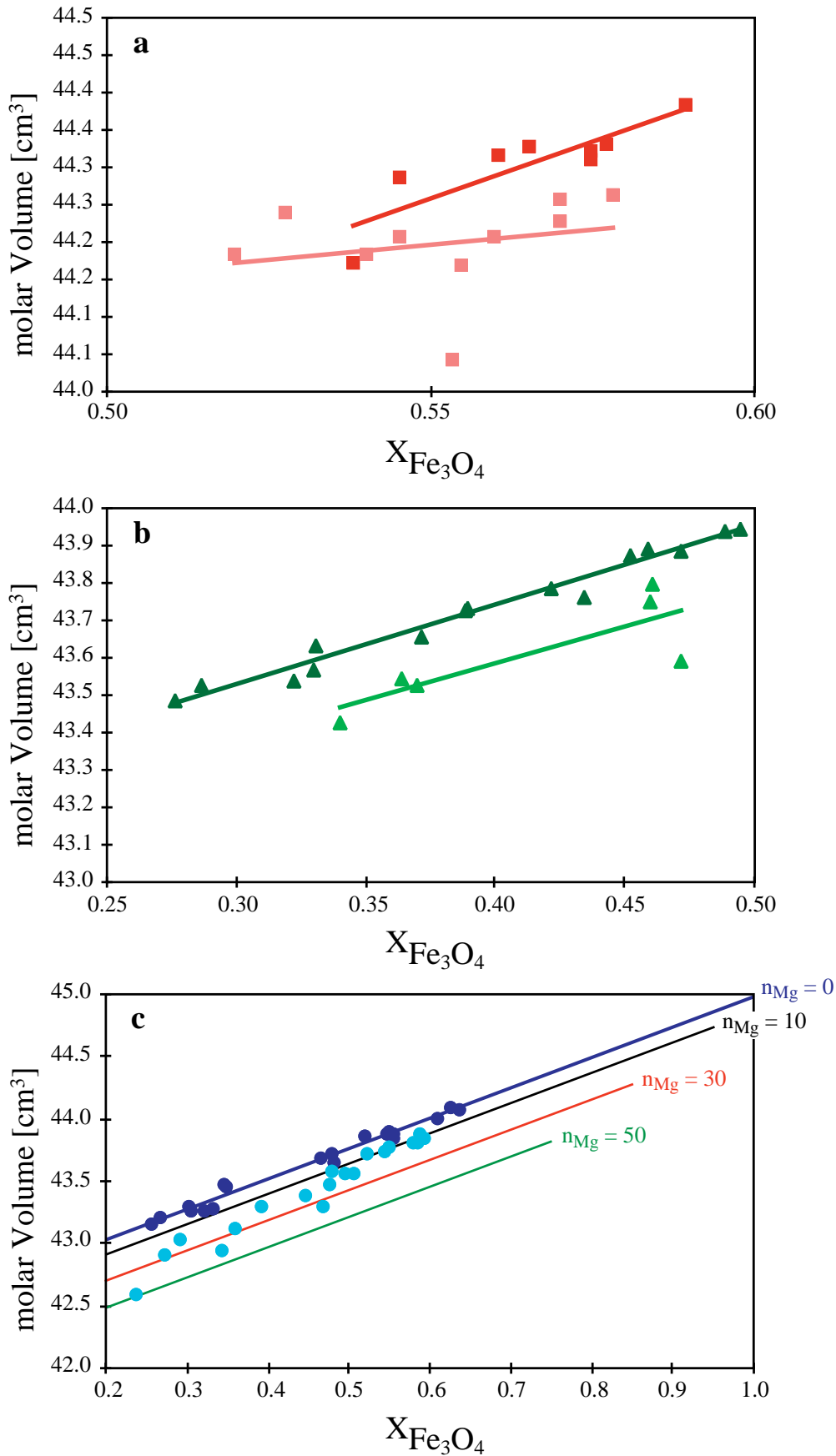
Fig. 5.6: Compositional dependence of the molar volumes of a) spinelloid II, b) spinelloid III and c) spinelloid V. The darker coloured data points are samples from the Mg-free system (Woodland & Angel 2000) and the lighter coloured data are from the Mg-bearing system (this study). The scatter is due to variable Fe_2SiO_4 and Mg_2SiO_4 contents, which also influence the molar volume. The lines are not fits to the data, but are meant to provide a visual guide for the compositional effects on the molar volume. In c) Mg-isopleths are shown, calculated assuming ideal mixing (see text).

For the spinelloid III structure, a number of measured values for $V°_{Mg_2SiO_4}$, as well as estimated values for $V°_{Fe_2SiO_4}$ exist in the literature (Table 5.3). The values of $V°_{Fe_2SiO_4}$ are based upon a long extrapolation of volume data for $(Mg,Fe)_2SiO_4$ wadsleyite solid solutions having compositions with $Fe^{2+}/(Fe^{2+}+Mg) \leq 0.25$ (Fig. 1.3). The estimate of $V°_{Fe_2SiO_4}$ derived from data of the Fe_3O_4–Fe_2SiO_4 subsystem should be more accurate since the available data lie closer in composition to this endmember ($X_{Fe_2SiO_4} = 0.50 - 0.72$, Woodland & Angel 2000). In addition, sufficient data are also available in this subsystem to test whether ideal mixing is a valid approximation for these spinelloids or not. A non-linear regression of 15 data points yielded $V°_{Fe_2SiO_4} = 43.04(21)$ cm^3 and $W_{V(mt-FeSi)} = -1.3(1.5)$ cm^3 with a $\chi^2 = 3.3$ (Table 5.3). The value of $W_{V(mt-FeSi)}$ lies within 1σ of zero, indicating that ideal mixing is a reasonable assumption for spinelloid III solid solutions along the Fe_3O_4–Fe_2SiO_4 binary, at least within the resolution of the available data. The rather large uncertainty is due to the absence of stable compositions that constrain behaviour near either of the endmembers. Although the fitted value of $V°_{Fe_2SiO_4}$ agrees within its uncertainty with literature values, it is recommended that the somewhat smaller value of $43.04(21)$ cm^3 be adopted since an even smaller value is obtained when assuming ideal mixing. The value of $V°_{Mg_2SiO_4}$ calculated using equation 5.2.1 is larger than measured values, but is in agreement within error (Table 5.3).

Table 5.3: Summary of molar volumes calculated for the different spinelloid polytypes.

Component	Phase	$V°$ [cm^3]	Reference
Fe_3O_4	spinelloid II	45.4(3)[a]	Woodland & Angel (2000)
Fe_2SiO_4	spinelloid II	43.0(7)[a]	Woodland & Angel (2000)
Fe_3O_4	spinelloid III	45.04(6)[a]	Woodland & Angel (2000)
Fe_2SiO_4	spinelloid III	42.89(10)[a]	Woodland & Angel (2000)
Fe_3O_4	spinelloid III	45.6(6)[b]	Woodland & Angel (2000)
Fe_2SiO_4	spinelloid III	43.04(21)[b]	Woodland & Angel (2000)
W_V (mt-FeSi)	spinelloid III	-1.3(1.5)[b]	Woodland & Angel (2000)
Fe_3O_4	spinelloid V	44.96(4)[a]	Woodland & Angel (2000)
Fe_2SiO_4	spinelloid V	42.53(8)[a]	Woodland & Angel (2000)
Fe_3O_4	spinelloid V	44.74(17)[b]	Woodland & Angel (2000)
Fe_2SiO_4	spinelloid V	42.27(12)[b]	Woodland & Angel (2000)
W_V (mt-FeSi)	spinelloid V	1.0(6)[b]	Woodland & Angel (2000)
Mg_2SiO_4	spinelloid II	41.3(1.3)[a]	this study
Mg_2SiO_4	spinelloid III	40.9(4)[a]	this study
Mg_2SiO_4	spinelloid V	40.4(3)[a]	this study
literature data			
Fe_2SiO_4	wadsleyite	43.08	Akaogi et al. (1989)
Fe_2SiO_4	wadsleyite	43.14	Fabrichnaya (1998)
Fe_2SiO_4	wadsleyite	43.15	Fei et al. (1991)
Fe_2SiO_4	wadsleyite	43.22	Jeanloz & Thompson (1983)
Mg_2SiO_4	wadsleyite	40.52	Jeanloz & Thompson (1983)
Mg_2SiO_4	wadsleyite	40.52	Horiuchi & Sawamoto (1981)
Mg_2SiO_4	wadsleyite	40.54	Fei et al. (1991)
Mg_2SiO_4	wadsleyite	40.54	Fabrichnaya (1998)

[a] value calculated assuming ideal mixing
[b] value calculated assuming a regular solid solution model

The large compositional gap observed between Mg-poor spinelloid III and Mg-rich wadsleyite (see section 4.1) suggests some non-ideal behaviour should exist, which could be responsible for the difference between the measured value of $V°_{Mg_2SiO_4}$ and that calculated here. However, the limited number of Mg-bearing spinelloid III samples (n = 8) and their restricted compositional range currently precludes a more detailed evaluation of possible non-ideal behaviour in these ternary compositions.

Spinelloid V is stable over a larger compositional range than spinelloids II and III in both the Fe_3O_4–Fe_2SiO_4 subsystem and in Mg-bearing compositions (e.g. Figs. 1.6, 4.9). Statistical analysis of data in Table 5.3 allows estimation of the molar volume of the hypothetical Mg_2SiO_4 endmember for the first time. However, to do this values for $V°_{Fe_2SiO_4}$ and $V°_{Fe_3O_4}$ must first be derived from the data in Woodland and Angel (2000) for Mg-free spinelloid V. A linear fit implying ideal mixing yields $V°_{Fe_2SiO_4}$ = 42.51(8) cm^3 and $V°_{Fe_3O_4}$ = 44.95(4) cm^3. Using these values together with data for the Mg-bearing spinelloid V samples listed in Table 4.3 and applying equation 5.2.1 gives $V°_{Mg_2SiO_4}$ = 40.4(3) cm^3. Substituting these V° values for the three endmembers in equation 5.2.1 permits theoretical molar volumes of spinelloid V solid solutions to be computed as a function of composition, as long as ideal mixing is valid. In this manner, isopleths of constant Mg content have been drawn in Figure 5.6c. In only a few cases are the data points inconsistent with the calculated isopleths.

A non-linear least squares regression of data from the Fe_3O_4–Fe_2SiO_4 subsystem following a regular solution model was performed to test for non-ideal behaviour. This yielded $W_{V(mt-FeSi)}$ = 1.0(6) cm^3 with a χ^2 = 8.5 (Table 5.3). The quite large calculated uncertainty and the associated large χ^2 value indicate that the data are not really sufficient to discern the extent of non-ideality with confidence ($W_{V(mt-FeSi)}$ lies < 2σ from zero). The probable reasons for the large uncertainty (poor fit) are scatter in the available data and the lack of data with compositions close to either endmember. Thus, although a certain degree of non-ideal behaviour is suggested from this analysis, it cannot be statistically resolved from the simpler case of ideal mixing. This means that evaluation of non-ideal mixing behaviour in the more complex Mg-bearing spinelloid V solid solutions is not currently feasible, and that the molar volumes of such compositions are best represented by an ideal mixing model, as illustrated by the isopleths in Figure 5.6c. Like for spinelloid III, synthesis of further compositions is needed to better constrain the solid solution behaviour of spinelloid V. However, it is likely that the necessary compositions lying near the Fe_2SiO_4, Fe_3O_4 and Mg_2SiO_4 endmembers are not stable, so that ideal mixing will remain the most reasonable mixing model for these spinelloids.

As a means to compare the volumes of solid solutions with the different spinelloid structures as well as with spinel a reduced volume parameter can be derived in a manner analogous to the derivation of the reduced *b*-parameter (see above and Appendix 9.3). Mirroring the relative behaviour of the reduced *b*-parameter, the reduced volume becomes smaller in the same sequence of phases: spinelloid II → spinelloid III → spinelloid V → spinel, for a given composition (Fig. 5.7). This is consistent with the relative stability of the spinelloid polymorphs with respect to pressure and reflects the stabilisation progressively denser structures with increasing pressure.
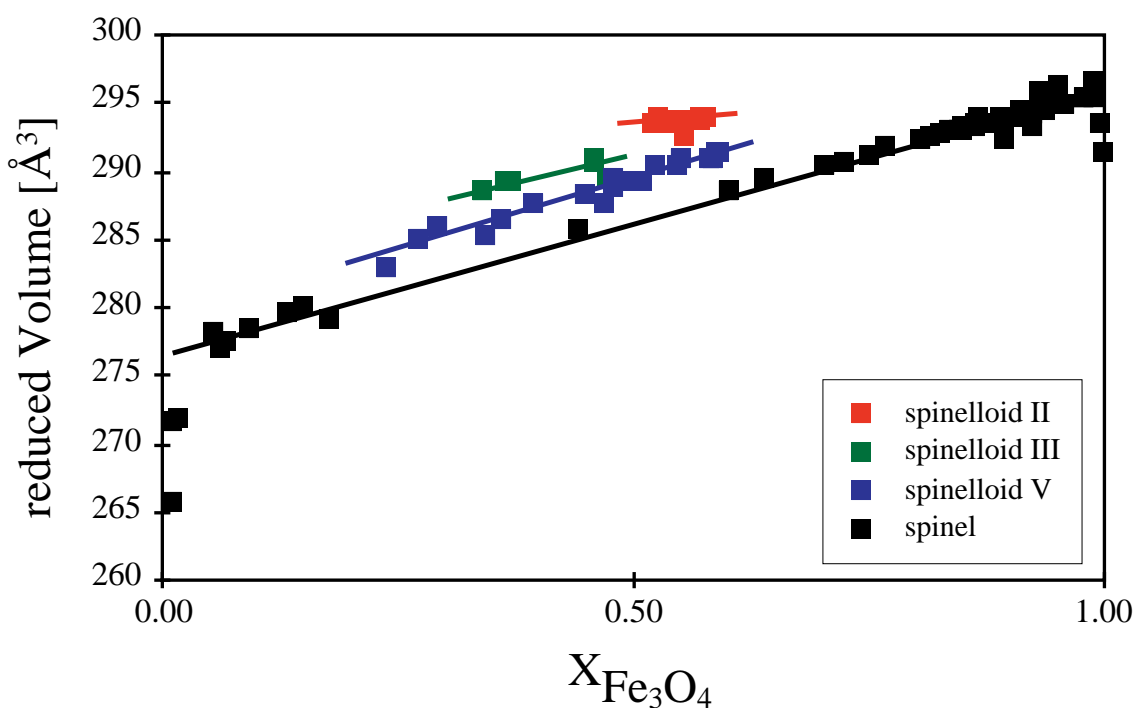
Fig. 5.7: Variation in the reduced volume of spinel and all three spinelloid polytypes with $X_{Fe_3O_4}$. The scatter is due to variable Fe_2SiO_4 and Mg_2SiO_4 contents, which also influence the cell volume. The lines are not fits to the data, but are meant to provide a visual guide for the compositional effects on the reduced volume. See text and Appendix 9.3 for details on the derivation of the reduced volume parameter.

5.2.3. Olivine

Olivine solid solutions exhibit a compositional variation in cell volume that is consistent with the data of Schwab and Küstner (1977), who synthesised their olivine solid solutions at atmospheric pressure (Fig. 5.8).

No systematic changes in this relation as a function of pressure have been observed, indicating that only negligible amounts of Fe^{3+} can be incorporated in olivine at high pressures, even in very Fe^{3+}-rich bulk compositions. In terms of the olivine composition, we find that no matter whether olivine coexists with spinelloid or spinel, its composition as measured by the microprobe begins to deviate slightly from ideal stoichiometry in the higher pressure experiments, where the bulk compositions studied were dominantly Mg-rich. Several samples were carefully reanalysed and didn't reveal any difference in chemical composition. This might suggest the incorporation of a small amount of Fe^{3+} (compare e.g. Fig. 4.2), however, considering the agreement with the molar volume data of Schwab and Küstner (1977), it would appear more likely that this small compositional deviation is an artefact, related either to the presence of finely divided Fe^{3+}-rich inclusions in the olivine or, more likely, to a small systematic problem with the microprobe calibration when analysing Mg-rich compositions. Further investigation of this issue is in progress by TEM analysis of selected samples.
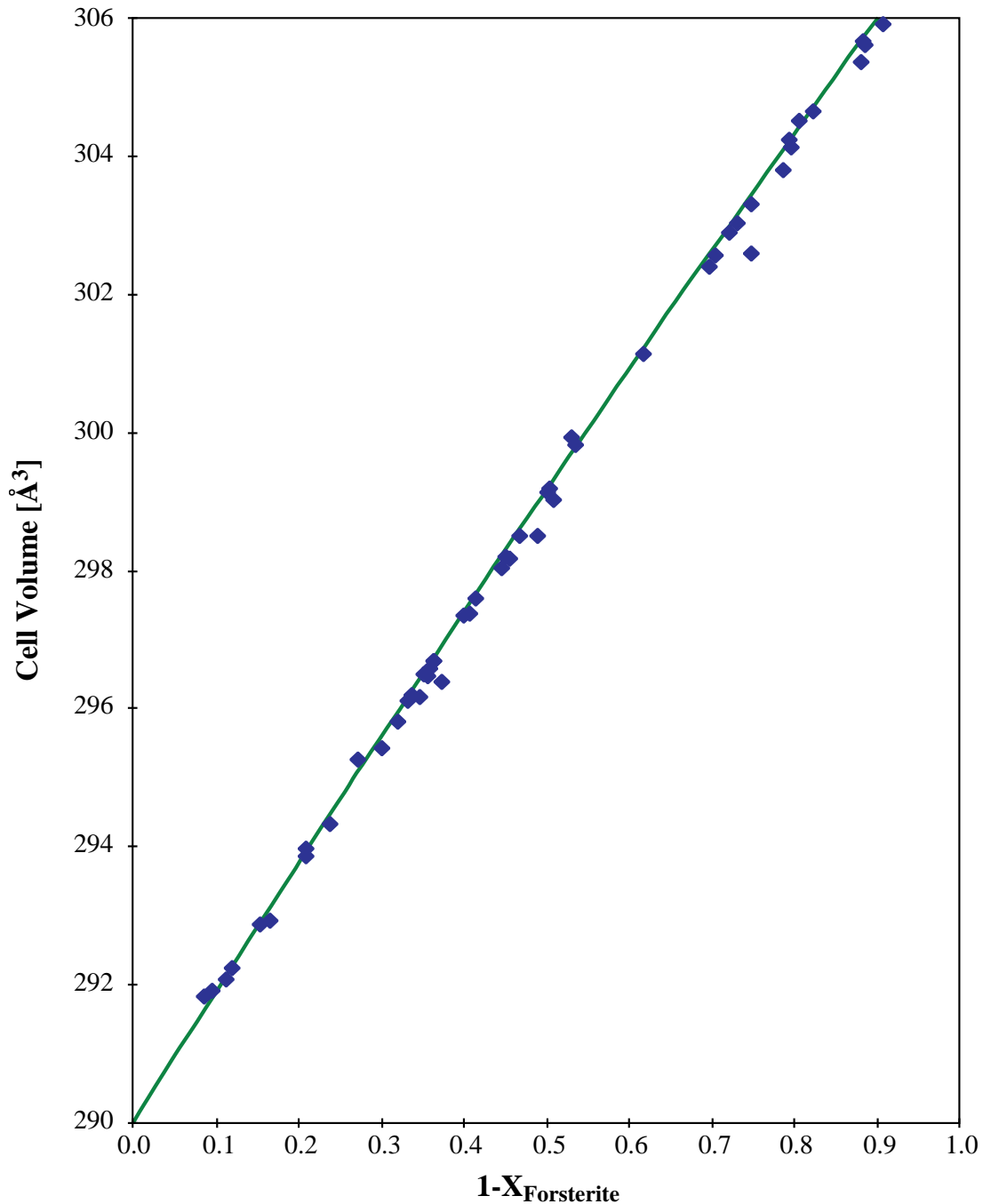
Fig. 5.8: Variation in the cell volume of olivine solid solutions as a function of composition. The green solid curve represents experimental data by Schwab and Küstner (1977). In general all synthesised olivines plot on this trend, indicating that olivine has not incorporated significant Fe^{3+} in its structure at high pressure.

5.3. T-dependent magnetic susceptibility of spinelloid and spinel solid solutions
Kontny et al. (2003)

The magnetic behaviour and Curie temperatures (T_C) of spinelloid and spinel solid solutions was investigated from magnetic susceptibility (MS) measurements in the temperature range from -192 to 700 °C. Samples used were from this study as well as from Woodland and Angel (2000). Only the most important results of these measurements will be described here. Further details can be found in Kontny et al. (2003).

5.3.1. Spinelloids

Spinelloid II is ferrimagnetic at room temperature and the MS measurements exhibit a characteristic critical temperature at 190 °C, which is perfectly reversible. This critical temperature is also observed in Mg-bearing samples along with a second transition temperature appearing at lower temperatures. The position of this lower transition temperature is compositionally dependent. Spinelloid III is paramagnetic over nearly the entire temperature range with a possible Néel temperature below -200 °C. Based on its crystal structure, spinelloid III is expected to have a perfect antiferromagnetic behaviour below its Néel temperature. However, the results are ambiguous due to the very weak signal from the samples investigated and further studies are needed to better understand the magnetic properties of this polytype. Mg-free spinelloid V is paramagnetic at room temperature and hysteresis loops at various low temperatures indicate that a ferri- to superparamagnetic transition occurs before reaching the T_C. The T_C varies nonlinearly with decreasing magnetite content from -50 to -183 °C (Fig. 5.9). The substitution of Mg in spinelloid V further decreases the T_C (Fig. 5.9), consistent with a diluting effect of Mg on Fe^{2+} in the octahedral sublattice. It is also known from Mössbauer spectroscopy (Woodland, personal communications) that spinelloid II and III are ferrimagnetic and paramagnetic, respectively and that spinelloid V is dominantly paramagnetic with a small ferrimagnetic component. These observations are in excellent agreement with the MS measurements. A contribution of spinelloids II and V to deep magnetic anomalies in the Earth's lithosphere can be excluded since they loose their magnetisation at relatively low temperatures. However, their relevance for magnetic anomalies on other planets such as Mars, where these high-pressure minerals could survive their exhumation or were formed by meteorite impacts, has to be further investigated.
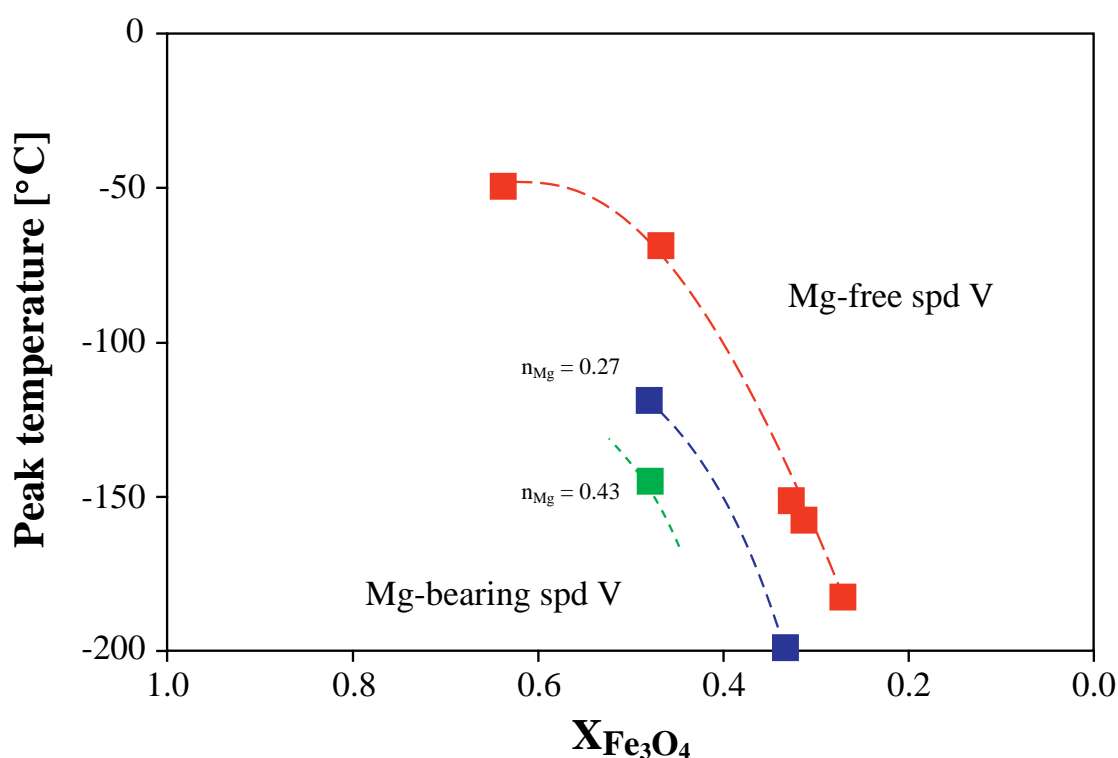
Fig. 5.9: Peak temperature plotted as a function of magnetite content in spinelloid V. Red squares resemble Mg-free, blue and green squares Mg-bearing spinelloid V samples. n_{Mg} refers to Mg cations calculated on the basis of 4 oxygens. Figure has been modified after Kontny et al. (2003).

5.3.2. Spinel

Spinels have T_C peaks between -261 and 580 °C, depending on their composition (Fig. 5.10); the temperature gradually decreasing with increasing Si content. Yamanaka and Okita (2001) postulated a ferrimagnetic to antiferromagnetic transition between compositions of $X_{Fe_3O_4} = 0.64$ and 0.21. The new set of measurements indicate that spinel is ferrimagnetic at least to a composition of $X_{Fe_3O_4} = 0.20$, dramatically narrowing the position of the magnetic transition to a range of ~10 mol % magnetite content (Fig. 5.10). Nevertheless it appears that the magnetic transition at $X_{Fe_3O_4} < 0.20$ is gradual rather than abrupt.
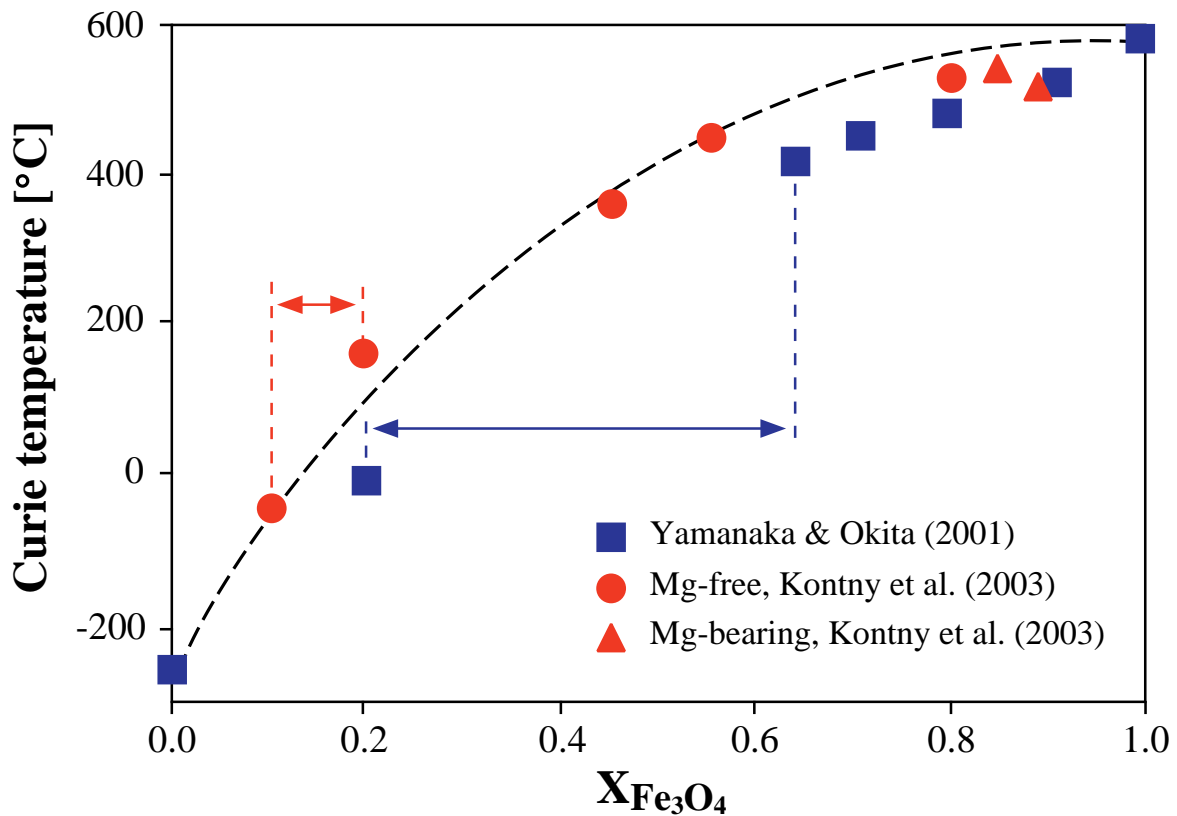
Fig. 5.10: Variation of Curie temperature of Mg-free and Mg-bearing spinel solid solutions as a function of composition. Blue and red colored arrows show the predicted compositional ranges where the ferrimagnetic to antiferromagnetic transition is supposed to occur according to Yamanaka and Okita (2001) and Kontny et al. (2003), respectively. Figure has been modified after Kontny et al. (2003).

6. Implications for the Earth's mantle

An important goal of this study is to better understand the effect of Fe^{3+} on the mineral assemblages expected to be present in the Earth's upper mantle and transition zone. In an essentially Fe^{3+}-free pyrolitic mantle model (see Fig. 1.1) the upper part of the transition zone should be composed of wadsleyite and majoritic garnet, while the lower portion should contain ringwoodite, majoritic garnet, and small amounts of Ca-Si-perovskite and ilmenite (e.g. Irifune & Ringwood 1987; Ringwood 1991). Spectroscopic measurements on mantle garnets (e.g. Luth et al. 1990; Canil & O'Neill 1996; Woodland & Koch 2003), as well as experimental data on synthetic majoritic garnets (O'Neill et al. 1993) indicate that substantial quantities of ferric iron can be accommodated in this phase. The phase relations determined for the Fe_2SiO_4–Mg_2SiO_4–Fe_3O_4 system reveal that the various intermediate spinelloid phases are stable only in Fe-rich bulk compositions, which are incompatible with a pyrolitic mantle (see section 4.1). $(Mg,Fe)_2SiO_4$-wadsleyite and the isostructural spinelloid III have distinctly separate stability fields in terms of composition and pressure and this suggests that substitution of Fe^{3+} in wadsleyite may be limited to a greater extent than suggested by Woodland and Angel (2000). However, this is not to say that the incorporation of Fe^{3+} into wadsleyite is unimportant or insignificant. For example, the four wadsleyites synthesised in this study contain 0.02-0.06 cations per formula unit Fe^{3+}, which corresponds to a $Fe^{3+}/\Sigma Fe = 0.05$-0.10 (Table 4.1). In addition, O'Neill et al. (1993) demonstrated that measureable amounts of Fe^{3+} can be incorporated in wadsleyite, even in the presence of Fe-metal and Fei et al. (1992) found $Fe^{3+}/\Sigma Fe = 0.08$ in their wadsleyite sample, which is similar to that found here. Canil et al. (1994) estimated a bulk $Fe^{3+}/\Sigma Fe = 0.035$ (i.e. 3.5% of the total Fe present is in the ferric form) for the primitive upper mantle. Assuming that the transition zone has the same bulk composition, a uniform distribution of Fe^{3+} among the phases present would imply ~0.25 wt% Fe_2O_3 in wadsleyite with a nominal composition of $X_{Mg_2SiO_4} = 0.9$, corresponding to ~0.005 cations per formula unit Fe^{3+}. This is significantly less than the maximum Fe^{3+} content observed in this study (see above) and suggests that although substitution of Fe^{3+} is rather limited in $(Mg,Fe)_2SiO_4$-wadsleyite, this phase can accommodate much more than the expected amount of Fe^{3+} present in the transition zone. This supports the assumption of a generally uniform distribution of ferric iron among the phases of the transition zone assemblage.

The incorporation of Fe^{3+} in wadsleyite involves a Fe_3O_4 component in the same fashion as is observed in spinelloid III, making spinelloid III indirectly relevant to the Earth's mantle from a crystal chemical point of view. The estimated molar volumes for the hypothetical Fe_2SiO_4 and Fe_3O_4 endmembers with the spinelloid III structure extracted from the data in this study are important input parameters for modelling the stabilities of transition zone assemblages. A small extrapolation of the results of Fei et al. (1991) from 1200 °C to 1100 °C for the nominally Fe^{3+}-free system (Fig. 1.3), places the olivine-wadsleyite phase transition at ~12.5 GPa. The observed stability of Fe^{3+}-wadsleyite at 12.0 GPa (sample 4f1v0233) at 1100 °C indicates that the presence of Fe^{3+} stabilises wadsleyite to somewhat lower pressures. In fact, the present results in Fe^{3+}-bearing compositions only constrain the phase boundary to lie between 10.5 and 12.0 GPa (Table 4.1), so that a shift of ~0.5 GPa must be considered as a minimum effect of Fe^{3+} incorporation in wadsleyite. Therefore, the presence of even

fairly small amounts of Fe^{3+} could cause a shift in the position of the olivine-wadsleyite phase transition and the "410 km" discontinuity to shallower depths, up to 15 km or more. However, the low Fe^{3+} contents expected in a primitive mantle bulk composition means that a noticeable shift would only occur locally in regions of relatively oxidised mantle, possibly in close proximity to subducting slabs. Unfortunately, the lack of experiments containing coexisting olivine and wadsleyite means that a further assessment of the width of the olivine-wadsleyite two-phase field in the presence of Fe^{3+} is not posssible. This is an important consideration since the addition of an extra component, such as Fe^{3+}, can in principle expand the pressure interval over which the two-phase field exists, thereby reducing the sharpness of the seismic discontinuity to the point where it is no longer discernible in seismic data. However, the observed amounts of Fe^{3+} in wadsleyite are quite small, making it unlikely that pressure interval of two-phase field will expand significantly.

Aside from $(Mg,Fe)_2SiO_4$-wadsleyite, spinelloid V has the highest pressure stability of any of the intermediate spinelloid phases found in the Mg_2SiO_4–Fe_2SiO_4–Fe_3O_4 ternary system. Its high-pressure stability limit is also expected to increase with increasing temperature. In addition, spinelloid V possesses the largest compositional range of any spinelloid polytype and can incorporate more Mg than either spinelloid II or III. At 9.0 GPa, spinelloid V can coexist with olivine having a composition of $X_{fo} = 0.72$, suggesting that spinelloid V could be present locally as an additional phase in the mantle assemblage in the deepest parts of the upper mantle and the upper portions of the transition zone where Fe enrichment, including Fe^{3+}, has occurred through metasomatic interaction (Table 4.1). It is conceivable that spinelloid V could be further stabilised by the incorporation of other cations such as Cr or Mn, the effects of which are currently unknown. As yet, there is no report of this phase in the rare natural samples that likely originated in the transition zone (i.e. inclusions in diamond). However, it is possible that this phase could either be mistaken for a spinel solid solution or it could react during the ascent to a mixture of olivine and spinel.

The local addition of significant amounts of Fe^{3+} through metasomatism could potentially stabilise either spinelloid V or even produce a Mg-bearing magnetite-rich spinel that can coexist with olivine, wadsleyite or ringwoodite. Interestingly, this additional spinel phase would be essentially Si-free in such Mg-rich compositions, which is contrary to the conventional expectation that high-P spinel should contain a significant amount of Si. However, for this to happen in the transition zone the fO_2 of the metasomatic agent must be very high in order to introduce enough Fe^{3+} to saturate wadselyite or ringwoodite. If this were to occur, the resulting fO_2 in the localised domain would be significantly higher than the surrounding ambient mantle, which could potentially be low enough for a metallic alloy phase to be stable (Woodland & Koch 2003). The high thermodynamic activity of an Fe^{3+} component in a minor phase of the mineral assemblage, such as magnetite-rich spinel, would reinforce the elevating effect on the resulting fO_2 (see O'Neill et al. 1993).

Another important aspect related in part to the oxidation state of the Earth's mantle is the possible protonation of nominally anhydrous mantle phases such as pyroxene, garnet, wadsleyite and ringwoodite (e.g. Rossman & Smyth 1990; Skogby et al. 1990; McMillan et al. 1991; Smyth 1987;

Knittle et al. 1993). The presence of water in the mantle can have numerous important chemical and physical effects including the depression of the rock solidus, leading to partial melting, changes in chemical differentiation, a decrease in magma viscosity and density, changes in seismic wave velocities and anisotropy, as well as changing the bulk electrical conductivity (e.g. Richard et al. 2002). Smyth (1994) and Kudoh et al. (1996) have demonstrated that significant OH can be incorporated in Mg_2SiO_4-wadsleyite and that the substitution of OH for O occurs uniquely on the O1 site. This site is the only O site bonded solely to octahedrally coordinated cations and implies a maximum H_2O content of 3.3 wt% when this site is completely occupied by OH groups. The theoretical maximum H_2O solubility has been experimentally confirmed by Inoue et al. (1995) with charge balance achieved by the formation of vacancies on the octahedral sites. However the presence of Fe^{3+} permits a further substitution mechanism to be considered in which Si + O are replaced by Fe^{3+} + OH via a coupled tetrahedral substitution that at the same time provides an adequate charge balancing mechanism (Woodland & Angel 2000). If this mechanism occurs, it could increase the number of sites in the structure where OH can be accommodated, thus elevating the maximum H_2O content above the theoretical maximum suggested by Smyth (1994) and Kudoh et al. (1996). With increasing pressure a third mechanism suggested by Prewitt and Finger (1993) could play an important role as well in which Si undergoes a transformation from four- to six-fold coordination that would permit hydrogen to be retained under extreme conditions. Although this mechanism is probably not relevant for wadsleyite, it could be important for OH incorporation in ringwoodite.

A new hydrous spinelloid phase, named hydrous wadsleyite II, was experimentally produced in a synthetic natural bulk compostion by Smyth and Kawamoto (1997). It has a structure closely related to spinelloid III, but with an expanded unit-cell in the *b*-direction. This phase is now considered to have the spinelloid IV structure (Smyth 2003, pers. comm.). The stability of this phase has been linked to the presence of Fe, particularly Fe^{3+} (Smyth & Kawamoto 1997) and emphasises the complex crystal chemistry of spinelloid phases and the close relationship between Fe^{3+} and OH in these structures. Whether other phases, such as spinelloid V, can be stabilised in more Mg-rich compositions (i.e. more mantle relevant compositions) or to higher pressures by the incorporation of OH awaits further investigation. In any case, this demonstrates the potential petrological importance of the entire family of spinelloid structures.

It is known that the magnetic and electrical properties of mixed oxides with the spinel structure, here in particular Mg-rich silicate spinels and magnetite-rich Mg-ferrites, are strongly dependent on the exact cation distribution and presence of vacancies within the structure (e.g. Lorimier et al. 2002). More detailed studies on single crystals of these phases need to be performed using for example TEM and in situ high-P and high-T XRD techniques in order to accurately determine their likely properties under mantle conditions. In addition, the potentially strong influence that a locally occurring magnetite-rich spinel phase could have on the electrical conductivity of the deepest portions of the upper mantle and transition zone would depend on its connectivity within the assemblage. Its abundance and distribution would be related to the local fO_2 and textural features, respectively.

7. Summary

Experiments in the system Mg_2SiO_4–Fe_2SiO_4–Fe_3O_4 produced three intermediate phases that are stable between ~4.0 and 9.0 GPa and 1100 °C. These phases are different spinelloid polytypes and are structural analogues to spinelloids II, III and V in the Ni-aluminosilicate system (Akaogi et al. 1982). The additional spinelloid polytypes I and IV, which are stable in the Ni-aluminosilicate system were not found in the ternary system studied here. The behaviour of spinelloid III was of particular interest since it is isostructural with the important mantle phase $(Mg,Fe)_2SiO_4$-wadsleyite. Spinelloid II is the first intermediate phase to appear at low pressures in Mg-poor compositions. With increasing pressure spinelloid II is replaced by an isochemical spinelloid V polytype between 6.0 and 6.5 GPa. Spinelloid III is relatively Si-rich and, depending on pressure, can coexist with either spinelloid II or V. At 1100 °C, spinelloid III gives way to the assemblage olivine + spinelloid V between 7.5 and 8.0 GPa and its maximum Mg content is limited to ~0.15 mol % Mg_2SiO_4 at 7.5 GPa. Thus there is a very large gap in composition and pressure separating the stability fields of spinelloid III and $(Mg,Fe)_2SiO_4$-wadsleyite. In general, the addition of Mg or an increase in temperature acts to shift the phase stabilities of the spinelloids to higher pressures. The stabilities of the spinelloid phases are limited to pressures < 10.0 GPa at 1100 °C. At 12.0 GPa, olivine is replaced by wadsleyite, that coexists with a spinel that contains a significant $MgFe_2O_4$ component. The stable compositional range of wadsleyite is rather narrow and corresponds well with the results from Fei et al. (1991). At 16.0 GPa ringwoodite replaces wadsleyite as the stable Si-rich phase. It also can coexist with a $MgFe_2O_4$-bearing spinel. The ringwoodite-wadsleyite two-phase field was not encountered in any experiment, but must be rather narrow, on the order of ~2.0 GPa, corresponding to a depth interval of ~60 km. It appears that the presence of Fe^{3+} has very little influence on the occurrence of this phase transition. Also no compelling evidence was found for the incorporation of significant amounts of Fe^{3+} in olivine, even at very high pressures. In Mg-rich compositions more relevant to the Earth's mantle, no spinelloid phase was found except for $(Mg,Fe)_2SiO_4$-wadsleyite at ≥ 12.0 GPa, and the assemblage $olivine_{ss}$ + $spinel_{ss}$ is stable over a wide range of pressure. In such bulk compositions, the Fe^{3+}-rich spinel is practically Si-free and contains a Mg-ferrite component. Thus there appears to be a mutual incompatibility between the Mg_2SiO_4 and Fe^{3+}-rich components in high-pressure spinels. It is conceivable that the presence of Fe^{3+} in a mantle assemblage (e.g. through metasomatism) could stabilise small quantities of either spinelloid V or a magnesioferrite-bearing spinel in equilibrium with olivine. Unlike the spinel that is considered to be present in the lower parts of the transition zone, this phase will contain little or no Si.

The interphase partitioning of Fe^{2+} and Mg for different mineral pairs yields consistent results with respect to bulk composition. Orthopyroxene, which appeared in experiments due to a minor amount of oxidation, exhibits Mg-Fe^{2+} partitioning with olivine in agreement with the experiments of von Seckendorff and O'Neill (1993). This indicates that despite minor oxidation in some experiments, Mg-Fe^{2+} equilibrium was achieved, at least on a local scale. The absence of any noticeable pressure dependence on partitioning between the spinelloid polytypes and spinel, suggests that these phases have only small, if any excess volumes of mixing.

X-ray diffraction patterns were obtained for all experimental run products to permit phase identification. In addition, structural parameters were derived by full-pattern Rietveld refinement. As expected, the unit-cells of the three spinelloid polytypes become smaller with the incorporation of Mg, due to its smaller ionic radius compared to Fe^{2+}. The most sensitive parameter is the *b*-parameter, which is distinct for each spinelloid polytype. This is because the spinelloid family of structures are related to each other by different stacking sequences of a common "basic structural unit" in the *b*-direction (e.g. Horiuchi et al. 1982). For a given spinelloid polytype, the *b*-parameter progressively decreases with decreasing Fe_3O_4 content, as does its unit-cell volume. Relative to a hypothetical Fe_3O_4 endmember, the incorporation of a Fe_2SiO_4 component lowers the unit-cell volume and the presence of a Mg_2SiO_4 component lowers it still further. The compositionally restricted stability fields of the different spinelloids indicate that their structures can only tolerate a limited amount of solid solution. Molar volumes for the hypothetical endmembers Fe_3O_4, Fe_2SiO_4 and Mg_2SiO_4 were derived by combination of structural data determined in this study and literature data (e.g. Woodland & Angel 2000). Although statistical analysis of the spinelloid III and V volume data suggest a small amount of non-ideal mixing behaviour, the resolution of available data does not yield a very reliable fit of the excess volumes and, at this point, these solid solutions should be considered to mix ideally. This permits a simple model to be used to predict molar volumes for the hypothetical endmember components and for any composition in the Mg_2SiO_4–Fe_2SiO_4–Fe_3O_4 ternary system. A molar volume of $43.04(21)$ cm^3 for Fe_2SiO_4 with the spinelloid III (wadsleyite) structure is proposed, which is somewhat smaller than previous estimates (e.g. Fei et al. 1991). Molar volumes of the hypothetical Mg_2SiO_4 endmember of spinelloid II and V have been derived for the first time, giving values of $V° = 41.3(1.3)$ and $40.4(3)$ cm^3, respectively.

Assessment of the composition–molar volume systematics in spinel is complicated by the fact that a subset of synthesised spinels contain a $MgFe_2O_4$ component as indicated by the fact that these spinels contain less Si than is necessary to produce a Mg_2SiO_4 component with the available Mg. Thus not all spinels produced in this study can be represented by the same three endmember components. Two sets of components were considered in the evaluation of the molar volume data of the spinel solid solutions, Fe_3O_4–Fe_2SiO_4–Mg_2SiO_4 and Fe_3O_4–Fe_2SiO_4–$MgFe_2O_4$, with many spinel compositions being able to be described by both sets. The assumption of ideal mixing behaviour comes reasonably close to describing the data, particularly for the set of spinels that can be represented by the Fe_3O_4, Fe_2SiO_4 and $MgFe_2O_4$ endmember components. However, a discrepancy between the calculated molar volume of the Mg_2SiO_4 endmember and published measurements suggests that modelling the spinel solid solutions requires an additional term to account for excess volumes of mixing. In fact, slightly non-ideal behaviour was previously reported for spinels in the Fe_3O_4–Fe_2SiO_4 subsystem by Woodland and Angel (2000). Using their result of $W_{V(mt-FeSi)} = -0.15(6)$ cm^3 for this binary, the regression of data from this study allowed Margules parameters to be derived for the other two binary systems, Fe_2SiO_4–Mg_2SiO_4 and Fe_3O_4–Mg_2SiO_4: $W_{V(FeSi-MgSi)} = 0.25(5)$ cm^3 and $W_{V(mt-MgSi)} = 1.6(5)$ cm^3. The much larger degree of non-ideality along the Fe_3O_4–Mg_2SiO_4 binary is consistent with the observed phase relations, where a large miscibility gap appears to be present between those Mg-

bearing spinels that are Si-rich and those that are Fe^{3+}-rich. A similar assessment using Fe_3O_4, Fe_2SiO_4 and $MgFe_2O_4$ as components confirmed the suggestion of virtually ideal behaviour in magnetite-magnesioferrite spinels. The result of the least squares regression was not wholly satisfying in that the parameter for the Fe_2SiO_4–$MgFe_2O_4$ binary, $W_{V(FeSi-mf)} = 10(43)$ cm^3, has an unacceptably large uncertainty due to the near absence of spinels in the data set that have compositions lying near to this join, compromising the ability to reasonably constrain this parameter.

A reduced molar volume parameter can be computed for each spinelloid polytype as well as for spinel, which represents the volume of common structural slabs and affords a direct comparison between these different structures. At constant composition, the following sequence is apparent: $V_{spd\ II} \rightarrow V_{spd\ III} \rightarrow V_{spd\ V} \rightarrow V_{sp}$. This mirrors the stabilities of these phases in terms of pressure, with denser packed structures becoming stable at progressively higher pressures.

This study further illustrates that simple chemical systems can have complex phase relations and that the physical properties of the stable phases can be complicated. In terms of the Earth's mantle, it is apparent that only limited amounts of Fe^{3+} can be incorporated in $(Mg,Fe)_2SiO_4$-wadsleyite, which is considered to be an important phase in the upper portion of the transition zone. However, considering the small amount of Fe^{3+} estimated to be present in a primitive mantle bulk composition, wadsleyite should have no difficulty incorporating its "share". Thus it is concluded that the Fe^{3+} budget will be distributed over the entire transition zone assemblage, leading to low Fe^{3+} contents in all phases. This also would mean low activities of Fe^{3+} components in the assemblage phases, which will act to keep the fO_2 of this part of the mantle low, potentially at the condition of metal saturation. In regions where the amount of Fe^{3+} is elevated through metasomatism, for example, a $MgFe_2O_4$-bearing spinel or spinelloid V might become locally stabilised. The discovery of a new type of Fe^{3+}-rich spinelloid related to the wadsleyite structure in experiments with a water-bearing synthetic natural bulk composition (hydrous wadsleyite II, Smyth & Kawamoto 1997), suggests a relationship between Fe^{3+} and OH incorporation in nominally anhydrous minerals. In addition, it emphasises the importance of studying the stabilities, crystal chemistry and properties of spinelloid phases, including wadsleyite since their stabilities could be influenced by the presence of minor elements such as Mn, Cr, or even H_2O.

8. References

Akaogi M, Akimoto S, Horioka K, Takahashi K, Horiuchi H (1982) The system $NiAl_2O_4$–Ni_2SiO_4 at high pressures and temperatures: spinelloids and spinel-related structures. J Solid State Chem 44: 257-267

Akaogi M, Ito E, Navrotsky A (1989) Olivine-modified spinel-spinel transitions in the system Mg_2SiO_4–Fe_2SiO_4: Calorimetric measurements, thermochemical calculation, and geophysical application. J Geophys Res 94: 15671-15685

Andrault D, Bolfan-Casanova N (2001) High-pressure phase transformations in the $MgFe_2O_4$ and Fe_2O_3–$MgSiO_3$ systems. Phys Chem Mineral 28: 211-217

Angel RJ, Woodland AB (1998) Crystal structure of spinelloid II in the system Fe_3O_4–Fe_2SiO_4. Eur J Mineral 10: 607-610

Barbier J (1989) New spinelloid phases in the $MgGa_2O_4$–Mg_2GeO_4 and $MgFe_2O_4$–Mg_2GeO_4 systems. Eur J Mineral 1: 39-46

Bina C, Wood BJ (1987) The olivine-spinel transition: Experimental and thermodynamic constraints and implications for the nature of the 400-km discontinuity. J Geophys Res 92: 4853-4866

Brey GP, Weber R, Nickel KG (1990) Calibration of a belt apparatus to 1800 °C and 6 GPa. J Geophys Res 95: 15603-15610

Canil D (1994) An experimental calibration of the "nickel in garnet" geothermometer with applications. Contrib Mineral Petrol 117: 410-420

Canil D, O'Neill HStC (1996) Distribution of ferric iron in some upper mantle assemblages. J Petrol 37: 609-635

Canil D, O'Neill HStC, Ross II CR (1991) A preliminary look at phase relations in the system γ-Fe_2SiO_4–Fe_3O_4 at 7 GPa. Terra Abstr 3: 65

Canil D, O'Neill HStC, Pearson DG, Rudnick R, McDonough WF, Carswell DA (1994) Ferric iron in peridotites and mantle oxidation states. Earth Planet Sci Lett 123: 205-220

Fabrichnaya O (1998) The assessment of thermodynamic parameters for solid phases in the Fe–Mg–O and Fe–Mg–Si–O systems. Calphad 22: 85-125

Fei Y, Mao H, Mysen BO (1991) Experimental determination of element partitioning and calculation of phase relations in the MgO–FeO–SiO_2 system at high pressure and high temperature. J Geophys Res 96: 2157-2169

Fei Y, Mao H-K, Shu J, Parthasarathy G, Bassett WA (1992) Simultaneous high-P, high-T X-ray diffraction study of β-$(Mg,Fe)_2SiO_4$ to 20 GPa and 900 K. J Geophys Res 97: 4489-4495

Fei Y, Frost DJ, Mao H-K, Prewitt CT, Häusermann D (1999) In situ structure determination of the high-pressure phase of Fe_3O_4. Am Mineral 84: 203-206

Flanagan MP, Shearer PM (1998) Global mapping of topography on transition zone velocity discontinuities by stacking *SS* precursors. J Geophys Res 103: 2673-2692

Frost DJ, Langenhorst F, van Aken PA (2001) Fe–Mg partitioning between ringwoodite and magnesiowüstite and the effect of pressure, temperature and oxygen fugacity. Phys Chem Mineral 28: 455-470

Gill R (1997) Electron beam methods. In: Gill R (ed) Modern analytical geochemistry - an introduction to quantitative chemical analysis for earth, environmental and materials scientists. Longman Publishing, Singapore, 215-234

Hammond R, Barbier J (1991) Spinelloids in the nickel gallosilicate system. Phys Chem Mineral 18: 184-190

Hazen RM, Finger LW, Ko J (1992) Crystal chemistry of Fe-bearing anhydrous phase B: Implications for transition zone mineralogy. Am Mineral 77: 217-220

Hill RJ, Craig JR, Gibbs GV (1979) Systematics of the spinel structure type. Phys Chem Mineral 4: 317-319

Horioka K, Takahashi K-I, Morimoto N, Horiuchi H (1981a) Structure of Nickel Aluminosilicate (Phase IV): A high-pressure phase related to spinel. Acta Cryst B37: 635-638

Horioka K, Nishiguchi M, Morimoto N, Horiuchi H (1981b) Structure of Nickel Aluminosilicate (Phase V): A high-pressure phase related to spinel. Acta Cryst B37: 638-640

Horiuchi H, Sawamoto H (1981) β-Mg_2SiO_4: Single-crystal X-ray diffraction study. Am Mineral 66: 568-575

Horiuchi H, Horioka K, Morimoto N (1980) Spinelloid: A systematics of spinel-related structures obtained under high-pressure conditions. J Mineral Soc Jpn 14: 253-264

Horiuchi H, Akaogi M, Sawamoto H (1982) Crystal structure studies on spinel-related phases, spinelloids: Implications to olivine-spinel phase transformation and systematics. In: Akimoto S, Manghnani MH (eds) High-Pressure Research in Geophysics, Advances in Earth and Planetary Sciences 12, Center for Academic Publishing Japan, Tokyo, 391-403

Hugh-Jones DA, Woodland AB, Angel RJ (1994) The structure of high-pressure C2/c ferrosilite and crystal chemistry of high-pressure C2/c pyroxenes. Am Mineral 79: 1032-1041

Inoue T, Yurimoto H, Kudoh Y (1995) Hydrous modified spinel, $Mg_{1.75}SiH_{0.5}O_4$: a new water reservoir in the mantle transition region. Geophys Res Lett 22: 117-120

Irifune T, Ringwood AE (1987) Phase transformations in primitive MORB and pyrolite compositions to 25 GPa and some geophysical implications. In: Manghnani MH, Syono Y (eds) High Pressure Research in Mineral Physics, Geophys Monograph 39, Am Geophys Union, Washington DC, 231-242

Ito E, Yamada H (1982) Stability relations of silicate spinels, ilmenites and perovskites. In: Akimoto S, Manghnani MH (eds) High-pressure research in geophysics. Center Acad Publ Jap, Tokyo, 405-419

Jeanloz R, Thompson AB (1983) Phase transitions and mantle discontinuities. Rev Geophys 21: 51-74

Katsura T, Ito E (1989) The system Mg_2SiO_4–Fe_2SiO_4 at high pressures and temperatures: Precise determination of stabilities of olivine, modified spinel, and spinel. J Geophys Res 94: 15663-15670

Knittle E, Hathorne A, Davis M, Williams Q (1993) A spectroscopic study of the high-pressure behaviour of the O_4H_4 substitution in garnet. In: Syono Y, Manghnani MH (eds) High Pressure

Research: Application to Earth and Planetary Sciences, Geophys Monograph 67, Am Geophys Union, Washington DC, 297-304

Koch M, Woodland AB, Angel RJ (2003) Stability of spinelloid phases in the system Mg_2SiO_4–Fe_2SiO_4–Fe_3O_4 at 1100 °C and up to 10.5 GPa. In: Rubie D, Duffy T, Ohtani E (eds) Special Volume of Physics of the Earth and Planetary Interiors (PEPI), New Developments in High-Pressure Mineral Physics and Applications to the Earth's Interior, Elsevier, in review

Kontny A, Woodland AB, Koch M (2003) Temperature-dependent magnetic susceptibility behaviour of spinelloid and spinel solid solutions in the systems Fe_2SiO_4–Fe_3O_4 and $(Mg,Fe)_2SiO_4$–Fe_3O_4. Phys Chem Mineral, in press

Krischner H, Koppelhuber-Bitschnau B (1994) Röntgenstrukturanalyse und Rietveldmethode - eine Einführung. Friedrich Vieweg & Sohn Verlag, Wiesbaden, 5. Auflage, 194 p

Kudoh Y, Inoue T, Arashi H (1996) Structure and crystal chemistry of hydrous wadsleyite, $Mg_{1.75}H_{0.5}SiO_4$: Possible hydrous magnesium silicate in the mantle transition zone. Phys Chem Mineral 23: 461-469

Larson AC, von Dreele RB (1988) GSAS, general structure analysis system manual. Rep LAUR 86-748, Los Alamos Nat Lab, Los Alamos, New Mexico, USA

Lindsley DH (1976) The crystal chemistry and structure of oxide minerals as exemplified by the Fe-Ti oxides. In: Rumble III D (ed) Oxide Minerals, Short Course Notes 3, Min Soc Am, Washington DC, L1-L60

Lorimier J, Bernard F, Niepce J-C, Guigue-Millot N, Isnard O, Bérar J-F (2002) Mixed valences in nanometric ferrites investigated by resonant powder diffraction. Appl Crystallogr 36: 301-307

Luth RW, Virgo D, Boyd FR, Wood BJ (1990) Ferric iron in mantle-derived garnets, implications for thermobarometry and for the oxidation state of the mantle. Contrib Mineral Petrol 104: 56-72

Ma C-B (1974) New orthorhombic phases on the join $NiAl_2O_4$ (spinel analog)–Ni_2SiO_4 (olivine analog): Stability and implications to the mantle mineralogy. Contrib Mineral Petrol 45: 257-279

Ma C-B, Sahl K (1975) Nickel Aluminosilicate, Phase III. Acta Cryst B31: 2142-2143

Ma C-B, Tillmanns E (1975) Nickel Aluminosilicate, Phase II. Acta Cryst B31: 2139-2141

Ma C-B, Sahl K, Tillmanns E (1975) Nickel Aluminosilicate, Phase I. Acta Cryst B31: 2137-2139

Marumo F, Isobe M, Akimoto S (1977) Electron-density distributions in crystals of γ-Fe_2SiO_4 and γ-Co_2SiO_4. Acta Cryst B33: 713-716

Matsubara S, Kato A (1979) Iwakiite, $Mn^{2+}(Fe^{3+},Mn^{3+})_2O_4$, a new tetragonal spinelloid mineral from the Gozaisho mine, Fukushima Prefecture, Japan. Mineral J 9: 383-391

McMillan PF, Akaogi M, Sato RK, Poe B, Foley J (1991) Hydroxyl groups in β-Mg_2SiO_4. Am Mineral 76: 354-360

Nell J, van den Berg JC (1988) Stability relations of iscorite (Fe_7SiO_{10}) in the system Fe–Si–O. Trans Instn Min Metall 97: C53-C60

Ohtaka O, Tobe H, Yamanaka T (1997) Phase equilibria for the Fe_2SiO_4–Fe_3O_4 system under high pressure. Phys Chem Mineral 24: 555-560

O'Neill HStC, Pownceby MI (1993) Thermodynamic data from redox reactions at high temperatures. I An experimental and theoretical assessment of the electrochemical method using stabilised

zirconia electrolytes, with revised values for the Fe–"FeO", Co–CoO, Ni–NiO and Cu–Cu_2O oxygen buffers, and new data for the W–WO_2 buffer. Contrib Mineral Petrol 114: 296-314

O'Neill HStC, McCammon CA, Canil D, Rubie DC, Ross II CR, Seifert F (1993) Mössbauer spectroscopy of mantle transition zone phases and determination of minimum Fe^{3+} content. Am Mineral 78: 456-460

Pouchou J-L, Pichoir FMA (1985) "PAP" $\phi(\rho Z)$ procedure for improved quantitative microanalysis. In: Armstrong JT (ed) Microbeam Analysis, San Francisco Press, California, USA, 104-106

Prewitt CT, Finger LW (1993) Crystal Chemistry of high-pressure hydrous magnesium silicates. In: Syono Y, Manghnani MH (eds) High Pressure Research: Application to Earth and Planetary Sciences, Geophys Monograph 67, Am Geophys Union, Washington DC, 269-274

Price GD (1983) Polytypism and the factors determining the stability of spinelloid structures. Phys Chem Mineral 10: 70-83

Richard G, Monnereau M, Ingrin J (2002) Is the transition zone an empty water reservoir? Inferences from numerical model of mantle dynamics. Earth Planet Sci Lett 205: 37-51

Ringwood AE (1967) The pyroxene-garnet transformation in the Earth's mantle. Earth Planet Sci Lett 2: 255-263

Ringwood AE (1991) Phase transformations and their bearing on the constitution and dynamics of the mantle. Geochim Cosmochim Acta 55: 2083-2110

Ringwood AE, Major A (1966) Synthesis of Mg_2SiO_4–Fe_2SiO_4 spinel solid solutions. Earth Planet Sci Lett 1: 241-245

Ringwood AE, Major A (1970) The system Mg_2SiO_4–Fe_2SiO_4 at high pressures and temperatures. Phys Earth Planet Inter 3: 89-108

Ringwood AE, Major A (1971) Synthesis of majorite and other high pressure garnets and perovskites. Earth Planet Sci Lett 12: 411-418

Ross II CR, Armbruster T, Canil D (1992) Crystal structure refinement of a spinelloid in the system Fe_3O_4–Fe_2SiO_4. Am Mineral 77: 507-511

Rossman GR, Smyth JR (1990) Hydroxyl contents of accessory minerals in mantle eclogites and related rocks. Am Mineral 75: 775-780

Sasaki S, Prewitt CT, Sato Y, Ito E (1982) Single-crystal X-ray study of gamma-Mg_2SiO_4. J Geophys Res 87: 7829-7832

Shannon RD (1976) Systematic studies of interatomic distances in oxides. In: Strens RGJ (ed) The physics and chemistry of minerals and rocks, John Wiley & Sons, London, 403-431

Shearer PM (1990) Seismic imaging of upper-mantle structure with new evidence for a 520-km discontinuity. Nature 344: 121-126

Shearer PM (1996) Transition zone velocity gradients and the 520-km discontinuity. J Geophys Res 101: 3053-3066

Schwab R-G, Küstner D (1977) Präzisionsgitterkonstantenbestimmung zur Festlegung röntgenographischer Bestimmungskurven für synthetische Olivine der Mischkristallreihe Forsterit-Fayalit. N Jb Mineral, Mh 5: 205-215

Skogby H, Bell DR, Rossman GR (1990) Hydroxide in pyroxene: Variations in the natural environment. Am Mineral 75: 764-774

Smuts J, Steyn JGD, Boeyens JCA (1969) The crystal structure of an iron silicate, Iscorite. Acta Cryst B25: 1251-1255

Smyth JR (1987) β-Mg_2SiO_4: A potential host for water in the mantle? Am Mineral 72: 1051-1055

Smyth JR (1994) A crystallographic model for hydrous wadsleyite: An ocean in the Earth's interior? Am Mineral 79: 1021-1024

Smyth JR, Kawamoto T (1997) Wadsleyite II: A new high pressure hydrous phase in the peridotite-H_2O system. Earth Planet Sci Lett 146: E9-E16

Tamada O, Shen B, Morimoto N (1983) The crystal structure of laihunite ($\square_{0.04}Fe^{2+}_{0.80}Fe^{3+}_{0.80}SiO_4$) —nonstoichiometric olivine-type mineral—. Mineral J 11: 382-391

Toby BH (2001) EXPGUI, a graphical user interface for GSAS. J Appl Cryst 34: 210-213

von Seckendorff V, O'Neill HStC (1993) An experimental study of Fe-Mg partitioning between olivine and orthopyroxene at 1173, 1273 and 1423 K and 1.6 GPa. Contrib Mineral Petrol 113: 196-207

Woodland AB (1998) The orthorhombic to high-P monoclinic phase transition in Mg-Fe pyroxenes: Can it produce a seismic discontinuity? Geophys Res Lett 25: 1241-1244

Woodland AB, Angel RJ (1997) Reversal of the orthoferrosilite – high-P clinoferrosilite transition, a phase diagram for $FeSiO_3$ and implications for the mineralogy of the Earth's upper mantle. Eur J Mineral 9: 245-254

Woodland AB, Angel RJ (1998) Crystal structure of a new spinelloid with the wadsleyite structure in the system Fe_2SiO_4–Fe_3O_4 and implications for the Earth's mantle. Am Mineral 83: 404-408

Woodland AB, Angel RJ (2000) Phase relations in the system fayalite-magnetite at high pressures and temperatures. Contrib Mineral Petrol 139: 734-747

Woodland AB, Koch M (2003) Variation in oxygen fugacity with depth in the upper mantle beneath the Kaapvaal craton, Southern Africa. Earth Planet Sci Lett, submitted

Woodland AB, O'Neill HStC (1993) Synthesis and stability of $Fe^{2+}_3Fe^{3+}_2Si_3O_{12}$ garnet and phase relations with $Fe_3Al_2Si_3O_{12}$–$Fe^{2+}_3Fe^{3+}_2Si_2O_{12}$ solutions. Am Mineral 78: 1002-1015

Woodland AB, Ross II CR (1994) A crystallographic and Mössbauer spectroscopy study of $Fe^{2+}_3Al_2Si_3O_{12}$–$Fe^{2+}_3Fe^{3+}_2Si_3O_{12}$, (Almandine-"Skiagite") and $Ca_3Fe^{3+}_2Si_3O_{12}$–$Fe^{2+}_3Fe^{3+}_2Si_3O_{12}$ (Andradite-"Skiagite") garnet solid solutions. Phys Chem Mineral 21: 117-132

Yagi T, Marumo F, Akimoto S (1974) Crystal structures of spinel polymorphs of Fe_2SiO_4 and Ni_2SiO_4. Am Mineral 59: 486-490

Yamanaka T, Okita M (2001) Magnetic properties of the Fe_2SiO_4–Fe_3O_4 spinel solid solutions. Phys Chem Mineral 28: 102-109

9. Appendix – Table of contents

9.1. Mineral calculations

The calculations of the cations per formula unit (c.p.f.u.) for spinels and spinelloids require the assumption of an ideal stoichiometry to determine the amounts of Fe^{3+} and Fe^{2+} present. Below is an identical calculation for olivine providing the necessary mathematical operations in brackets ([]).

	SiO_2	MgO	FeO	Σ	
wt%	30.83	61.07	7.74	99.64	
atom wt	60.09	40.21	71.85		
mol %	0.51	0.19	0.85	1.56	[wt% / atom wt]

	Si	Mg	$Fe^{2+}_{(tot)}$	Fe^{3+}	Σ
cpfu	0.99	0.37	1.64	0.02	3.00

$[3 * mol \% / Σ \ mol \%]$

$[2 * (4 - (cpfu \ Fe^{2+} + 2Si + Mg))]$

From the cation occupancies the spinel and spinelloid composition can then be expressed in terms of endmember components. Spinels usually have compositions that plot in the three component system of Mg_2SiO_4–Fe_2SiO_4–Fe_3O_4, but from our experimental results it is clear that the substitution of Mg and Si is decoupled from one another, making it necessary to add a fourth component ($MgFe_2O_4$) to the system. However, even for such situations only three components are necessary to completely describe the spinel composition. In general each composition can be described by more than one set of three endmember components, all of which are equally correct from a thermodynamic perspective. For example the four component composition space can be subdivided according to whether enough Si is present to account for all Mg as a Mg_2SiO_4 component or not:
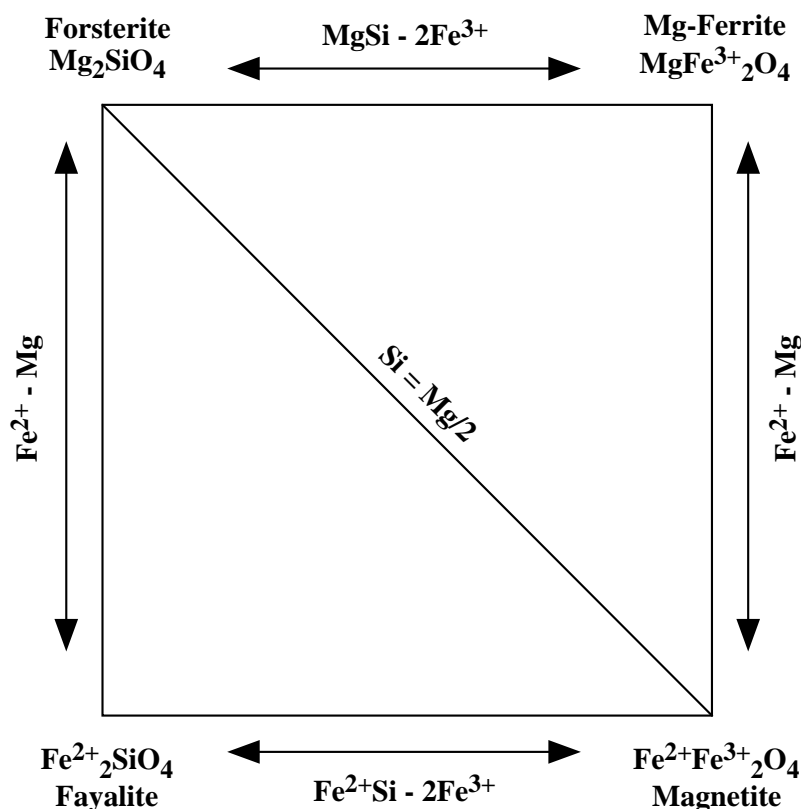
Here, the Si-rich spinels and many of the magnetite-rich spinels produced in the experiments can be considered in terms of the components Mg_2SiO_4, Fe_2SiO_4 and Fe_3O_4. The assignement of molar proportions of these three components is made as follows:

Calculation of molar proportions in the Fo-Fa-Mt triangle from cpfu:

	Si	Mg	Fe^{2+}	Fe^{3+}	
cpfu	0.08	0.12	0.96	1.84	Magnetite
Mt			0.92	1.84	all Fe^{3+} goes into Mt, together with half this amount of Fe^{2+}
rest	0.08	0.12	0.04	0.00	---> $X_{mt} = 0.92 = Fe^{3+} / 2$
Fa	0.02		0.04		the rest of Fe^{2+} goes into Fa, together with half this amount of Si
rest	0.06	0.12	0.00	0.00	---> $X_{fa} = 0.02 = (Fe^{2+} - X_{mt}) / 2$
Fo	0.06	0.12			the rest of Mg goes into Fo, together with half this amount of Si
rest	0.00	0.00	0.00	0.00	---> $X_{fo} = 0.06 = Mg / 2$

Spinels with Si < 2Mg c.p.f.u. fall within the $MgFe_2O_4$-Mg_2SiO_4-Fe_3O_4 subsystem, which necessitates a somewhat different cation assignment to derive the molar proportions of these endmembers:

Calculation of molar proportions in the Fo-Mt-Fer triangle from cpfu:

	Si	Mg	Fe^{2+}	Fe^{3+}	
cpfu	0.01	0.21	0.80	1.98	Mg-Ferrite
Fo	0.01	0.02			all Si goes into Fo, together with double this amount of Mg
rest	0.00	0.19	0.80	1.98	---> $X_{fo} = 0.01 = Si$
Fer		0.19		0.38	the rest of Mg goes into Fer, together with double this amount of Fe^{3+}
rest	0.00	0.00	0.80	1.60	---> $X_{fer} = 0.19 = Mg - (2 * X_{fo})$
Mt			0.80	1.60	the rest of Fe^{3+} goes into Mt, together with half this amount of Fe^{2+}
rest	0.00	0.00	0.00	0.00	---> $X_{mt} = 0.80 = 0.5 * Fe^{3+} - (2 * X_{fer})$

Alternatively, in order to assess the volume systematics of Si-bearing spinels together with those that contain a $MgFe_2O_4$ component, another set of components can be considered:
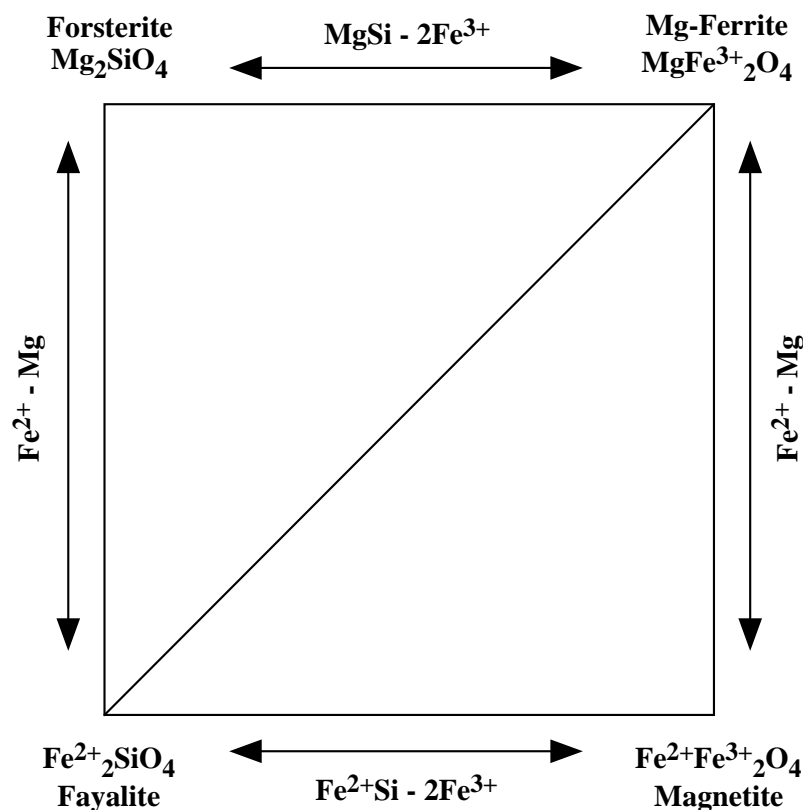
In this case, a large number of spinel compositions can be computed in terms of the $MgFe_2O_4$, Fe_2SiO_4 and Fe_3O_4 components, with the calculation of molar proportions of these endmember components as follows:

Calculation of molar proportions in the Fa-Fer-Mt triangle from cpfu:

	Si	Mg	Fe^{2+}	Fe^{3+}	
cpfu	0.08	0.12	0.96	1.84	Magnetite
Fa	0.08		0.16		all Si goes into Fa, together with double this amount of Fe^{2+}
rest	0.00	0.12	0.80	1.84	---> $X_{fa} = 0.08 = Si$
Mt			0.80	1.60	the rest of Fe^{2+} goes into Mt, together with double this amount of Fe^{3+}
rest	0.00	0.12	0.00	0.24	---> $X_{mt} = 0.80 = Fe^{2+} - (2 * X_{fa})$
Fer		0.12		0.24	the rest of Fe^{3+} goes into Fer, together with half this amount of Mg
rest	0.00	0.00	0.00	0.00	---> $X_{fer} = 0.12 = 0.5 * Fe^{3+} - (2 * X_{mt})$

The Si-rich compositions (i.e. the true wadsleyites) lie within the $MgFe_2O_4$–Mg_2SiO_4–Fe_2SiO_4 subsystem and the molar proportions of these endmember components can be derived in an analagous fashion:

Calculation of molar proportions in the Fo-Fer-Fa triangle from cpfu:

	Si	Mg	Fe^{2+}	Fe^{3+}	
cpfu	0.99	0.37	1.62	0.02	Olivine
Fa	0.81		1.62		all Fe^{2+} goes into Fa, together with half this amount of Si
rest	0.18	0.37	0.00	0.02	---> X_{fa} = 0.81 = Fe^{2+} / 2
Fo	0.18	0.36			the rest of Si goes into Fo, together with double this amount of Mg
rest	0.00	0.01	0.00	0.02	---> X_{fo} = 0.18 = Si - X_{fa}
Fer		0.01		0.02	the rest of Mg goes into Fer, together with double this amount of Fe^{3+}
rest	0.00	0.00	0.00	0.00	---> X_{fer} = 0.01 = Fe^{3+} / 2

9.2. Chemical compositions of pyroxene and iscorite

Average chemical analyses for pyroxenes and iscorite are provided in the Tables below with the cation occupancies calculated assuming ideal stoichiometry based on 6 and 12 oxygens per formula unit, respectively. "n" = number of analyses, values in parantheses indicate 1σ standard deviation error.

9.2.1. Pyroxene

opx		wt%				c.p.f.u.			
	n	SiO_2	FeO	MgO	Total	$Fe^{2+}_{(tot)}$	Si	Mg	Fe^{3+}
8f8b0271	5	45.88(31)	49.48(25)	3.54(02)	98.90(20)	1.79(1)	1.98(1)	0.23	0.03(2)
8f9b1196	17	46.83(30)	46.07(29)	6.63(15)	99.52(31)	1.62(1)	1.97(1)	0.42(1)	0.07(2)
8f5b1180	5	52.75(09)	25.19(41)	21.75(06)	99.70(46)	0.79(1)	1.98	1.22(1)	0.03(1)
8f8v0095	5	49.32(45)	38.50(24)	12.48(15)	100.31(41)	1.29(1)	1.97(1)	0.74(1)	0.06(2)
3f8v0082	5	49.90(38)	35.16(71)	14.55(53)	99.60(24)	1.16(3)	1.98(1)	0.86(3)	0.05(2)
8f8v0082	3	48.61(88)	37.63(81)	13.22(16)	99.47(28)	1.26(3)	1.95(3)	0.79(1)	0.10(6)
8f8v0126	6	50.03(53)	34.75(72)	15.04(33)	99.83(25)	1.14(3)	1.97(1)	0.89(2)	0.06(3)
3f5h1136	14	55.01(98)	17.12(62)	28.97(90)	101.10(57)	0.51(2)	1.95(3)	1.54(4)	0.09(7)
8f5h1136	7	53.28(23)	24.81(56)	22.93(43)	101.01(17)	0.77(2)	1.97(1)	1.27(2)	0.06(1)
3f8h1137	4	50.67(62)	33.33(52)	16.39(45)	100.39(58)	1.08(3)	1.97(1)	0.92(2)	0.07(2)
8f8h1137	7	50.71(29)	34.36(80)	15.51(50)	100.58(65)	1.12(3)	1.98	0.90(3)	0.05(1)
4f8v0083	5	52.57(33)	29.21(18)	19.19(14)	100.97(60)	0.92	1.99	1.09	0.02(1)
8f8v0083	3	49.64(42)	36.15(77)	14.50(18)	100.29(24)	1.19(3)	1.96(2)	0.85(1)	0.09(3)
4f5v0084	6	54.46(29)	21.85(64)	24.86(29)	101.17(36)	0.67(2)	1.98(1)	1.35(1)	0.04(2)
8f5v0084	4	53.84(35)	23.53(69)	23.23(37)	100.60(32)	0.73(2)	1.99(1)	1.28(2)	0.02(2)
5f9v0180	10	49.10(38)	39.19(42)	11.76(32)	100.05(50)	1.32(2)	1.97(1)	0.71(2)	0.05(2)
4f5v0096	4	54.34(51)	20.43(57)	25.84(31)	100.61(29)	0.62(2)	1.98(2)	1.40(1)	0.05(3)
5f5v0096	4	54.99(33)	18.76(31)	27.14(38)	100.89(40)	0.56(1)	1.98(1)	1.46(1)	0.04(2)
8f5v0128	5	53.30(49)	21.85(30)	24.61(12)	99.77(17)	0.67(1)	1.97(2)	1.36(1)	0.06(3)

cpx		wt%				c.p.f.u.			
	n	SiO_2	FeO	MgO	Total	$Fe^{2+}_{(tot)}$	Si	Mg	Fe^{3+}
4f5v0081	3	55.32(16)	19.00(20)	26.66(04)	100.98(30)	0.57	1.99	1.44(1)	0.01(1)
3f5h0998	10	56.26(53)	13.95(35)	30.83(26)	101.03(81)	0.41(1)	1.97(1)	1.62(1)	0.05(1)
8f8v0053	4	52.05(70)	30.22(17)	18.77(27)	101.05(26)	0.96(1)	1.98(2)	1.06(2)	0.05(5)
4f1v0098	3	57.56(13)	7.58(25)	35.63(41)	100.77(60)	0.22(1)	1.97(1)	1.82(1)	0.07(3)
5f8v0099	7	51.45(49)	30.37(30)	18.25(14)	100.07(59)	0.98(1)	1.98(1)	1.05(1)	0.05(2)
4f5v0129	9	55.03(37)	16.52(51)	29.13(26)	100.68(78)	0.49(1)	1.96(1)	1.55(1)	0.08(2)
4f5v0055	20	56.59(57)	12.57(54)	31.77(34)	100.94(70)	0.37(2)	1.98(1)	1.66(1)	0.05(3)
4f8v0085	6	53.24(46)	26.12(26)	21.60(40)	100.97(75)	0.81(1)	1.98	1.20(1)	0.03(1)
5f5v0100	10	56.03(51)	15.00(79)	29.60(86)	100.62(71)	0.44(3)	1.99(1)	1.57(3)	0.03(2)
8f5v0100	4	56.53(38)	13.55(91)	30.76(49)	100.84(42)	0.40(3)	1.99(1)	1.62(2)	0.03(1)
4f1v0127	12	56.93(53)	6.42(19)	36.84(28)	100.19(67)	0.18(1)	1.94(1)	1.88(1)	0.12(1)
8f1v0127	3	56.56(54)	6.59(54)	36.34(46)	99.49(35)	0.19(2)	1.94(1)	1.87(1)	0.11(2)
4f1v0233	3	58.47(60)	6.18(55)	37.19(50)	101.85(69)	0.17(2)	1.96	1.86(1)	0.08(1)
8f1h1646	7	58.18(57)	5.14(41)	37.41(46)	100.73(64)	0.15(1)	1.97(1)	1.89(1)	0.07(3)
4f5z0133	4	56.50(43)	10.37(57)	33.63(21)	100.50(19)	0.30(2)	1.96(1)	1.74(1)	0.08(2)

9.2.2. Iscorite

isc		wt%				c.p.f.u.			
	n	SiO_2	FeO	MgO	Total	$Fe^{2+}_{(tot)}$	Si	Mg	Fe^{3+}
5f9b1197	11	9.87(15)	86.29(41)	0.87(8)	97.03(35)	6.93(2)	0.95(2)	0.12(1)	2.11(3)
8f9b1197	12	10.19(10)	86.26(49)	0.66(1)	97.11(41)	6.93(1)	0.98(1)	0.10	2.04(3)
5f9b1194	12	10.27(08)	86.02(26)	1.25(3)	97.53(21)	6.85(1)	0.98(1)	0.18	2.05(2)
8f9b1194	3	10.32(11)	86.14(07)	0.80(1)	97.26(07)	6.90(1)	0.99(1)	0.11	2.02(2)

9.3. Normalised unit-cell parameters for spinelloids

The structural relationship between the unit-cells of spinel and those of spinelloid are:

stacking direction: *b* (spinelloid) // [110] spinel

                                c (spinelloid) // [001] spinel

which means that: *a* (spinelloid) // [1-10] spinel

b (spinel)

View of a spinel lattice (F cubic) projected down the *c*-axis

b **(spinelloid)**

Spinel cell is illustrated in black
Spinelloid setting in red

closed squares: lattice points at height 0 on *z*
open: lattice points at height 1/2 on *z*

a **(spinel)**
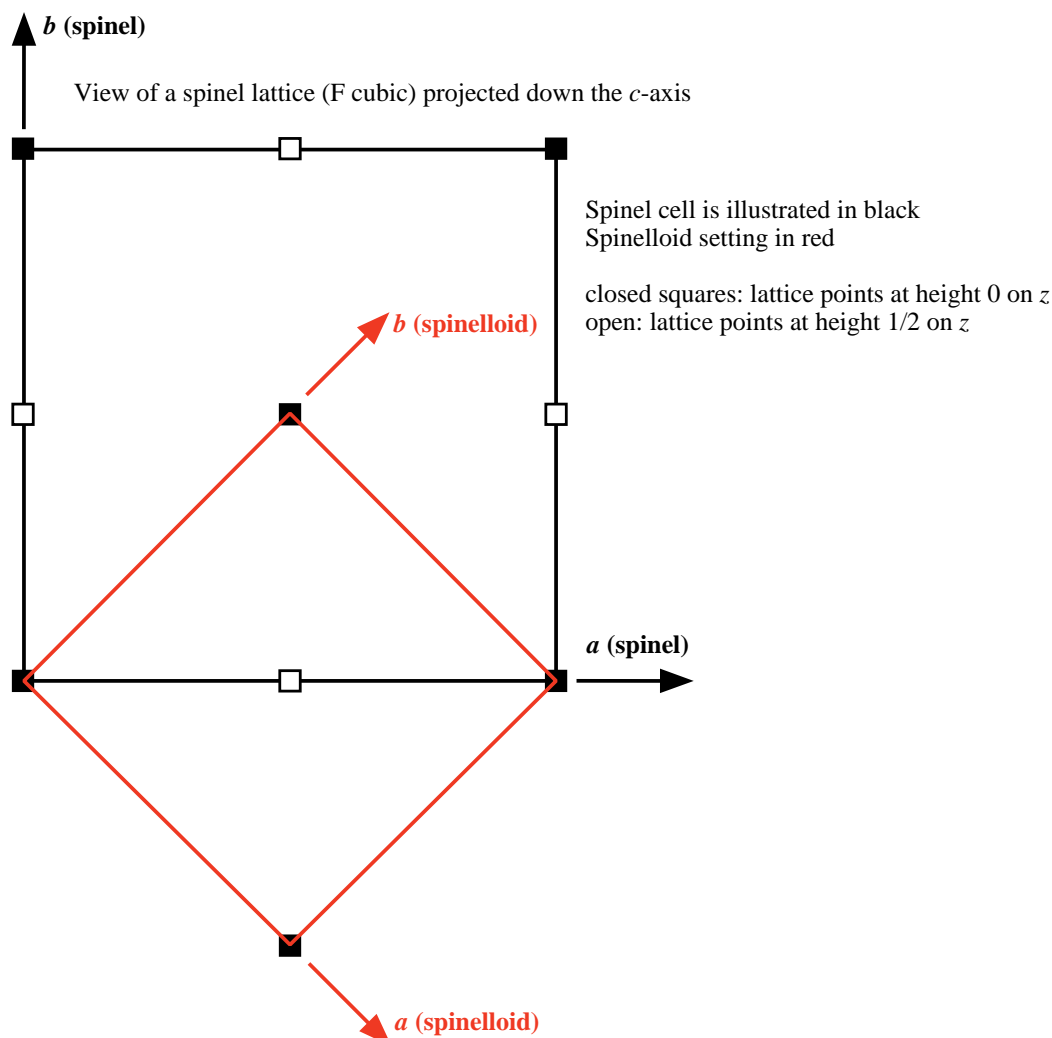
a **(spinelloid)**

Since spinel has a F-lattice there are lattice points in the middle of the faces (e.g. 1/2,1/2,0 and -1/2,1/2,0) as well as at the corners of the unit cell. Therefore, the unit-cell parameters of spinel in the spinelloid setting are:

b (spinelloid) = *b* (spinel) / sqrt(2)

c (spinelloid) = *c* (spinel)

a (spinelloid) = *a* (spinel) / sqrt(2)

Multiplying (*a*b*c*) will give V(spinelloid) = V(spinel) / 2

This "normalized cell" actually contains two slabs of tetrahedra of the spinel structure, one pointing "up" and the other "down". So the true slab width is *b* (spinelloid) / 2 or about 2.97 Å. If the *b* unit-cell parameters of various spinelloids are divided by 2.97 Å the number of layers are obtained (compare Table 1.1):

II: *b* = 18.0 Å, *b* / 2.97 ~ 6 slabs, which is the stacking sequence uuuddd

III: *b* = 11.9 Å, *b* / 2.97 ~ 4 slabs, sequence uudd

V: *b* = 8.93 Å, *b* / 2.97 = 3 slabs, sequence uud

Acknowledgements

Erklärung

Hiermit erkläre ich, Mario Koch, geboren am 19.11.1970 in Ludwigshafen/Pfalz, dass ich die vorgelegte Dissertation selbst verfaßt und mich dabei keiner anderen als der von mir ausdrücklich bezeichneten Quellen und Hilfen bedient habe.

Desweiteren erkläre ich, dass ich an keiner anderen Stelle ein Prüfungsverfahren beantragt habe und die Dissertation weder in dieser oder anderer Form bereits anderweitig als Prüfungsarbeit verwendet, noch einer anderen Fakultät als Dissertation vorgelegt wurde.

Heidelberg, den 15. Mai 2003